Appendix B – Part I

Results from Prior Support (one-pagers)

As examples of the breadth and vitality of the scientific achievements of the COMPRES community, Appendix B of this proposal provides 143 research "one-pagers" that have been submitted by research groups in preparation of this proposal that summarize selected published results enabled by COMPPRES investment in community facilities and infrastructure from 2012-2016.

Table of Contents – One-Pagers

Hidden carbon in Earth's inner core revealed by shear softening in dense Fe_7C_3

Bin Chen[a,b,c,1], Zeyu Li[a], Dongzhou Zhang[d], Jiachao Liu[a], Michael Y. Hu[e], Jiyong Zhao[e], Wenli Bi[b,e], Esen E. Alp[e], Yuming Xiao[f], Paul Chow[f], Jie Li[a,1]

[a]Department of Earth and Environmental Sciences, University of Michigan; [b]Department of Geology, University of Illinois at Urbana-Champaign, [c]Hawaii Institute of Geophysics and Planetology, University of Hawaii at Manoa, [d]Seismological Laboratory, California Institute of Technology, [e]Advanced Photon Source, Argonne National Laboratory, [f]HPCAT, Geophysical Laboratory, Carnegie Institution of Washington

The iron carbide Fe_7C_3 has recently emerged as a leading candidate component of the inner core because at core pressures it is likely the first phase to solidify from a liquid containing iron and a small amount of carbon. In the study, we employed diamond-anvil cell techniques in combination with a suite of advanced synchrotron methods including the Nuclear Resonant Inelastic X-ray Scattering (NRIXS), Synchrotron Mössbauer Spectroscopy (SMS), and X-ray Emission Spectroscopy (XES), in order to probe the acoustic sound velocities and magnetic transitions of Fe_7C_3 under high pressures. We found exceptionally low shear-wave velocity (v_S) in the low-spin and non-magnetic phase of iron carbide Fe_7C_3 at high pressures. The anomalously low v_S of the Earth's inner core could be explained by low-spin Fe_7C_3, thus eliminating the need to invoke partial melting or a postulated large temperature effect. This study was supported by the National Science Foundation and by the Department of Energy through the CDAC (Carnegie-DoE-Alliance Center), and partly by COMPRES.

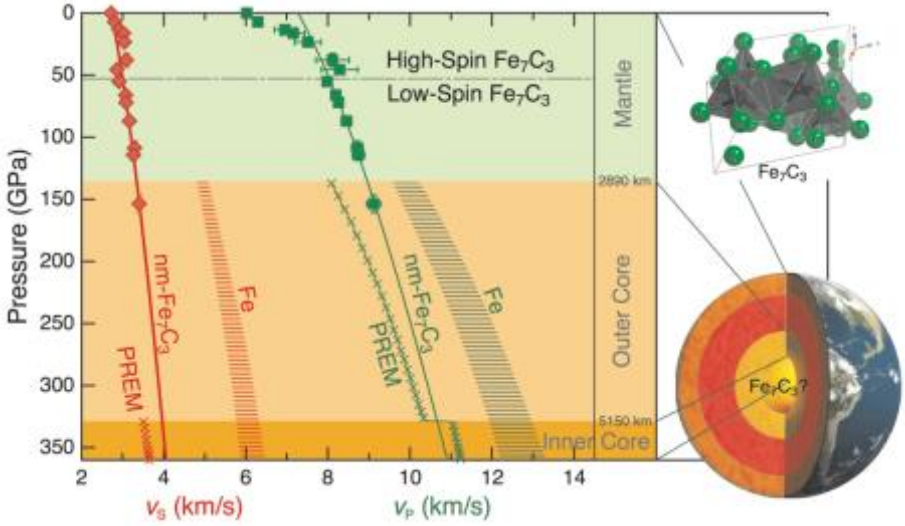

Figure 1. Observations at APS have provided the first-ever estimates of the seismic wave velocities of Fe_7C_3 at high pressure. The S-wave velocity data points are represented by red diamonds, while the P-wave velocity data points are green squares. The solid lines show the extrapolations towards inner core pressures at room temperature. For comparison, the dashed line regions show the seismic wave estimates for pure iron.

Reference:

Chen, B., Z. Li, D. Zhang, J. Liu, M. Y. Hu, J. Zhao, W. Bi, E. E. Alp, Y. Xiao, P. Chow, J. Li (2014), Hidden carbon in Earth's inner core revealed by shear softening in dense Fe_7C_3. *Proc. Nat. Acad. Sci. U.S.A.*, 111(50), 17755–17758, doi:10.1073/pnas.1411154111

Magneto-elastic coupling in compressed Fe_7C_3 supports carbon in Earth's inner core

Bin Chen, Jie Li
Department of Earth and Environmental Sciences, University of Michigan, Ann Arbor
Lili Gao, Esen E. Alp, Jiyong Zhao
Advanced Photon Source, Argonne National Laboratory
Barbara Lavina, Przemyslaw Dera
Center for Advanced Radiation Sources, The University of Chicago

We have employed diamond anvil cell and high brilliance X-ray to probe a candidate iron alloy for the inner core at high pressures. Single crystals of an iron carbide Fe_7C_3, a candidate inner core component were squeezed to megabar pressure in the diamond anvil cell and probed by X-rays. As a result of a pressure-induced magnetic transition, the iron carbide unexpectedly becomes more compressible at about half an megabar pressure, leading to a close match to the inner core density under relevant inner core conditions. Such observation supports the scenario of inner core mainly composed of Fe_7C_3 and the proposition that the core is potentially the largest carbon reservoir in Earth. This study is partially supported by CDAC, COMPRES, NSF grants EAR-102379 and EAR-1291881.

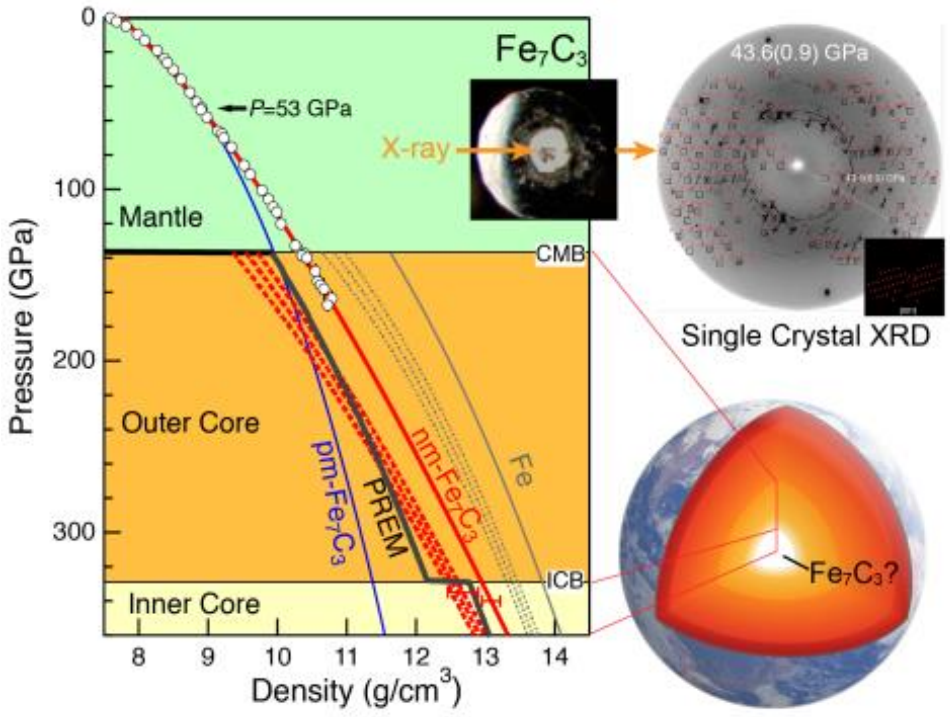

Figure 1. The measured and calculated density of Fe_7C_3 in comparison with and seismic observations, indicating that the non-magnetic (nm) Fe_7C_3 can match the inner core density according to the Preliminary Reference Earth Model (PREM). Top right panel shows the single crystal loading in a diamond anvil cell and representative single crystal X-ray diffraction data and the projection of the Fe_7C_3 crystal structure in the reciprocal space.

Reference:

Chen, B., L. Gao, B. Lavina, P. Dera, E. E. Alp, J. Zhao, and J. Li (2012), Magneto-elastic coupling in compressed Fe_7C_3 supports carbon in Earth's inner core, *Geophys. Res. Lett.*, *39*(18), L18301, doi:10.1029/2012GL052875.

Equation of state and phase diagram of Fe–16Si alloy as a candidate component of Earth's core

Rebecca A. Fischer [a], Andrew J. Campbell [a], Razvan Caracas [b], Daniel M. Reaman [a], Przymyslaw Dera [c], Vitali B. Prakapenka [c]

[a] University of Chicago, [b] Ecole Normale Supérieure de Lyon, [c] GSECARS

(COMPRES-related facilities: COMPRES gas-loading system; NSLS X17C; ALS 12.2.2)

The outer core of the Earth contains several weight percent of one or more unknown light elements, which may include silicon. Therefore it is critical to understand the high pressure–temperature properties and behavior of an iron–silicon alloy with a geophysically relevant composition (16 wt% silicon). We experimentally determined the melting curve, subsolidus phase diagram, and equations of state of all phases of Fe–16 wt%Si to 140 GPa, finding a conversion from the $D0_3$ crystal structure to a B2+hcp mixture at high pressures. The melting curve implies that 3520 K is a minimum temperature for the Earth's outer core, if it consists solely of Fe–Si alloy, and that the eutectic composition in the Fe– Si system is less than 16 wt% silicon at core–mantle boundary conditions. Comparing our new equation of state to that of iron and the density of the core, we find that for an Fe–Ni–Si outer core, 11.3±1.5 wt% silicon would be required to match the core's observed density at the core–mantle boundary. We have also performed first-principles calculations of the equations of state of Fe_3Si with the $D0_3$ structure, hcp iron, and FeSi with the B2 structure using density-functional theory.

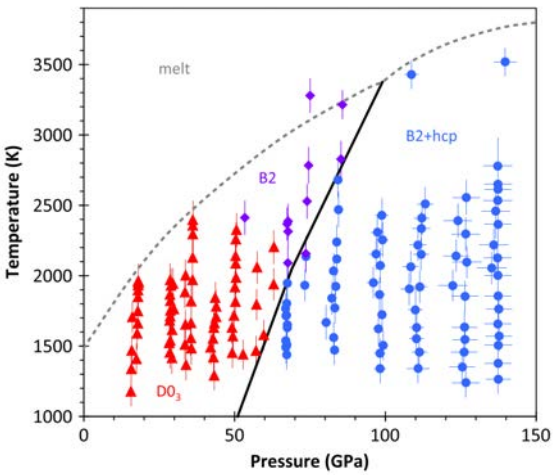

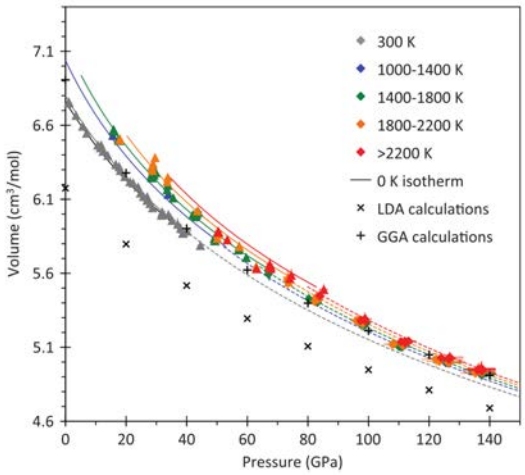

Left: Phase diagram of Fe–16Si. **Right:** Equation of state of Fe–16Si.

Reference: Fischer R. A., Campbell A. J., Caracas R., Reaman D. M., Dera P., and Prakapenka V. B. (2012) Equation of state and phase diagram of Fe–16Si alloy as a candidate component of Earth's core. *Earth Planet. Sci. Lett.*, **357-358**, 268-276.

Equations of state in the Fe-FeSi system at high pressures and temperatures

Rebecca A. Fischer [a], Andrew J. Campbell [a], Razvan Caracas [b], Daniel M. Reaman [a], Dion L. Heinz [a], Przymyslaw Dera [c], Vitali B. Prakapenka [c]

[a] University of Chicago, [b] Ecole Normale Supérieure de Lyon, [c] GSECARS

(COMPRES-related facilities: COMPRES gas-loading system; ALS 12.2.2)

Earth's core is an iron-rich alloy containing several weight percent of light element(s), possibly including silicon. Therefore, the high pressure-temperature equations of state of iron-silicon alloys can provide understanding of the properties of Earth's core. We performed X-ray diffraction experiments using laser-heated diamond anvil cells to achieve simultaneous high pressures and temperatures, up to ~200 GPa for Fe–9 wt% Si alloy and ~145 GPa for stoichiometric FeSi. We determined equations of state of the $D0_3$, hcp+B2, and hcp phases of Fe–9Si, and the B20 and B2 phases of FeSi. We also calculated equations of state of Fe, $Fe_{11}Si$, Fe_5Si, Fe_3Si, and FeSi using ab initio methods, finding that iron and silicon atoms have similar volumes at high pressures. By comparing our experimentally determined equations of state to the observed core density deficit, we find that the maximum amount of silicon in the outer core is ~11 wt %, while the maximum amount in the inner core is 6–8 wt %, for a purely Fe-Si-Ni core. Bulk sound speeds predicted from our equations of state also match those of the inner and outer core for similar ranges of compositions. We find a compositional contrast between the inner and outer core of 3.5–5.6 wt % silicon, depending on the seismological model used. We find a good match to the observed density, density profile, and sound speed of the Earth's core, suggesting that silicon is a viable candidate for the dominant light element.

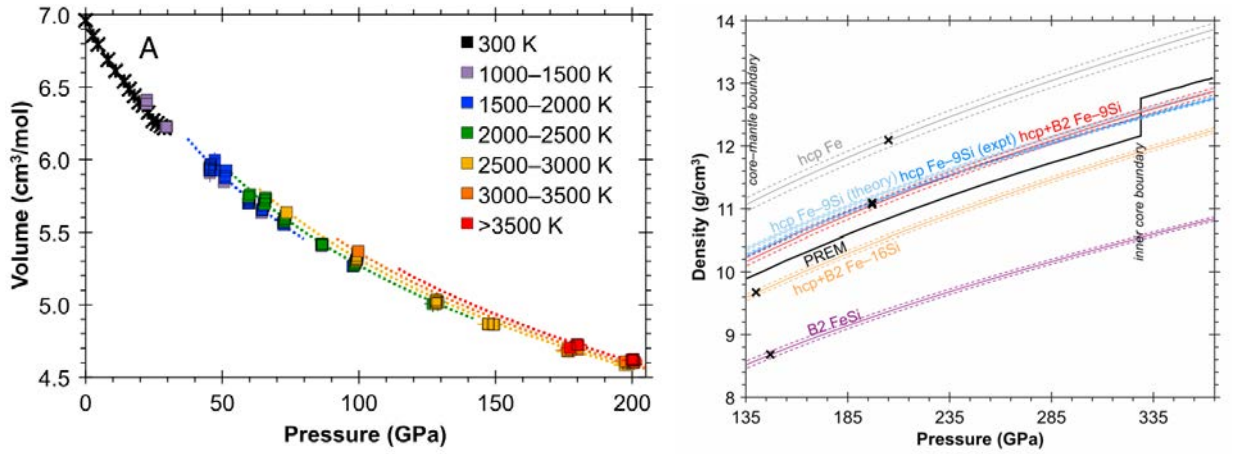

Left: Phase diagram of Fe–9Si. Crosses: $D0_3$ phase; Squares: hcp+B2 phase.

Right: Comparison between equations of state of Fe–Si alloys and PREM density model of Earth's core.

Reference: Fischer R. A., Campbell A. J., Caracas R., Reaman D. M., Heinz D. L., Dera P., and Prakapenka V. B. (2014) Equations of state in the Fe–FeSi system at high pressures and temperatures. *J. Geophys. Res.* **119**, 2810-2827.

Properties of iron and iron compounds to high pressure:
Implications for the Earth's mantle and core

A. E. Gleason & W. Mao, Stanford Univ. & LANL

(COMPRES-related facility: ALS 12.2.2)

Two separate studies on pure iron and an iron-oxy-hydroxide provide new constraints on the state of the Earth's mantle and core revealing: 1) pure iron is surprising weak to Earth core conditions supporting a dislocation creep mechanism for solid state flow and possible mechanism for observed seismic anisotropy in the core, and 2) measurements of structural and electronic spin transitions in e-FeOOH show a connection between water content and spin transition pressure to mantle pressures. The high pressure x-ray (axial and radial) diffraction for both of these studies were collected, in part, at the ALS beamline 12.2.2.

Figure 1.

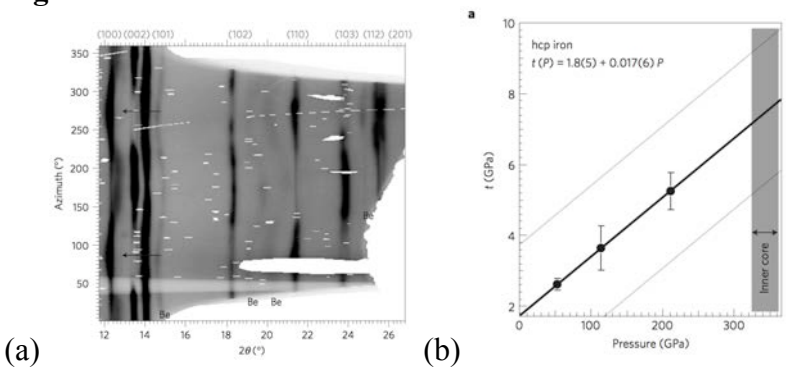

(a) (b)

Fig. 1 Representative caked diffraction pattern (a) combined with acoustic sound speeds extracted from NRIXS provide new constraints on the bulk strength of iron to high pressure (b) indicating pure iron is much weaker than previously thought and likely to flow under Earth core conditions.

Figure 2.

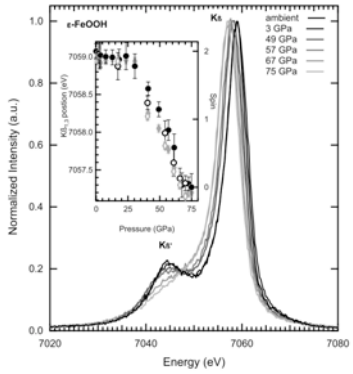

Fig. 2 XES spectra of e-FeOOH at high pressure. These data combined with DFT and XRD provide evidence for a spin transition in Fe3+ preceded by a second order phase transition whose main characteristic is given by a symmetrization of hydrogen bonds and uncovered a connection between water content and iron spin transitions at mid- to lower-mantle

References:

Gleason, A.E., Mao, W.L. and Zhao, J. "Sound velocities for hexagonally close-packed iron compressed hydrostatically to 136 GPa from phonon density of states" 2013 Geophysical Research Letters, 40, 2983-2987.

Gleason, A.E., Quiroga, C.E., Otte, K., Suzuki, A., Pentcheva, R. and Mao, W.L. "Symmetrization driven spin transition in e-FeOOH at high pressure" 2013 Earth and Planetary Science Letters, 39, 49-55.

Gleason, A.E. and Mao, W.L. "Strength of iron at core pressures and evidence for a weak Earth's inner core" 2013 Nature Geoscience, 6, 571-574.

Seismic parameters of Fe and Fe-alloys at high pressure and temperature by Momentum-resolved IXS

Ahmet Alatas[1], Michael Y. Hu[1], Jiyong Zhao[1], Wenli Bi[1,3], Jin Liu[2], Jung-Fu Lin[2], Leonid Dubrovinsky[4]
[1]Advanced Photon Source, Argonne National Laboratory, Argonne, Illinois 60439
[2]Department of Geological Sciences, Jackson School of Geosciences, University of Texas at Austin, Austin, Texas 78712,
[3]Department of Geology, University of Illinois at Urbana-Champaign, Urbana, Illinois 61801
[4] Bayerisches Geoinstitut, Universität Bayreuth, Bayreuth, Germany
(COMPRES-related facilities: Advanced Photon Source, beamline 3-ID)

Earth's core is predominantly constituted of Fe, alloyed with Ni and a certain amount (approximately 10 wt.%) of elements lighter than Fe (thus named light elements). A plethora of studies have concentrated on the identity and concentration of candidate light elements incorporated into the Earth's core from cosmochemical, geochemical, geophysical, and mineral physics perspectives; though, the crystal structure and the amount of the major light element alloyed with Fe in the Earth's core remain highly debated.

Inelastic x-ray scattering technique with milli electron volt energy resolution provides unique opportunity to study phonon dispersion that is directly related to compressional and shear sound velocities of the system. Small beam size and penetration of x-rays to most of the sample make it unique for studying iron and iron alloys under high pressure and/or high temperature combined with x-ray diffraction and nuclear resonant inelastic x-ray scattering technique. Some of the recent results are shown in the figure provides a multifactored geophysical constraint on compositional model of the inner core which is consistent with silicon being major light element alloyed with Fe and 5 wt % Ni as well as certain portion of the bcc Fe-Si alloy with the lattice preferred orientation may produce compressional and shear velocity anisotropies to potentially account for the observed seismic anisotropy in the inner core.

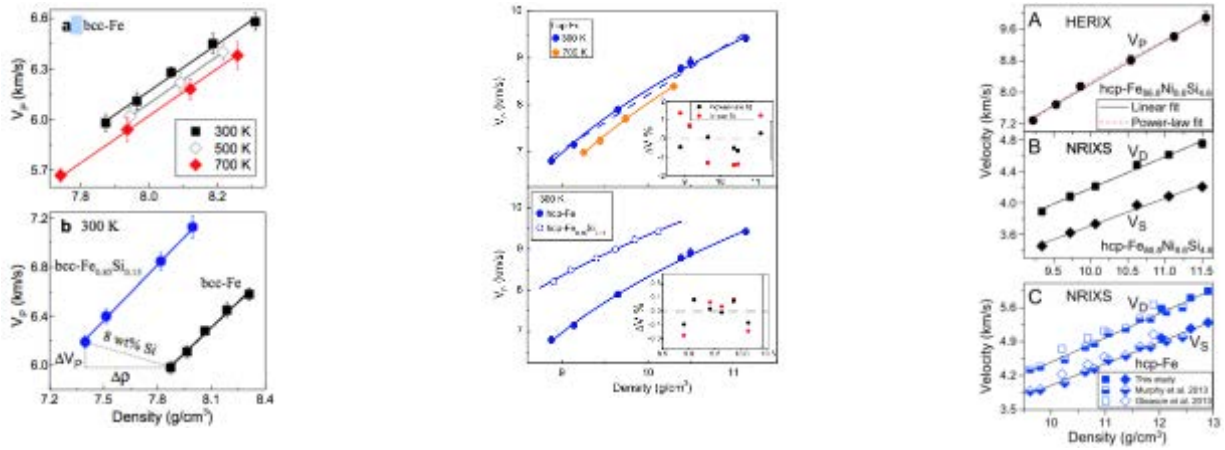

Figure: (Left) Compressional wave velocity (V_P) and density relation of bcc-Fe (a) and Fe-Si alloy (b) at high pressure and high temperature[1]. (Center) V_P and density relation of fcc-Fe at room and high temperature (a) and hcp-Fe and Fe-Si alloy at room temperature (b) [2]. (Right) Sound velocities of ^{57}Fe-enriched hcp-Fe and hcp-$Fe_{86.8}Ni_{8.6}Si_{4.6}$ alloy as a function of density. (a) V_P of hcp-$Fe_{86.8}Ni_{8.6}$ $Si_{4.6}$ alloy derived from HERIX measurements. (b) V_D and V_S of hcp-$Fe_{86.8}Ni_{8.6}Si_{4.6}$ alloy derived from NRIXS measurements. (c) V_D and V_S of hcp-Fe derived from NRIXS measurements. V_S reported in this study were calculated from the V_P and V_D[3].

1) J. Liu et al. Physics of the Earth and Planetary Interiors 233 (2014) 24–32.
2) Z Mao et. al. Proceedings of the National Academy of Sciences 109 (2012) 10239-10244.
3) J. Liu et. al. Journal of Geophysical Research: Solid Earth 121 (2016) 1-14.

Use of the Advanced Photon Source, an Office of Science User Facility operated for the U.S. Department of Energy (DOE) Office of Science by Argonne National Laboratory, is sup-ported by the U.S. DOE under Contract No. DE-AC02-06CH11357

Temperature dependence of bcc to hcp transition in iron studied with synchrotron Mössbauer spectroscopy using hybrid-filling mode of the APS (*)

E. E. Alp[1], W. Bi[,21], J. Zhao[1], M. Y. Hu[1], T.S. Toellner[1], S. Sinogeikin[3]

[1]Advanced Photon Source, Argonne National Laboratory
[2]Department of Geology, University of Illinois at Urbana-Champaign
[3] HP-CAT, Geophysical Laboratory, Carnegie Institute of Washington

The transformation of iron from bcc to hcp phase under pressure is studied using synchrotron Mössbauer spectroscopy during a special filling mode at the Advanced Photon Source. In this so-called **"Hybrid Filling Mode"** a single bunch containing 16 *mA* is isolated from the remaining bunches by 1.594 *microseconds* gaps. Compared to ^{57}Fe half life of 97.8 nsec, this mode represents a unique opportunity to record the nuclear decay over 10 lifetimes. This has been exploited for the first time to determine the boundaries of the phase transition accurately, and obtain Clausius-Clapeyron slope, dependence of hyperfine field on temperature and pressure, and identify the nature of the phase transition.

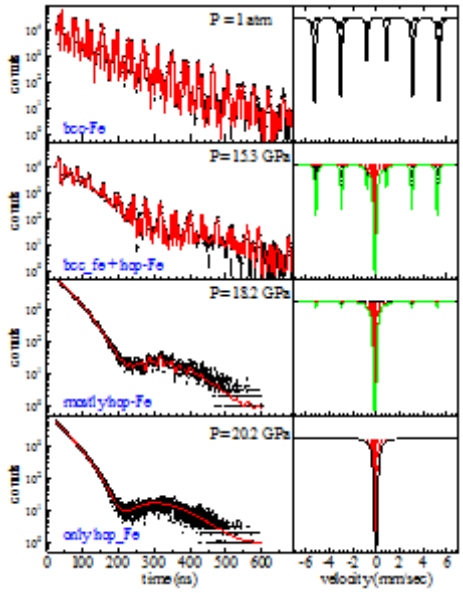

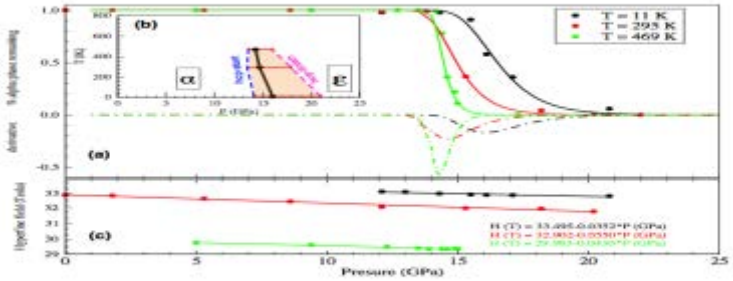

Left figure: *Nuclear decay of iron metal at ambient temperature and under high pressure of 15.3, 18.2 and 20.2 GPa. The bcc iron (magnetic) transforms to hcp iron (non-magnetic) between ~ 14-20 GPa. In the mixed state, it is possible to determine fraction of each phase, and their hyperfine parameters reliably if data is available over several lifetimes ($t_{1/2}$=97.8 nsec). The data on the left column are fitted using CONUSS program, and then it is used to simulate the corresponding energy spectrum on the right column. The magnetic phase (bcc) gives the split lines, and non-magnetic phase (hcp) gives the single absorption line.* ***Right figure: (a):*** *Transformation of bcc to hcp as a function of pressure, (b) The temperature-pressure diagram of the studied region between 11 and 469 K, and (c) dependence of magnetic hyperfine field as a function of pressure at different temperatures.*

(*) This work is supported by U.S. Department of Energy (DOE), Office of Science, Basic Energy Sciences under contract DE-AC02-06CH11357, and the Consortium for Materials Properties Research in Earth Sciences (COMPRES) [National Science Foundation (NSF) EAR 06-49658]. E. Alp thanks W. Sturhahn for discussion on the data analysis.

Iron-carbon nonstoichiometric solutions: cementite and 'Fe_7C_3' explored

During COMPRES II, melting and element partitioning relations were explored in metallic liquid solutions involving Fe-S-C. Those studies have been extended during COMPRES III to include Fe-S-C-H liquids. H is found to be a much more effective agent of freezing point depression than oxygen (Buono and Walker, 2014). Several studies of the solid Fe_3C-like material [cohenite for mineralogists or cementite for metallurgists] grew out of the initial efforts. The trace siderophile element partitioning between cohenite and metallic liquid was explored (Buono et al., 2013). A surprising discovery in this study was that cohenite can have a very wide range of Fe/C, all in the cohenite Pnma X-ray structure. The properties and compositional range of these variable composition cohenites were explored in some depth using diffusion couple methods by Walker et al. (2013). It was also shown in that study that the Eckstrom-Adcock carbide, nominally Fe_7C_3, also has a wide range of possible compositions. Both carbides are better regarded as intermetallic solutions than as stoichiometric compounds. These finding have considerable impact on the potential stability and magnetic properties of the Fe-based carbides. The stability of the ferromagnetic phase of Fe_3C was experimentally determined by Walker et al. (2015) using both direct magnetometer-within-a-multi-anvil device methods and by tracking volumetric proxies for magnetic state [thermal expansion and compressibility] using DAC devices on station 12.2.2 at the ALS supported by COMPRES. Ferromagnetic cementite becomes paramagnetic above 6-7 GPa. The Curie temperature and pressure were also shown to be sensitive to the composition of the cementite solution measured. Cumulatively these studies show the potential for carbide stability in the mantle as well as demonstrating the range of possibilities opened by the discovery of nonstoichiometry in the carbides. This discovery should not have been surprising from the perspective of the nonstoichiometries already well known in the Fe oxides, hydrides, sulfides, and nitrides.

Publications from this project:

AS Buono and D Walker (2014) H, not O or pressure, causes eutectic T depression in the Fe-FeS System to 8 GPa. *Meteoritics & Planetary Science 1–8 [Drake Volume] doi: 10.1111/maps.12372*

AS Buono, R Dasgupta, C-TA Lee, D Walker (2013) Siderophile element partitioning between cohenite and liquid in the Fe–Ni–S–C system and implications for geochemistry of planetary cores and mantles. *Geochimica et Cosmochimica Acta 120 239–250*

D Walker, R Dasgupta, J Li, AS Buono (2013) Nonstoichiometry and growth of some Fe carbides. *Contrib Mineral Petrol* 166:935–957, DOI 10.1007/s00410-013-0900-7

D Walker, J Li, B Kalkan SM Clark (2015) Thermal, compositional, and compressional demagnetization of cementite. *American Mineralogist, 100, 2610–2624* .doi.org/10.2138/am-2015-5306

Elastic softening in Fe_7C_3 with implications for Earth's deep carbon reservoirs.

Jiachao Liu[1], Jie Li[1], and Daijo Ikuta[2]
[1]Department of Earth and Environmental Sciences, University of Michigan, Ann Arbor, Michigan, USA,
[2]High Pressure Collaborative Access Team, Geophysical Laboratory, Carnegie Institution of Washington, Argonne, Illinois, USA

Synchrotron x-ray diffraction (XRD) measurements were performed on hexagonal Fe_7C_3, a potential host of reduced carbon in Earth's mantle and a candidate component of the inner core, up to 70 GPa at 300 K by using symmetric type diamond anvil cell (DAC). In order to avoid bridging between two diamonds and investigate pressure gradient in the sample chamber, the dimension of sample was well controlled and multiple pressure standards (two ruby balls, Au powder on top of the sample, separate Au flake) were loaded; on the other hand, Fe flake was loaded in the same sample chamber for comparison. Neon was loaded into the sample chamber as a hydrostatic pressure medium and an additional pressure standard. Compared with the smooth compression curve of pure iron, the compression curve of hexagonal Fe_7C_3 reveals elastic softening between 7 GPa and 20 GPa, which can be attributed to noncollinear alignment of spin moments in a state between the ferromagnetic and paramagnetic phases, as expected for Invar-type alloys. The volume reduction associated with the softening would enhance the stability of Fe_7C_3 in the deeper part of the upper mantle and transition zone. As a result of subsequent spin crossover at higher pressures, Fe_7C_3 at inner core conditions likely occurs as the nonmagnetic phase, which remains a candidate for the major component of the Earth's central sphere.

Reference: Liu, J., Li, J., Ikuta, D. (2016) Elastic softening in Fe_7C_3 with implications for Earth's deep carbon reservoirs. *J. Geophys. Res. Solid Earth*, 121, doi:10.1002/2015JB012701.

Neon was loaded into the sample chamber as a hydrostatic pressure medium and an additional pressure standard by using the COMPRES/GSECARS gas-loading system at the Advanced Photon Source (APS), Argonne National Laboratory.

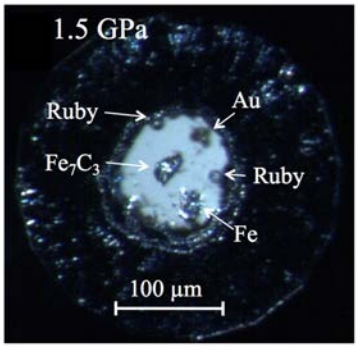

Optical images showing the sample configuration.

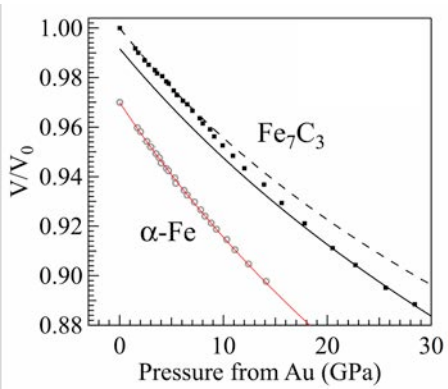

Normalized volumes of Fe_7C_3 (solid squares) and α-Fe (open circles) up to 30 GPa. The third-order Birch-Murnaghan equations of state fits to the Fe_7C_3 data reveal softening in Fe_7C_3 between 7 and 20 GPa.

Experiments: "Compressional anelasticity of HCP metals: a key to the dynamics of Earth's core" (Andrew Walker, University of Leeds)

Team: Andrew Walker, Simon Hunt, Ollie Lord, Ed Bailey, Lewis Schardong, Lora Armstrong, Stephen Stackhouse and Matt Whitaker

We undertook two experimental sessions in 2014 with the objective of beginning to constrain the anelasticity of Earth's inner core with a view understanding its microstructure (which would provide information on inner core deformation) and temperature (independently from that available from the melting point iron alloys at extreme pressure). Our proposal included two experimental strands: (a) Measurements of the anelastic response of HPC metal analogues using the D-DIA apparatus installed on the X17B2 beamline. The approach for these experiments follows that described by Li and Weidner (2007; Rev. Sci. Instrum. 78:053902). (b) Direct experiments on HCP iron using the new DTcup installed on the X17B2ss beamline. Although the approach is the same, these experiments would be the first using the new, higher pressure, deformation apparatus.

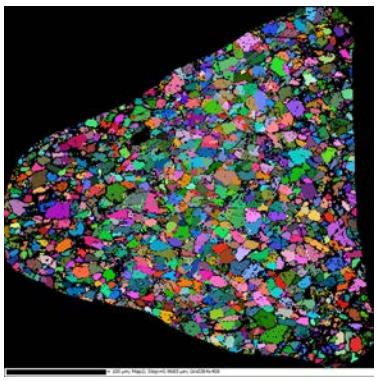

Data from EBSD analysis of recovered Zn sample showing grain orientation (colours relate to Euler angles of crystallographic orientation) and microstructure.

The two experimental sessions were marred by machine problems (specifically, problems with the superconducting wiggler's cryogenic system, leading to the loss of around half of the allocated time) but did yield useful insight. Experiments on a zinc analogue show clear evidence for frequency dependent Young's modulus developing at high temperature. Furthermore, the degree of this frequency dependent softening appears to be strongly correlated with the microstructure of the sample, with samples manufactured from packed powder showing less softening than those manufactured from extruded wire. The experiments on HCP iron were less successful. Although we were able to transform iron powder into the high-pressure HCP structure, the DTcup was unable to generate sufficient differential stress to measurably deform the sample at seismic frequencies. Work to understand the cause of this difficulty (which appears to related to an asymmetry in the behavior of the upper and lower differential anvils) is ongoing.

The W-WO_2 oxygen fugacity buffer (WWO) at high pressure and temperature: Implications for fO_2 buffering and metal-silicate partitioning

Gregory A. Shofner[1]*, Andrew J. Campbell[2], Lisa R. Danielson[3], Kevin Righter[4], Rebecca A. Fischer[2], Yanbin Wang[5], and Vitali Prakapenka[5]
[1]Towson University, [2]University of Chicago, [3]Jacobs Technology,
[4]NASA Johnson Space Center, [5]GSECARS

(COMPRES-related facilities: COMPRES Multianvil Assembly; NSLS X17C)

The high pressure and temperature equation of state of tungsten and tungsten oxide were measured up to 70 GPa and 2300 K using synchrotron X-ray diffraction in conjunction with a multianvil press and laser heated and externally heated diamond anvil cells at GSECARS, Sector 13, APS and at NSLS X17C. Three phases were observed in WO_2 with structures in the *P2₁/c*, *Pnma* and *C2/c* space groups; the *C2/c* phase is newly described here. Using the W and WO_2 equations of state determined in this study, the W-WO_2 buffer (WWO) was calculated to high pressures. The WWO buffer is at a higher fO_2 than the iron-wüstite (IW) buffer, but the magnitude of this difference decreases at higher pressures. This implies an increasingly lithophile character for W at higher pressures, in agreement with experiemental metal-silicate partitioning studies.

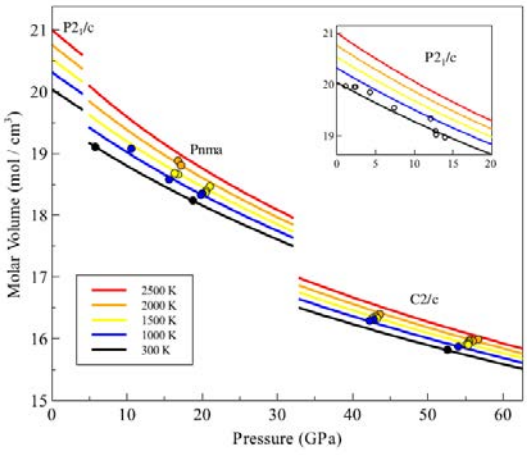

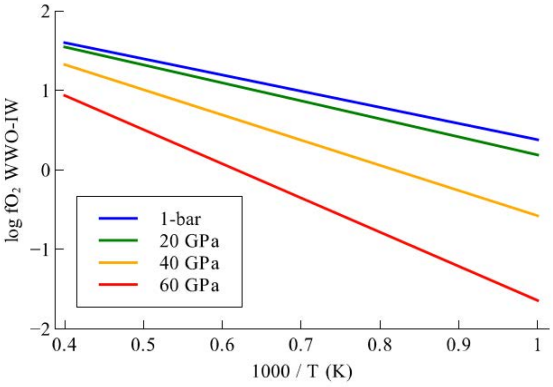

Left: Equations of state for WO_2 plotted along isotherms. Each of the three phases (*P2₁/c*, *Pnma*, *C2/c*) are plotted over pressures in which they are stable.

Right: Difference between the WWO and IW buffers at various pressures.

Reference: Shofner G. A., Campbell A. J., Danielson L., Righter K., Fischer R. A., Wang Y., and Prakapenka V. B. (2016) The W–WO_2 oxygen fugacity buffer (WWO) at high pressure and temperature: Implications for fO_2 buffering and metal-silicate partitioning. *Am. Mineral.* **101**, 211-221.

Sound velocities of FeHx: Implications for the Earth's core

Thompson, E.C.[1]; Chidester, B.A.[1]; Fischer, R.A. [2];
Prakapenka, V.B.[3]; Bi, W.L.[4]; Alp, E.E.[4] and Campbell, A.J.[1]

[1]Department of the Geophysical Sciences, University of Chicago;
[2]National Museum of Natural History, Smithsonian Institution and the Department of Earth and Planetary Sciences, University of California Santa Cruz;
[3]Center for Advanced Radiation Sources, University of Chicago;
[4]Argonne National Lab, Advanced Photon Source

(COMPRES-related facilities: APS Sector 3)

Earth's core is composed of an iron-rich alloy, and includes a light element component that accounts for the difference between seismically obtained densities and the density of pure Fe at relevant pressure and temperature conditions. As the most abundant and lightest element in the solar system, hydrogen is a plausible contributor to this core density deficit. Although hydrogen solubility in iron at atmospheric conditions is low, its solubility increases with pressure, increasing the likelihood of FeH_X formation within the Earth's interior. This study combines synchrotron x-ray diffraction (XRD) *P-V-X* data and density of state information from high-pressure nuclear resonant inelastic scattering (NRIXS) experiments and literature EoSs to better constrain the compressional behavior of FeH_X. Stoichiometry of quenched FeH_X samples was determined using new *fcc* FeH_X equation of state, to calculate sound velocities from NRIXS data on *fcc* FeH_X in our sample as a function of pressure and composition (i.e., varying hydrogen). Using this methodology, the acoustic velocities of the *fcc* phase of FeH_X are higher than those reported for the hcp phase but not those of the dhcp phase.

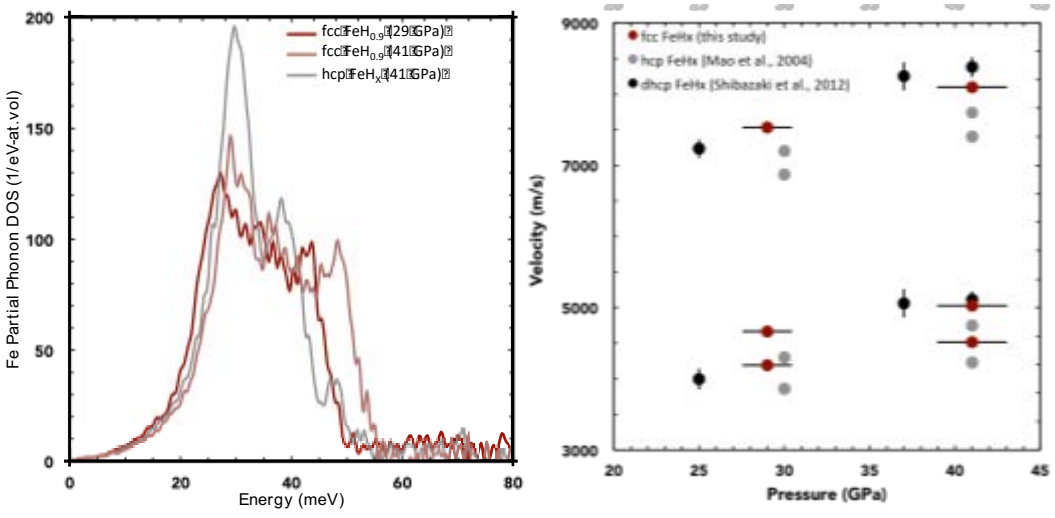

Figure 1. (left) Partial phonon density of states of *fcc* and *hcp* iron hydride at 29 and 41 GPa. **(right)** Calculated Debye velocities, V_P and V_S for iron hydride as a function of pressure.

References:
Mao *et al.* (2004) Geophys. Res. Lett. 31.
Shibazami *et al.* (2012) Earth Planet. Sci. 313-314.
Thompson *et al.* (in prep)

Equation of state of pyrite to 80 GPa and 2400 K

Thompson, E.C.[1], Chidester, B.A.[1], Fischer, R.A.[2], Myers, G.I. [1], Heinz, D.L.[1], Prakapenka, V.B.[3], Campbell, A.J.[1]

[1]Department of the Geophysical Sciences, University of Chicago,
[2]National Museum of Natural History, Smithsonian Institution and the Department of Earth and Planetary Sciences, University of California Santa Cruz,
[3]Center for Advanced Radiation Sources, University of Chicago

(COMPRES-related facilities: COMPRES gas-loading system at GSECARS)

We performed X-ray diffraction measurements on FeS_2 achieving pressures from 15 to 80 GPa and temperatures up to 2400 K using laser-heated diamond anvil cells. No phase transitions were observed in the pyrite structure over the pressure and temperature ranges investigated. Combining our new *P-V-T* data with previously published room temperature compression and thermochemical data, we fit a Debye temperature of 624(14) K and determined a Mie-Grüneisen equation of state for pyrite having bulk modulus $K_T = 141.2(18)$ GPa, pressure derivative $K_T' = 5.56(24)$, Grüneisen parameter $\gamma_0 = 1.41$, anharmonic coefficient $A_2 = 2.53(27)\times10^{-3}$ $JK^{-2}mol^{-1}$, and $q = 2.06(27)$. These findings are compared to previously published equation of state parameters for pyrite from static compression, shock compression, and ab initio studies. This revised equation of state for pyrite is consistent with an outer core density deficit satisfied by 11.4(10) wt% sulfur, yet matching the bulk sound speed of PREM requires an outer core composition of 4.8(19) wt% S. This discrepancy suggests that sulfur alone cannot satisfy both seismological constraints simultaneously and cannot be the only light element within Earth's core, and so the sulfur content needed to satisfy density constraints using our FeS_2 equation of state should be considered an upper bound for sulfur in the Earth's core.

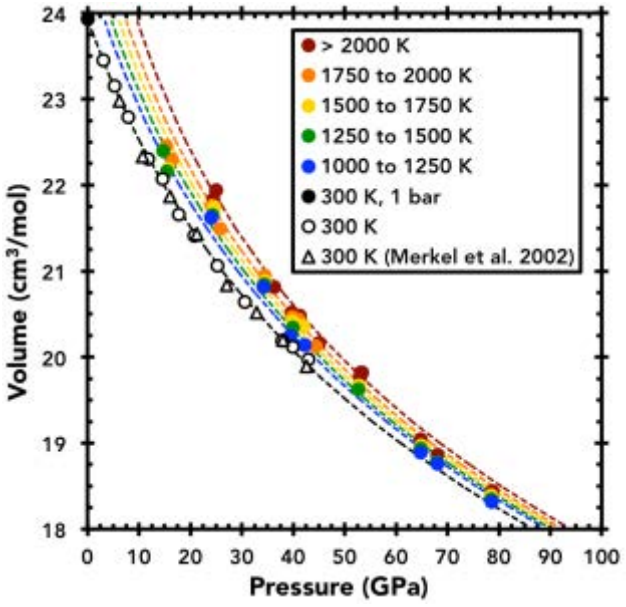

Figure 1. Vinet equation of state of pyrite-FeS_2 up to 80 GPa. Circles are measured volumes from this study, triangles are data from Merkel et al. (2002), and color-coded dashed lines are isotherms calculated at the median temperature of the data within each indicated temperature range.

References:

Thompson E.C., Chidester, B.A., Fischer, R.A., Myers, G.I., Heinze, D.L., Prakapenka, V.B., and Campbell A.J. (2016) In-situ infrared spectra of hydroxyl in amphiboles at high pressure. *American Mineralogist*. **101**, 1046-1051.

Temperature of Earth's core constrained from melting of Fe and $Fe_{0.9}Ni_{0.1}$ at high pressures

D. Zhang[1,2,3], J. M. Jackson[1], J. Zhao[2], W. Sturhahn[1], E. E. Alp[2], M. Y. Hu[2], T. S. Toellner[2], C. A. Murphy[1], and V. B. Prakapenka[4]

1. California Institute of Technology, 1200 E California Blvd, Pasadena, CA 91125
2. Advanced Photon Source, Argonne National Laboratory, 9700 S. Cass Ave, Argonne, IL 60439
3. University of Hawaii at Manoa, 1680 East-West Rd, Honolulu, HI 96822
4. GSECARS, University of Chicago, 9700 S. Cass Ave, Argonne, IL 60439

(COMPRES-related facilities: APS XSD 3-ID-B and GSECARS 13-ID-D)

The melting points of *fcc*- and *hcp*-structured $Fe_{0.9}Ni_{0.1}$ and Fe are measured up to 125 GPa using laser heated diamond anvil cells, synchrotron Mössbauer spectroscopy, and a recently developed fast temperature readout spectrometer. The onset of melting is detected by a characteristic drop in the time-integrated synchrotron Mössbauer signal which is sensitive to atomic motion. The thermal pressure experienced by the samples is constrained by X-ray diffraction measurements under high pressures and temperatures. The obtained best-fit melting curves of *fcc*-structured Fe and $Fe_{0.9}Ni_{0.1}$ fall within the wide region bounded by previous studies. We are able to derive the *fcc–hcp*–liquid triple point of Fe and the quasi triple point of $Fe_{0.9}Ni_{0.1}$. Using previously measured phonon density of states of *hcp*-Fe, we calculate melting curves of *hcp*-structured Fe and $Fe_{0.9}Ni_{0.1}$ using our (quasi) triple points as anchors. The extrapolated $Fe_{0.9}Ni_{0.1}$ melting curve provides an estimate for the upper bound of Earth's inner core–outer core boundary temperature. The temperature within the liquid outer core is then approximated with an adiabatic model, which constrains the upper bound of the temperature at the core side of the core–mantle boundary. We discuss a potential melting point depression caused by light elements and the implications of the presented core–mantle boundary temperature bounds on phase relations in the lowermost part of the mantle.

Reference: Zhang, D., J.M. Jackson, J. Zhao, W. Sturhahn, E.E. Alp, M.Y. Hu, T.S. Toellner, C.A. Murphy, and V.B. Prakapenka (2016): Temperature of Earth's core constrained from melting of Fe and $Fe_{0.9}Ni_{0.1}$ at high pressures. *Earth and Planetary Science Letters*, 447, 72-83.

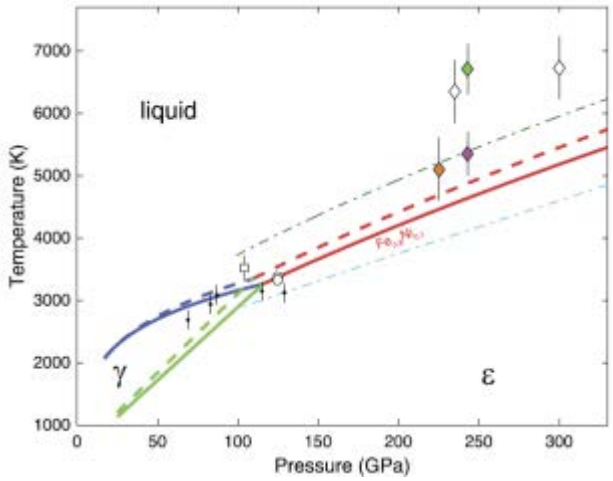

Fig 1: Phase boundaries of Fe and $Fe_{0.9}Ni_{0.1}$. Dashed curves and solid curves are for Fe and $Fe_{0.9}Ni_{0.1}$, respectively, where the *fcc–hcp* boundaries of Fe and $Fe_{0.9}Ni_{0.1}$ are adapted from Komabayashi et al., (2009, 2012).

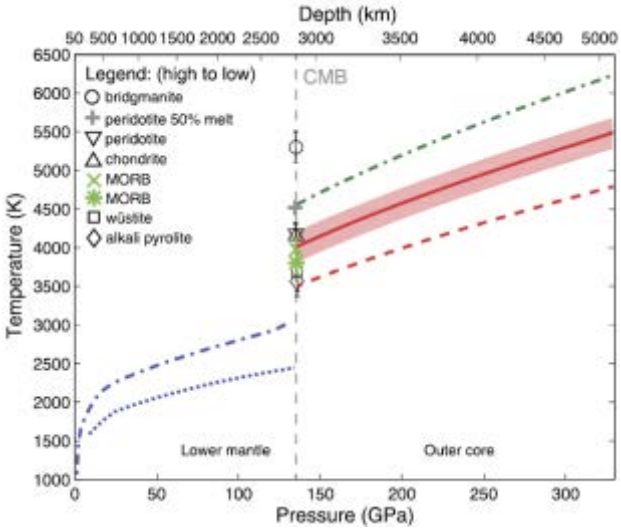

Fig 2: Proposed thermal profiles of Earth's interior and melting points of minerals. Red curves: adiabatic outer core temperature profile calculated from this study without (solid curve) and with light elements (dashed

Compression and structure of brucite to 31 GPa from synchrotron X-ray diffraction and infrared spectroscopy studies

Maining Ma[1,2], Wei Liu1, 1 Zhiqiang Chen,3 Zhenxian Liu,4 and Baosheng Li1,*
[1]Mineral Physics Institute, Stony Brook University, Stony Brook, New York 11794, U.S.A.
[2]Key Laboratory of Computational Geodynamics of Chinese Academy of Sciences, Graduate University of Chinese Academy of Sciences, Beijing 100049, China
[3]Department of Geosciences, Stony Brook University, Stony Brook, New York 11794, U.S.A.
[4]Geophysical Laboratory, Carnegie Institution of Washington, Washington, D.C. 20015, U.S.A.

(COMPRES-related facilities: National Synchrotron Light Source Beamline X17C, IR U2)

Synchrotron X‐ray powder diffraction and infrared (IR) spectroscopy studies on natural brucite were conducted up to 31 GPa using diamond-anvil cell (DAC) techniques at beamlines X17C and U2A of National Synchrotron Light Source (NSLS). The lattice parameters and unit-cell volumes were refined in P3m1 space group throughout the experimental pressure range. The anisotropy of lattice compression decreases with pressure due to a more compressible c axis and the compression becomes nearly isotropic in the pressure range of 10–25 GPa. The unit-cell volumes are fitted to the third-order Birch-Murnaghan equation of state, yielding K0 = 39.4(1.3) GPa, K0′ = 8.4(0.4) for the bulk modulus and its pressure-derivative, respectively. No phase transition or amorphization was resolved from the X‐ray diffraction data up to 29 GPa, however, starting from ~4 GPa, a new infrared vibration band (~3638 cm–1) 60 cm–1 below the OH stretching A2u band of brucite was found to coexist with the A2u band and its intensity continuously increases with pressure. The new OH stretching band has a more pronounced redshift as a function of pressure (–4.7 cm–1/GPa) than the A2u band (–0.7 cm–1/GPa). Comparison with first-principles calculations suggests that a structural change involving the disordered H sublattice is capable of reconciling the observations from X‐ray diffraction and infrared spectroscopy studies.

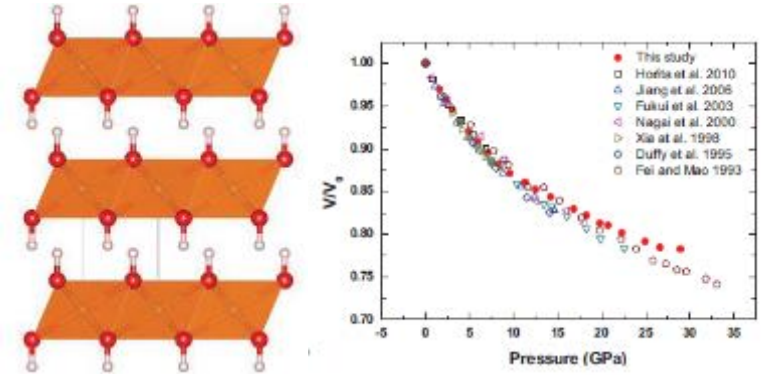

Fig. 1. (Left) Crystal structure of brucite and (right) compression curve of brucite and its comparison with previous studies.

Reference

Ma, M., W. Liu, Z. Chen, Z. Liu, B. Li (2013). Compression and Structure of brucite to 31 GPa from synchrotron X-ray diffraction and Infrared spectroscopy studies, *Am Min*, 98 33-40.

Dehydration Melting at the Top of the Lower Mantle

Brandon Schmandt[1], Steven D. Jacobsen[2], Thorsten W. Becker[3], Zhenxian Liu[4], and Kenneth G. Dueker[5]

[1]*Department of Earth and Planetary Science, University of New Mexico, Albuquerque NM, USA*
[2]*Department of Earth and Planetary Sciences, Northwestern University, Evanston IL, USA*
[3]*Department of Earth Sciences, University of Southern California, Los Angeles CA, USA*
[4]*Geophysical Laboratory, Carnegie Institution of Washington, Washington DC, USA*
[5]*Department of Geology and Geophysics, University of Wyoming, Laramie WY, USA*

The recent discovery of a hydrous ringwoodite inclusion in diamond (Pearson et al. 2014) indicates a partially hydrated mantle transition zone. To examine the potential for regional-scale hydration, we combined laboratory experiments and seismic observations to detect dehydration melting below 660 km in regions of downwelling beneath North America. The research involved a partnership between two NSF-COMPRES facilities (GSECARS/APS and U2A/NSLS) and the NSF-Earthscope, USArray. In lab experiments, hydrated ringwoodite was used to synthesize the bridgmanite plus ferropericlase assemblage, which routinely produced dehydration melt. In the seismic study, we generated over 100,000 receiver functions recorded by 2,244 stations to create a common conversion point (CCP) image of P-to-S converted phases in the depth range of 500-900 km. Negative amplitude Ps conversions (indicative of negative velocity gradients) were observed in regions where geodynamic models show downwelling across the 660-km discontinuity, a likely indicator of widespread hydration of the mantle transition zone.

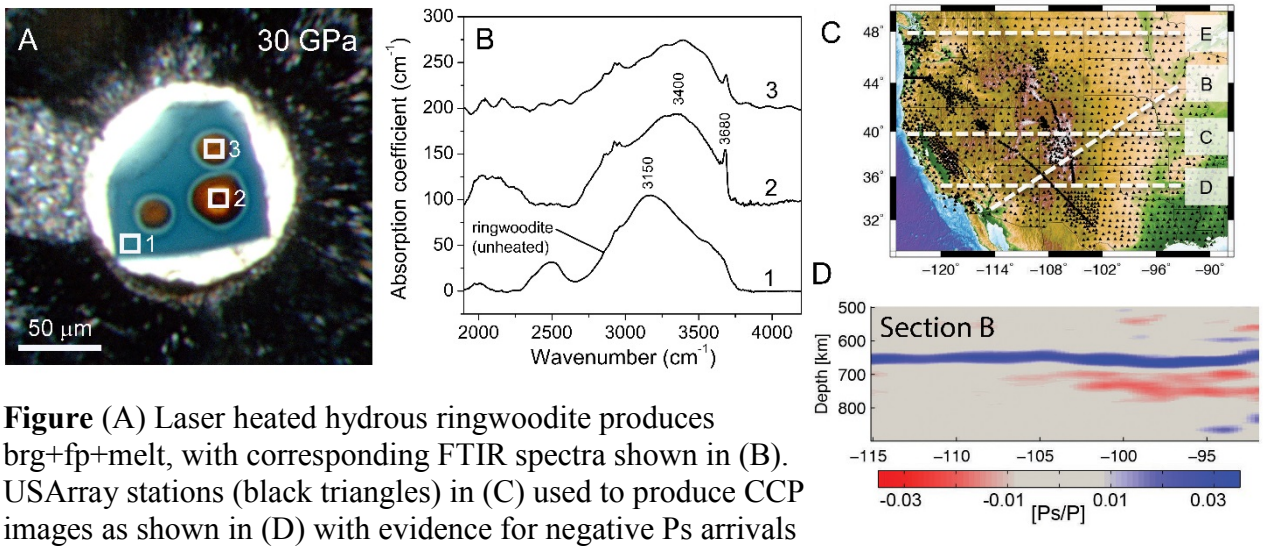

Figure (A) Laser heated hydrous ringwoodite produces brg+fp+melt, with corresponding FTIR spectra shown in (B). USArray stations (black triangles) in (C) used to produce CCP images as shown in (D) with evidence for negative Ps arrivals indicative of partial melting below 660 km.

Reference: Schmandt, B., S.D. Jacobsen, T.W. Becker, Z. Liu, and K.G. Dueker (2014) Dehydration melting at the top of the lower mantle. *Science* 344, 1265-1268.

Acknowledgements: This research was partially supported by COMPRES under NSF Cooperative Agreement EAR 11-57758, and by NSF EAR-0748707 to SDJ and EAR-1215720 to TWB. Facility support included: GSECARS (EAR-1128799, DOE DE-FG02-94ER14466); APS (DOE DE-AC02-06CH11357); U2A (COMPRES & NNSA DOE DE-FC-52-08NA28554, CDAC); NSLS (DOE DE-AC02-98CH10886); EarthScope USArray (NSF EAR-0733069, EAR-1261681, IRIS).

Evidence for H_2O-bearing fluids in the lower mantle from diamond inclusion

Mederic Palot[1], Steven Jacobsen[2], Joshua Townsend[2], Fabrizio Nestola[3], Katharina Marquardt[4], Nobuyoshi Miyajima[4], Jeffrey Harris[5], Thomas Stachel[1], Catherine McCammon[4], and Graham Pearson[1]

[1]*Department of Earth and Atmospheric Sciences, University of Alberta, Edmonton, Canada*
[2]*Department of Earth and Planetary Sciences, Northwestern University, Evanston IL, USA*
[3]*Dipartimento di Geoscienze, Università di Padova, 35131 Padua, Italy*
[4]*Bayerisches Geoinstitut, Universität Bayreuth, Bayreuth, Germany*
[5]*School of Geographical and Earth Sciences, University of Glasgow, Glasgow, United Kingdom*

We report the first direct evidence for water-bearing melt/fluid in the lower mantle from a natural ferropericlase (fp) crystal contained within a diamond from São Luíz, Brazil. The ferropericlase, ($Mg_{0.83}Fe_{0.17}O$), exhibits exsolution of magnesioferrite, which places the origin of the assemblage in the uppermost lower mantle. The presence of brucite–$Mg(OH)_2$ precipitates in the fp crystal reflects the later-stage quenching of an H_2O-bearing fluid film, previously trapped between the inclusion and diamond host cavity. Magnesioferrite exsolution occurs topotaxially in the ferropericlase, but also along pre-existing dislocations near the inclusion surface, indicating that exsolution occurred subsequent to ascent and applied stress on the inclusion surface from the diamond cavity. Quenching of the fluid, likely at transition zone conditions or shallower, resulted in the nano-precipitates of brucite. Dehydration melting may be one of the key processes involved in transporting water across the 660-km discontinuity, generating volatile-rich fluids and a diamond factory near the top of the lower mantle.

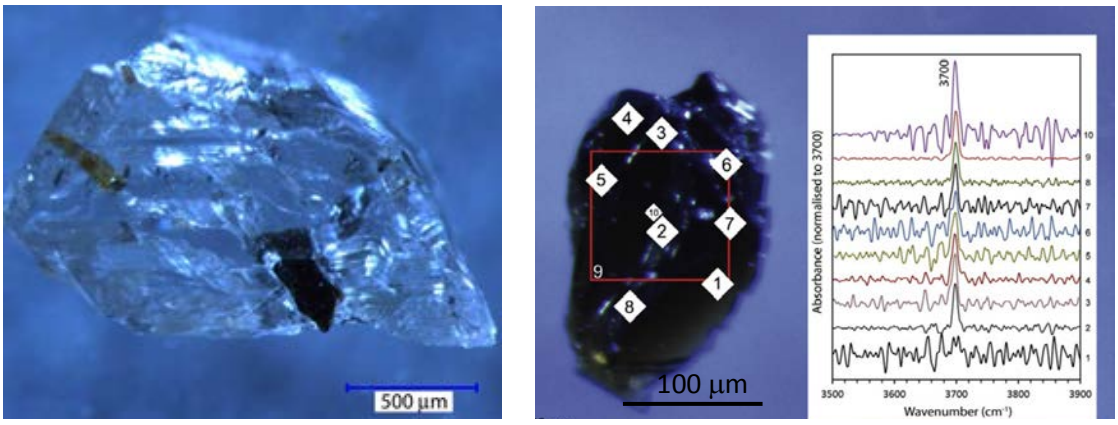

Figure: (*Left*) Fp included in a type-II diamond from Juina, Brazil. (*Right*) a fragment of the fp crystal shows signatures of nano-precipitates of brucite throughout, as evidenced by the ~3700 cm^{-1} O-H stretching mode. To achieve the high spatial resolution shown, we used synchrotron-IR spectroscopy at beamline U2A, National Synchrotron Light Source (NSLS). Each white box represents a 5-10 µm aperture for individually labeled spectra.

Reference: Palot, M., S.D. Jacobsen, J.P. Townsend, F. Nestola, K. Marquardt, N. Miyajima, J.W. Harris, T. Stachel, C.A. McCammon, and D.G. Pearson (2016). Evidence for H_2O-bearing fluids in the lower mantle from diamond inclusion. Lithos, *in press*, doi: 10.1016/j.lithos.2016.06.023.

Acknowledgements: This study utilized NSLS beamline U2A, which was partially supported by COMPRES (EAR 11-57758).

Synthesis of FeO_2 and the Fe-O-H system in the deep Earth

Qingyang Hu[1,4], Duck Young Kim[1,4], Wenge Yang[2,4], Liuxiang Yang[2,4], Yue Meng[3], Li Zhang[1,4], Ho-Kwang Mao[1,4]

1. Geophysical Laboratory, Carnegie Institution, Washington DC 20015, USA
2. High Pressure Synergetic Consortium (HPSynC), Geophysical Laboratory, Carnegie Institution, Argonne, Illinois 60439, USA
3. High Pressure Collaborative Access Team (HPCAT), Geophysical Laboratory, Carnegie Institution, Argonne, Illinois 60439, USA
4. Center for High Pressure Science and Technology Advanced Research (HPSTAR), Shanghai 201203, China

(COMPRES-related facilities: Partnership for Extreme Crystallography)

The Earth's geochemistry can be regarded as a ternary system of oxygen, its most abundant element by atomic fraction, iron, its major redox ingredient, and hydrogen, its most mobile element responsible for electron transfer. The oxygen rich atmosphere and iron rich earth core represent the two end members of the O-Fe system, overlapping the entire pressure-temperature (*P-T*) range of the planet. We explored the chemical reaction in the system of Fe-O-H at high-pressure and high-temperature that mimics deep lower mantle (DLM) conditions. When haematite is compressed in O_2 and heated above 76 GPa and 1800 K, a new FeO_2 phase is identified through X-ray diffraction conducted at synchrotron beamlines, including the Partnership for Extreme Crystallography at Advanced Photon Source, Argonne National Laboratory. The spotty FeO_2 diffraction pattern was solved by the so-called multigrain crystallographic method. The newly discovered FeO_2 phase holds an excessive amount of oxygen and has the same atomic structure as FeS_2. We went on to show that the mineral goethite (FeOOH) can also decompose to FeO_2 at 92 GPa and 2050 K by releasing hydrogen. In DLM situation, the hydrogen released from FeOOH would diffuse, infiltrate or react to form hydrocarbon or other volatiles. At the same time, FeO_2 patches are left in DLM and cumulate through plate tectonics. Such process provides an alternative interpretation to the origin of seismic and many geochemical signatures in the DLM.

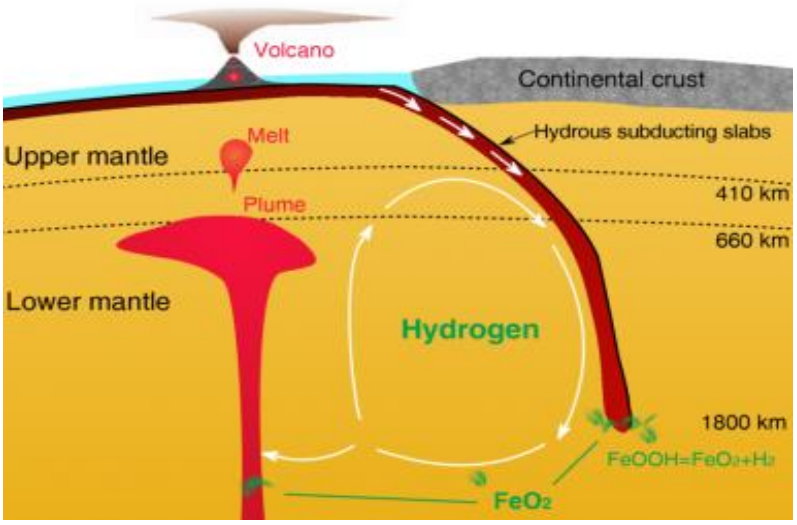

Figure 1: Hydrogen and oxygen cycles in the lower mantle.

Reference: Q. Hu, *et al.* FeO_2 and FeOOH under deep lower-mantle conditions and Earth's oxygen–hydrogen cycles. *Nature*, **531**, 241-244 (2016).

Structural and spectroscopic studies of alkali-metal exchanged Stilbites

Yanmei Ma, Zhenxian Liu, Aihui Geng, Thomas Vogt , Yongjae Lee

(COMPRES-related facilities: U2A beamline of the National Synchrotron Light Source (NSLS-1))

Synchrotron IR spectra were obtained at U2A beamline of the National Synchrotron Light Source (NSLS-1) at Brookhaven National Laboratory (BNL). To avoid possible saturated absorption, pure sample powders were placed between two diamond anvils and compressed to a thin film before measurements. The far-IR spectra were collected using a Bruker IFS 66v/S FTIR spectrometer in combination with a custom-made vacuum microscope system equipped with a liquid helium cooled bolometer detector (Infrared Laboratories) and a 3.5 mm thick Mylar beam splitter. More details on the optical layout of the beamline have been described elsewhere. The mid-IR spectra were collected in transmission mode with a Bruker Vertex 80v FTIR spectrometer and a Hyperion 2000 IR microscope with a nitrogen-cooled MCT detector at the U2A side station. The spectra were collected in the range of 100-700 cm^{-1} for the far-IR and 600-4500 cm^{-1} for the mid-IR. A spectral resolution of 4 cm^{-1} was applied to all IR measurements.

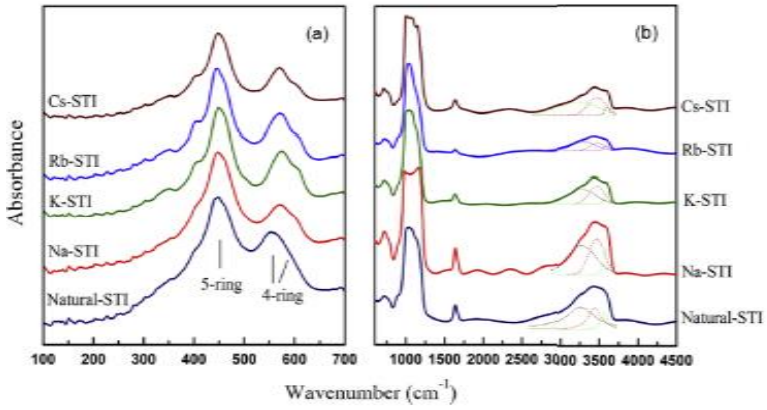

Fig. 1. (a) The far-IR spectra in the range of 100-700 cm^{-1} and (b) the mid-IR spectra in the range of 600-4500 cm^{-1} of the hydrated alkali-metal exchanged and natural stilbite at ambient conditions. The dotted curves in the right panel are the Lorentzian peak-fitting to the broad O-H stretching vibrational bands.

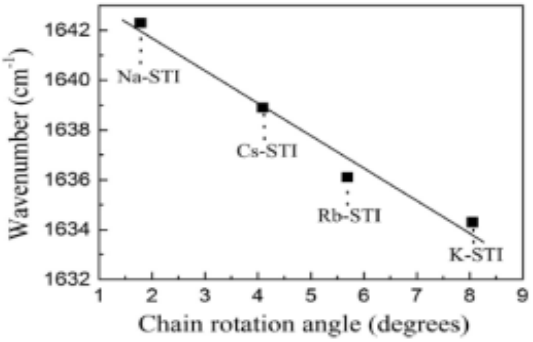

Fig. 2. Frequency dependency of the IR H-O-H bending mode on the chain rotation angle α. The straight line is drawn only as a guide. We observe a gradual increase in the frequency of the H-O-H bending band from 1634 to1642 cm^{-1} with increasing chain rotation angle α for the M-STI series (M = Na, Rb, Cs, K)

References: Z. Liu, J. Hu, H.K. Mao, R.J. Hemley, (2002), High-pressure synchrotron x-ray diffraction and infrared microspectroscopy: applications to dense hydrous phases. J. Phys. Condens. Matter **14**, pp.10641-10646.

The high-pressure behavior of micas: Vibrational spectra of muscovite, biotite, and phlogopite to 30 GPa

Q. Williams, E. Knittle (UCSC), H.P. Scott (Indiana U. SB), Z.X. Liu (Geophysical Lab, CIW)

(COMPRES-related facility: NSLS-U2A)

The infrared spectra of natural samples of muscovite, biotite and phlogopite were characterized to pressures of ~30 GPa, as is the Raman spectrum of muscovite to ~8 GPa. Both far-infrared and mid-infrared data are collected for muscovite, and mid-infrared data for biotite and phlogopite. The response of the hydroxyl vibrations to compression differs markedly between the dioctahedral and trioctahedral micas: the hydrogen bonding in dioctahedral environments increases with pressure, as manifested by negative shifts of the hydroxyl stretching vibrations, while cation-hydrogen repulsion likely produces positive mode shifts of the hydroxyl vibrations within trioctahedral environments. An abrupt decrease in frequency and increase in band-width of the hydroxyl stretching vibration in muscovite is observed at pressures above ~18-20 GPa, implying that the previously documented pressure-induced disordering is associated with the local environment and shifts in location of the hydroxyl unit in this material. The far-infrared vibrations of muscovite indicate that the compressional mechanism of this material shifts above 5-8 GPa, as the K-O stretching vibration with a zero-pressure frequency near 112 cm^{-1} shifts in its pressure dependence from 6.9 cm^{-1}/GPa below this pressure range to 0.78 cm^{-1}/GPa above it. Hence, there appears to be a transition from a dominance of interlayer compaction to more of a mixture of interlayer and intralayer compaction in the compressional behavior of this material. The mid-infrared bands that are primarily produced by vibrations of the tetrahedral layer broaden under pressure in both muscovite and biotite: within biotite, a spectral region that may be associated with higher coordination of tetrahedral cations increases in amplitude above about 25 GPa. The corresponding bands in phlogopite undergo less broadening, and their behavior is fully reversible on decompression.

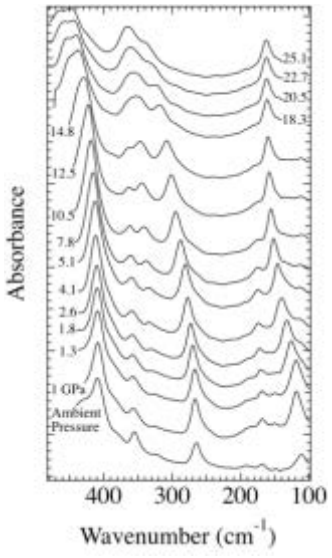

Figure 1. Far-infrared spectrum of $K_{0.92}Na_{0.08}Al_3Si_3O_{10}(OH)_2$ muscovite mica to 25 GPa. Note that the peaks at 325 and 355 cm^{-1} at ambient pressure coalesce between 15 and 18 GPa. The combination of this coalescence and the concomitant splitting of the 408 cm^{-1} band (each of which are consistent with a shift in symmetry and/or bonding environments) indicate that there is a structural change in muscovite near this pressure. This change is consistent with a disordering of the hydrogen environment near this pressure, a result supported by both our mid-IR spectra and consistent with past x-ray diffraction data.

Reference: Q. Williams, E. Knittle, H.P. Scott and Z.X. Liu, The high-pressure behavior of micas: Vibrational spectra of muscovite, biotite and phlogopite to 30 GPa, *American Mineralogist, 97,* 241-252, 2012.

Hydrous ringwoodite to 5 K and 35 GPa: Multiple hydrogen bonding sites resolved with FTIR spectroscopy

Panero, W. R., J. R. Smyth, J. S. Pigott, Z. Liu, and D. J. Frost, *American Mineralogist* 98, no. 4, 637-642, 2013.

Multiple substitution mechanisms for hydrogen in γ-$(Mg,Fe)_2SiO_4$, ringwoodite, lead to broad, overlapping and difficult-to-interpret FTIR spectra. Through combined low-temperature, high-pressure synchrotron-based FTIR spectroscopy, the multiple bonding sites become evident, and can be traced as a function of temperature and compression. Multiple OH stretching bands can be resolved in iron-bearing and iron-free samples with 0.79-2.5(3) wt% H_2O below 200 K at ambient pressure, with cooling to 5K at 35 GPa and 23 GPa resulting in the resolution of possibly as many as 5 OH stretching bands traceable at room temperature from 23 GPa down to 8 GPa. A distribution of defect mechanisms between $V_{Mg}''+2(H^{\bullet})$ at 3100 cm^{-1}, 3270 cm^{-1}, and possibly 2654 cm^{-1}, $V_{Si}''''+4(H^{\bullet})$ at 3640 cm^{-1}, and $Mg_{Si}''+2(H^{\bullet})$ at 2800 cm^{-1} can then be resolved. These multiple defect mechanisms can therefore explain the higher electrical and proton conductivity in ringwoodite when compared to wadsleyite, and therefore may be applied to resolve spatial variations in water storage in the Earth's transition zone.

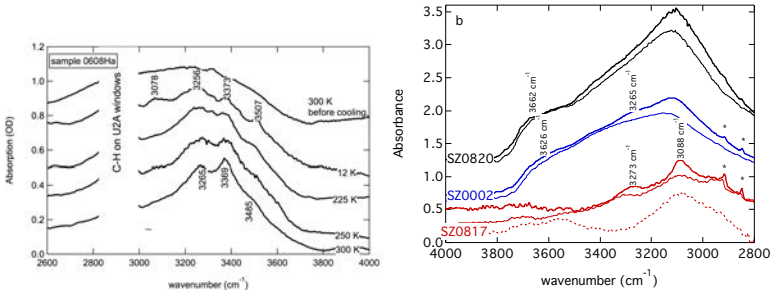

Left. OH absorption of sample SZ0817 with decreasing temperature on first cooling cycle showing the development of a new peak at ~3260 cm^{-1} as the 3100 cm^{-1} peak narrows with cooling. The process is reproducible with a second cooling cycle. Stars (*) indicate residual Loctite on the sample as well as C-H on the synchrotron mirrors. Curves are offset vertically for clarity. **Right**. Spectra of each sample (SZ0820, black, SZ0002, blue, SZ0817 red) normalized to 100 μm thickness for the X-OH bending region (a) and OH stretching (b). Curves are shifted vertically for clarity. Labels reflect the frequencies at low temperature (thick lines) with no significant shift observed at room temperature (thin lines) before (dashed) and after temperature cycling (solid). Sample 817 demonstrates narrowing and splitting of peaks upon cooling, without significant additional peaks. Stars (*) indicate residual Loctite on the sample as well as C-H on the synchrotron mirrors.

Infrared spectroscopy was carried out at the National Synchrotron Light Source (NSLS) beamline U2A using the low-temperature cryostat purchased through COMPRES infrastructure development made possible by COMPRES, the Consortium for Materials Properties Research in Earth Sciences under NSF Cooperative Agreement EAR 11-57758.

Dry $(Mg,Fe)SiO_3$ perovskite in the Earth's lower mantle

W. R. Panero, J. S. Pigott, D. M. Reaman, J. E. Kabbes, Z. Liu, *JGR, 120(2)*, 894-908, 2015.

Combined synthesis experiments and first-principles calculations show that $MgSiO_3$-perovskite with minor Al or Fe does not incorporate significant OH under lower mantle conditions. Perovskite, stishovite, and residual melt were synthesized from natural enstatite samples (Mg/(Fe+Mg) = 0.89 and 0.93; Al_2O_3 < 0.1 wt% with 35 and 2065 ppm wt H_2O, respectively) in the diamond anvil cell at 1600-2000 K and 25-65 GPa. Combined Fourier transform infrared (FTIR) spectroscopy, x-ray diffraction, and *ex-situ* transmission electron microscopy (TEM) analysis demonstrates little difference in the resulting perovskite as a function of initial water content. Four OH vibrational stretching bands are evident upon cooling below 100 K, suggesting 4 bonding sites for OH in perovskite with a maximum water content of 220 ppm wt H_2O, and likely no more than 10 ppm wt H_2O. Complementary, Fe-free, first-principles calculations predict multiple potential bonding sites for hydrogen in perovskite, each with significant solution enthalpy (0.2 eV/defect). We calculate that perovskite can dissolve less than 37 ppm wt H_2O (400 ppm H/Si) at the top of the lower mantle, decreasing to 31 ppm wt H_2O (340 ppm H/Si) at 125 GPa and 3000 K in the absence of a melt or fluid phase. We propose that these results resolve a long-standing debate of the perovskite melting curve and explain the order of magnitude increase in viscosity from upper to lower mantle.

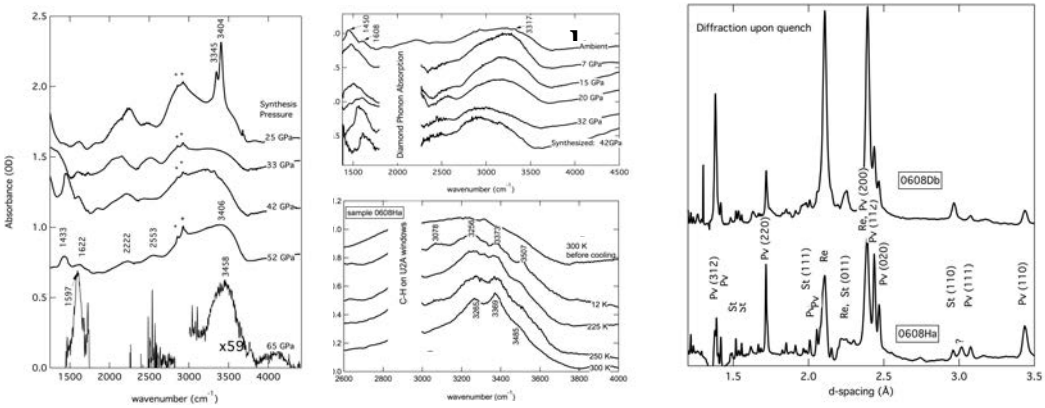

Left: Quench FTIR spectra of perovskite synthesized from enstatite with 2065 ppm wt H_2O as a function of synthesis pressure. The lower curve is the spectrum of a sample with 35 ppm wt H_2O vertically expanded by a factor of 59. **Middle, top** Decompression of the hydrous sample laser heated at 42 GPa to ambient pressure. **Middle, bottom** FTIR of the hydrous sample cooled to 12 K after synthesis and recovery. Four peaks become evident below 100 K and three are retained upon returning to 300 K. **Right**: XRD patterns of a hydrous sample (bottom) and dry sample (top) quenched to ambient pressure.

The *in-situ* X-ray diffraction experiments were carried out at the X-17C beamline of the National Synchrotron Light Source (NSLS), and infrared spectroscopy was carried out at NSLS U2A using the low-temperature cryostat purchased through COMPRES infrastructure development made possible by COMPRES, the Consortium for Materials Properties Research in Earth Sciences under NSF Cooperative Agreement EAR 11-57758.

Smyth Group University of Colorado, Boulder

Joe Smyth's group at University of Colorado has been studying hydration and water storage in planetary interiors by doing mineral synthesis at high pressure in collaboration with colleagues at University of Bayreuth (Germany) and characterizing the phases by single-crystal X-ray diffraction and Raman and FTIR spectroscopy in their laboratory at CU Boulder. The group also collaborates with other groups on secondary ion mass spectroscopy (SIMS) and University of Hawaii and Brillouin spectroscopy at UT Austin, Raman spectroscopy at Northwestern University. We provide well characterized oriented samples of hydrous high-pressure phases. We have found up to 3000 ppm H_2O in Al-bearing bridgmanite. We have explored the crystal chemistry of cation ordering in wadsleyite by synthesizing samples with 1-3wt% NiO, CoO, ZnO, V_2O_3, Cr_2O_3, and TiO_2. We found that transition metal cation ordering in wadsleyite is controlled by crystal field effects, rather than by cation radius (Zhang et al, 2016). Using COMPRES supported IR beam line at NSLS we identified several different proton sites in hydrous ringwoodite (Panero et al., 2013). At GSECARS we measured compression of akimotoite (Ye et al 2013), wadsleyite, ringwoodite (Chang et al., 2015), and chondrodite (Ye et al, 2015). A complete list of publications is here (http://ruby.colorado.edu/~smyth/Research/Papers/Papers.html), and a list of recent publications using COMPRES facilities is listed below.

1. Chang, Y.-Y., S.D. Jacobsen, C. R. Bina, S.-M. Thomas, J.R. Smyth, D.J. Frost. T. Boffa-Ballaran, C.A. McCammon, E.H. Hauri, T. Inoue, Y. Meng, P. Dera (2015) Comparative compressibility of wadsleyite and ringwoodite: Effect of H_2O on dK/dP and implications for detecting water in the transition zone. *Journal of Geophysical Research.* DOI 10.1002/2015JB012123.
2. Ye, Y., Jacobsen, S.D., Mao, Z. Duffy, T.S., Hirner S.M., Smyth, J.R. (2015) Crystal structure, thermal expansivity and elasticity of OH-chondrodite: Trends among dense hydrous magnesium silicates. *Contributions to Mineralogy and Petrology* 169, 43. DOI 10.1007/s00410-015-1138-3.
3. Panero, W. R., J. R. Smyth, J.S. Pigott, Z. Liu, and D.J. Frost (2013) Hydrous ringwoodite to 5K and 35 GPa: Multiple H bonding sites resolved with FTIR spectroscopy. American Mineralogist 98, 637-642.
4. Ye, Y., J.R. Smyth, T. Katsura, S.D. Jacobsen, P. Dera, D.A. Brown, C. Goujon (2013) Crystal structure, equation of state, and Raman and IR spectroscopy of akimotoite (ilmenite-type $MgSiO_3$). *Contributions to Mineralogy and Petrology* 165, 563-574.

In-situ infrared spectroscopic studies of hydroxyl in amphiboles at high pressure

Elizabeth C. Thompson[1*], Andrew J. Campbell[1], and Zhenxian Liu[2],
[1]Department of the Geophysical Sciences, University of Chicago, U.S.A.
[2]Geophysical Laboratory, Carnegie Institution of Washington, U.S.A.

(COMPRES-related facilities: NSLS U2A, COMPRES gas-loading system at GSECARS)

In this study, twelve natural amphibole samples spanning a range of ten compositions were probed with synchrotron infrared spectroscopy at room temperature and pressures up to 60 GPa. Infrared spectra were collected at atmospheric pressure and at regular intervals during compression, allowing for the collection of spectra centered on the typical O-H stretching region at 3600–3700 cm^{-1} as they evolved with pressure for each composition. The number of O-H bands within each sample was found to vary with composition, but the pressure dependence of O-H frequency shifting more closely correlated with mode frequency at ambient pressure than with composition. Combined with earlier results, these data reveal a linear relationship between mode frequency at ambient pressure and pressure dependence of O-H stretching modes in amphiboles and sheet silicates.

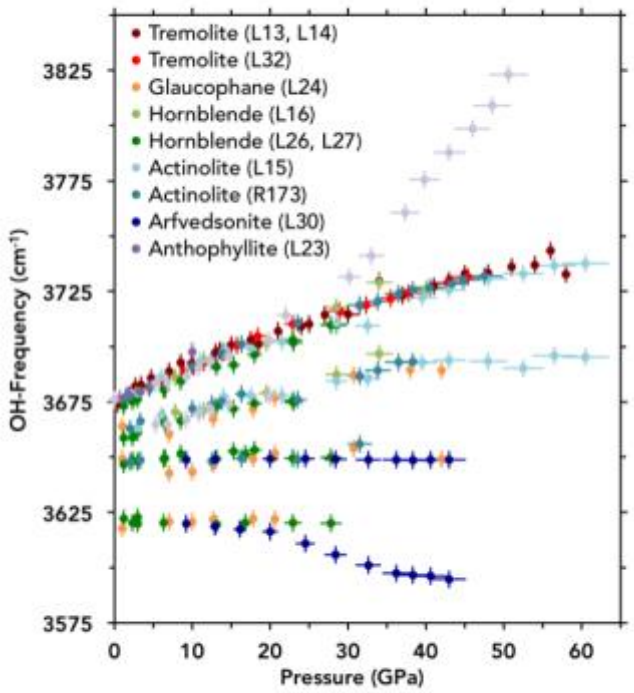

Two sample preparation methods utilized in this study allowed for direct comparison between quasi-hydrostatic neon-loaded sample conditions and the conditions achieved with a KBr pressure medium. Samples loaded in neon preserved sharper peaks, allowing greater spectral resolution, especially at higher pressures when peaks are most likely to broaden or disappear due to crystalline disorder and pressure gradients across the sample. This new quasi-hydrostatic loading method proved valuable to tracing O-H stretching behaviour in amphiboles to higher pressures than previously obtained and will lend itself to future study of O-H stretching pressure dependence in a wide range of hydrous minerals.

Figure 1. High pressure, room temperature measurements of O-H frequencies within each sample composition in this study. Circles: individual peak positions. Different symbol colours are used for different compositions, and sample numbers appear in parenthesis. Error bars represent 1σ uncertainties both in frequency and in pressure.

References:

Thompson E.C., Campbell A.J., and Liu Z. (2016) In-situ infrared spectra of hydroxyl in amphiboles at high pressure. *American Mineralogist*. **101**, 706-712.

In-situ synchrotron infrared spectroscopic studies of hydroxyl in mantle phases at high pressure

Elizabeth C. Thompson[1*], Zhenxian Liu[2], Mary M. Reagan[3], and Andrew J. Campbell[1]
[1]Department of the Geophysical Sciences, University of Chicago, U.S.A.
[2]Geophysical Laboratory, Carnegie Institution of Washington, U.S.A.
[3]Department of the Geological Sciences, Stanford University, U.S.A.

(COMPRES-related facilities: ALS 1.4.3, COMPRES gas-loading system at GSECARS)

Combining in situ infrared spectroscopy with the high pressure generated by diamond anvil cells allows for the direct detection of the O-H bond stretching frequency within a hydrogen bond (O-H…O) as it changes with pressure. In this study, room temperature infrared spectra of both natural and synthetic hydrous phases were collected at 1 bar and at pressure intervals up to 65 GPa, allowing a detailed assessment of the evolution of hydroxyl band frequencies as a function of pressure. Combining this new high-resolution infrared data, in conjunction with the findings of previous high-pressure studies, reveals systematics in the pressure dependence of hydroxyl bands in various mineral phases. For example, within the amphibole group the starting 1-bar hydroxyl band frequency linearly correlates with the hydroxyl pressure-dependence, while composition plays a secondary role. By examining a wider suite of hydrous minerals it is possible to better understand the complex interplay between local hydroxyl bonding environment, initial hydrogen bond frequency, pressure, and OH-band pressure-evolution, augmenting ab initio computational predictions concerning hydrogen bond symmetrization in a range of hydrous deep Earth phases. These systematics reveal which O-H modes tend toward symmetrization or not, and can also be used to predict changes in D/H partitioning behavior at high pressures.

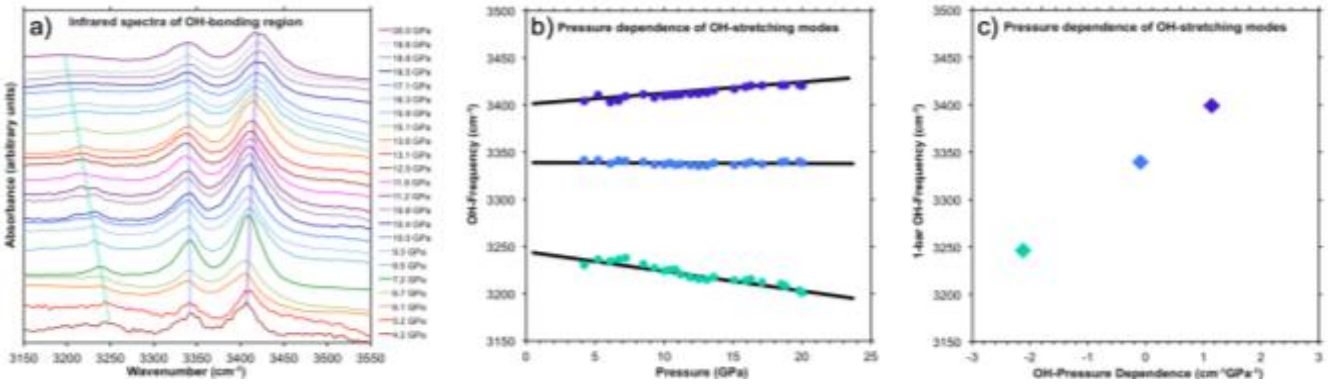

Figure 1. Representative high-pressure infrared data for hydrous minerals. This example is phase D [$MgSi_2O_4(OH)_2$]. **(a)** Room temperature spectra are collected at regular pressure intervals to determine peak positions as a function of pressure. **(b)** In the absence of symmetry transitions, OH-frequencies often trend linearly with pressure. **(c)** Plotting these slopes against initial frequency allows us to determine broader pressure dependence trends in groups of minerals with similar OH-bonding environments.

References: Thompson *et al.* (unpublished)

Compressibility and thermal expansion of hydrous ringwoodite with 2.5(3) wt% H_2O

Ye, Y., D. A. Brown, J. R. Smyth, W. R. Panero, S. D. Jacobsen, Y.-Y. Chang, J. P. Townsend, S. M. Thomas, E. H. Hauri, P. Dera, D. J. Frost, *Am Min*, 97, 573-582, 2012.

Ringwoodite (γ-Mg_2SiO_4) is the cubic spinel polymorph of olivine stable in the lower transition zone at depths of 525-660 km. It can incorporate percent levels of H_2O as hydroxyl charge compensated by cation vacancies at Mg and possibly also at Si sites. We have synthesized pure Mg ringwoodite with about 2.6 % H_2O by weight and measured compressibility at ambient temperature by both single-crystal and powder X-ray diffraction and thermal expansion at ambient pressure**.** Third-order B-M EOS gives values of K_{T0} = 159(7) GPa, K' = 6.7(7) for single-crystal XRD; K_{T0} = 161(4) GPa, K' = 5.4(6) for powder XRD; with K_{T0} = 160(2) GPa, K' = 6.2(3) for the combined data sets. This is consistent with hydration in silicates in transition zone causing a decrease in bulk modulus and seismic velocities, but an increase in K', causing larger velocity at higher pressure. Unlike hydrous wadsleyite, hydrous ringwoodite has been observed to break down by an irreversible unit cell expansion above 586 K at ambient pressure that may be related to the hydration mechanism. In order to better understand this phenomenon, single crystal intensity scans were conducted at various temperatures up to 736 K in our lab. Based on the experimental data and previous work of ^{29}Si NMR study, we speculate that during the irreversible expansion, a small mount of H^+ cations in Mg sites could transfer to Si sites without changing the cubic spinel structure of ringwoodite, and the substituted Si^{4+} cations might move to the normally vacant octahedral site at (½ , ½, 0).

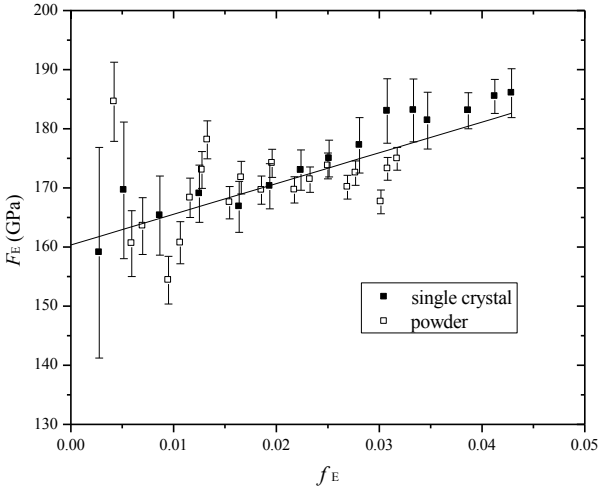

Birch normalized pressure (F_E) vs. Euler finite strain (f_E) plots with vertical error bars for the uncertainties of F_E. For f_E > 0.02 (P > 11 GPa), the plotted points for single-crystal are systematically and significantly above the fitting line, while the points for powder are below the fitting line, because of larger K' for single-crystal.

Samples for X-ray diffraction experiments loaded in neon using the Consortium for Materials Properties Research in Earth Sciences (COMPRES) gas loading system, under NSF Cooperative Agreement EAR 11-57758.

Crystal structure, Raman and FTIR spectroscopy, and equations of state of OH-bearing $MgSiO_3$ akimotoite

Ye, Y., J. Smyth, S. Jacobsen, W. Panero, D. Brown, T. Katsura, Y-Y Chang, J. Townsend, P. Dera, S. Tkachev, C. Unterborn, Z. Liu, C. Goujon, *Contrib. Min. Pet.* 166 , 2013.

Ilmentite-type $MgSiO_3$ (akimotoite) is stabilized relative to majorite-garnet under lower temperature geotherms within steeply subducting slabs. Two compositions of Mg-akimotoite were synthesized under similar conditions; one sample contains about 550 ppm wt. H_2O and was synthesized at 22 GPa and 1500ºC, and the other was synthesized at 22GPa and 1250ºC and is nominally anhydrous. Crystal structures of the two samples were refined from single-crystal X-ray diffraction with nearly identical results within error. Thermal expansivity at ambient pressure, and compressibility at ambient temperature are measured by single crystal X-ray diffraction. The anisotropies of axial thermal expansion and compressibility are similar for this sample. Akimotoite is 28% stiffer in the *a* direction than the *c* direction, and the *c*/*a* ratio increases with increased temperature and decreases with increased pressure. Hydration of akimotoite may increase both the bulk thermal expansivity and compressibility, and decrease the anisotropies of both axial thermal expansivity and compressibility. Complementary Raman and FTIR spectroscopy show multiple structural hydration sites. Low-temperature and high-pressure FTIR spectroscopy (15-300 K and 0-25 GPa) confirm that the multiple sites are structurally unique, with zero-pressure intrinsic anharmonic mode parameters between $-1.02(12)\times10^{-5}$ and $+1.7\times10^{-5}$ K^{-1}, indicating both weak OH..O bonding as well as strong OH bonding due to long O-O distances.

Left: Fractional unit-cell parameters versus temperature for the hydrous (solid symbols) and Ashida et al. (1988) (open symbols). **Right**: Zero-pressure, low-temperature FTIR spectra of the same sample.

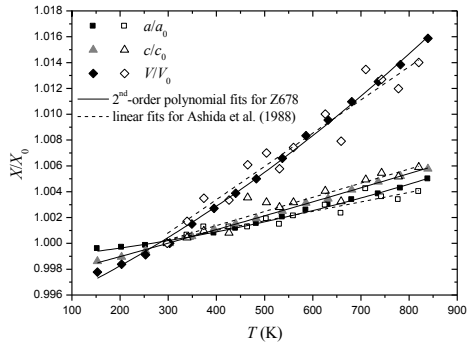

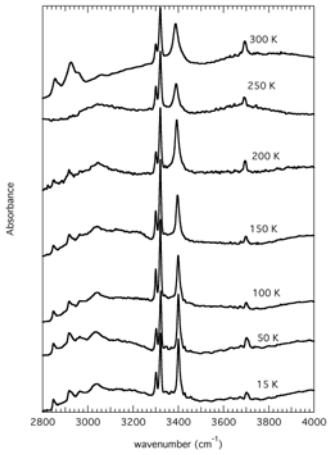

Samples for X-ray diffraction experiments loaded in neon using the Consortium for Materials Properties Research in Earth Sciences (COMPRES) gas loading system, under NSF Cooperative Agreement EAR 11-57758. Infrared spectroscopy was carried out at COMPRES-supported beamline NSLS U2A using the low-temperature cryostat purchased through COMPRES infrastructure development made possible by COMPRES.

High-pressure elastic behavior of $Ca_4La_6(SiO_4)_6(OH)_2$ a synthetic rare-earth silicate apatite: A powder X-ray diffraction study up to 9.33 GPa

Dawei Fan[1], Shuyi Wei[1], Maining Ma[2], Zhiqiang Chen[3], Baosheng Li[3], Hongsen Xie[1]
[1]Laboratory for High Temperature and High Pressure Study of the Earth's Interior, CAS, Guiyang, China
[2]Key Laboratory of Computational Geodynamics, CAS, Beijing, China
[3]Mineral Physics Institute, Stony Brook University, USA

(COMPRES-related facilities: National Synchrotron Light Source Beamline X17C)

The compression behavior of a synthetic $Ca_4La_6(SiO_4)_6(OH)_2$ has been investigated to about 9.33 GPa at 300 K using in situ angle-dispersive X-ray diffraction and a diamond anvil cell. No phase transition has been observed within the pressure range investigated. The values of zero pressure volume V0, K0, and K 0 0 refined with a third-order Birch–Murnaghan equation of state are V_0 = 579.2 ± 0.1 A^3, K_0 = 89 ± 2 GPa, and K_0' =10.9(0.8). If K_0' is fixed at 4, K_0 is obtained as 110 ± 2 GPa. Analysis of axial compressible modulus shows that the a-axis (K_{a0} = 79 ± 2 GPa) is more compressible than the c-axis (K_{c0} = 121 ± 7 GPa). A comparison between the high-pressure elastic response of $Ca_4La_6(SiO_4)_6(OH)_2$ and the iso-structural calcium apatites is made. The possible reasons of the different elastic behavior between $Ca_4La_6(SiO_4)_6(OH)_2$ and calcium apatites are discussed.

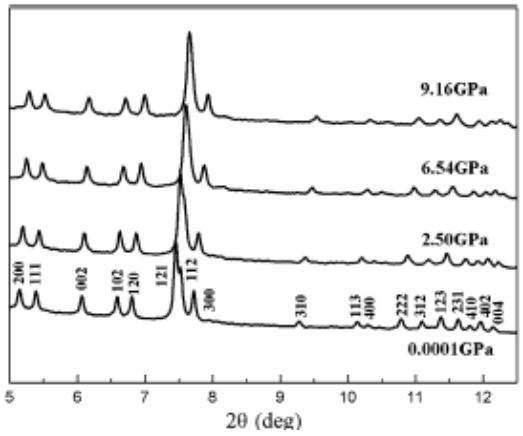

Fig. 1. Evolution of the X-ray diffraction pattern as a function of pressure to 9.33 GPa.

Reference

Fan, D., S. Wei, M. Ma, Z. Chen, B. Li, and H. Xie (2013) High-pressure elastic behavior of $Ca_4La_6(SiO_4)_6(OH)_2$ a synthetic rare-earth silicate apatite: a powder X-ray diffraction study up to 9.33 GPa, Phy. Chem. Min., DOI 10.1007/s00269-013-0626-0

In-situ synchrotron X-ray diffraction study of scorodite at high pressure

Dawei Fan[1], Maining Ma[2], Shuyi Wei[1], Baosheng Li[3], Zhiqiang Chen[3], Hongsen Xie[1]
[1]Laboratory for High Temperature and High Pressure Study of the Earth's Interior, CAS, Guiyang, China
[2]Key Laboratory of Computational Geodynamics, CAS, Beijing, China
[3]Mineral Physics Institute, Stony Brook University, USA

(COMPRES-related facilities: National Synchrotron Light Source Beamline X17C)

The compression behavior of a natural scorodite has been investigated to about 8.21 GPa at 300 K for the fist time using in situ angle-dispersive X-ray diffraction and a diamond anvil cell at beamline X17C, National Synchrotron Light Source, Brookhaven National Laboratory. Over this pressure range, no phase change or disproportionation has been observed. The isothermal equation of state was determined for the first time. The values of V0, K0, and K′ 0 refined with a third-order Birch-Murnaghan equation of state are V_0 = 934.2 ± 0.3 Å^3, K_0 = 61.8 ± 2.5 GPa, and K_0' = 6.6 ± 0.9. Furthermore, we confirm that the linear compressibilities (β) along a, b and c directions of scorodite is elastically anisotropic..

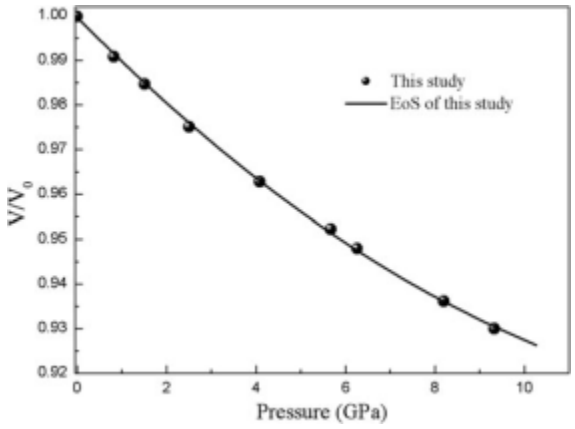

Fig. 1. Compression curve at 300K from this study.

Reference

Fan, D. W., Ma, M. N., Wei, S. Y., Li, B. S., Chen, Z. Q., Xie, H. S.(2013) In-situ synchrotron X-ray diffraction study of scorodite at high pressure, High Temperatures-High Pressures, 42, 203-209

P-V-T equation of state and high-pressure behavior of CaCO3 aragonite

Ying Li[1,2], Yongtao Zou[1], Ting Chen[3], Xuebing Wang[3], Xintong Qi[3], Haiyan Chen[1], Jianguo Du[2] and Baosheng Li[1]
[1]Mineral Physics Institute, Stony Brook University, U.S.A.
[2]Institute of Earthquake Science, China Earthquake Administration, China
[3]Department of Geosciences, Stony Brook University, Stony Brook, U.S.A.

(COMPRES-related facilities: National Synchrotron Light Source beamline X17B2)

The equation of state of aragonite was determined by in situ synchrotron X‐ray diffraction experiments on a hot-pressed polycrystalline specimen of aragonite within its stability field up to 5.8 GPa and 1173 K. As a complement to this experimental study, first-principle density functional theory calculations were performed up to 20 GPa at 0 K. Thermoelastic parameters for aragonite ($CaCO_3$) were derived by a least-squares fit of the experimental P-V-T data to the third-order Birch-Murnaghan equation of state (EOS), yielding the bulk modulus and its pressure and temperature derivatives K_0 = 65.24 ± 0.24 GPa, K'_0 = 4.95 ± 0.12, $(\partial K_T/\partial T)P$ = –0.024 ± 0.002 GPa/K and volume thermal expansion a300 = (6.1 ± 0.7) × 10-5 K-1. The analyses of the axial compressibility at ambient temperature show that the c-axis is much more compressible than the a- and b-axes. Based on first-principle calculations, the anisotropic compression behavior of aragonite structure is explained by the heterogeneous shortening of <Ca-O> and <C-O> bond lengths and the rotation of <O-C-O> angles along the a-, b-, and c-axes, whereas the unit-cell volume change of aragonite under compression is accommodated by comparable compression rate of the CaO_9 polyhedra and the voids in the crystal lattice. The results attained from this study provide important thermoelastic parameters for understanding the thermodynamic behavior and chemical reactions involving aragonite at subduction zone conditions.

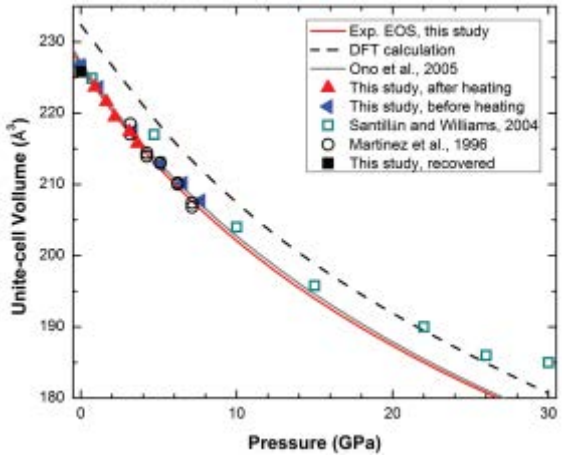

Fig. 1. *P-V* relations of aragonite at 300 K obtained in this study, in comparison with previous studies. Solid black curve represents the result of fitting the data of this study. Cold compression data were included for comparison but not used in the fit.

Reference

Li, Y., Y. Zou, X. Wang, T. Chen, X. Qi, H. Chen, J. Du, B. Li (2015) P-V-T equation of state and high-pressure behavior of CaCO3 aragonite, Am Min., 100, 2323-2329.

Elasticity and phase transformation at high pressure in coesite from experiments and first-principles calculations

Ting Chen[1], Xuebing Wang[1], Xintong Qi[1], Maining Ma[2], Zhishuang Xu[2], and Baosheng Li[3]
[1]Department of Geosciences, Stony Brook University, Stony Brook, New York 11794, U.S.A.
[2]University of Chinese Academy of Sciences, Beijing 100049, China
[3]Mineral Physics Institute, Stony Brook University, Stony Brook, New York 11794, U.S.A.

(COMPRES-related facilities: National Synchrotron Light Source Beamline X17C)

The crystal structure and equation of state of coesite (space group C2/c) and its high-pressure polymorph coesite-II (space group P21/n) under pressure have been studied using X-ray powder diffraction in a diamond-anvil cell (DAC) up to 31 GPa at room-temperature and first-principles calculations at 0 K up to 45 GPa. New diffraction peaks appear above 20 GPa, indicating the formation of coesite-II structure. The calculated enthalpies provide theoretical support for the pressure-induced phase transformation from coesite to coesite-II at ~21.4 GPa. Compared with coesite, the coesite-II structure is characterized by a "doubled" b-axis and the breakdown of the linear Si1-O1-Si1 angle in coesite into two distinct angles-one is ~176°, close to linear, whereas the other decreases by 22 to 158°. Coesite is very anisotropic with the a-axis the shortest and twice more compressible than the b- and c-axis. By comparison, coesite-II is not so anisotropic with similar compressibilities in its *a*-, *b*-, and *c*-axis. As analyzed by a third-order Eulerian finite strain equation of state, the bulk modulus of coesite at 21.4 GPa is 182.3 GPa, and that of coesite-II is 140.8 GPa, indicating that coesite-II is much more compressible than coesite. The existence of coesite-II in the coldest subduction zone will change the elasticity and anisotropic properties of the subducting materials dramatically.

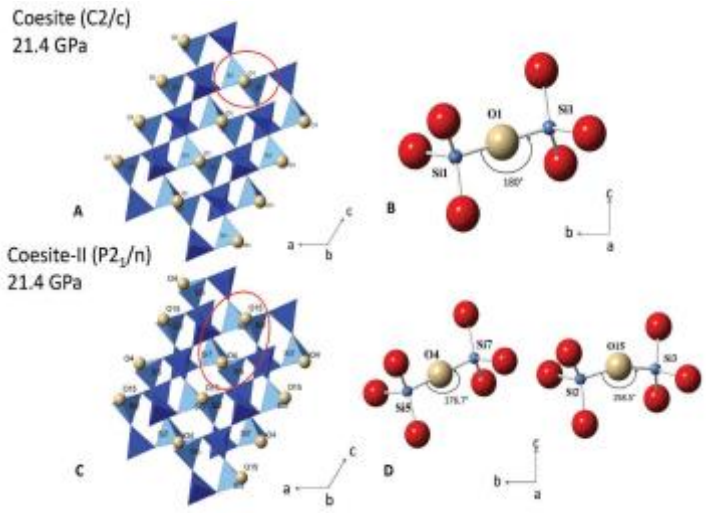

Figure 1. Structure of coesite and coesite-II at 21.4 GPa from DFT calculations. (**A** and **C**) Polyhedral illustration of the silica tetrahedral for coesite and coesite-II at 21.4 GPa, respectively, viewed down the *b*-axis. (**B** and **D**) Illustration of the Si1-O1-Si1 angle in coesite and its evolved angles Si5-O4-Si7 and Si2-O15-Si3 in coesite-II viewed down the *a*-axis (circled out in **A** and **C**).

Reference

Chen, T., X. Wang, X. Qi, M. Ma, Z. Xu, B. Li (2016). Elasticity and phase transformation at high pressure in coesite from experiments and first-principles calculations, *Am. Min.*, 101, 1190-1196.

The elasticity of natural hypersthene and the effect of Fe and Al substitution

Zhishuang Xu[1], Maining Ma, Baosheng Li[2], Xinguo Hong[2], Lin Han[1], and Xiaoya Zhou[1]
[1]Key Laboratory of Computational Geodynamics, Chinese Academy of Sciences of China
[2]Mineral Physics Institute, Stony Brook University, Stony Brook, USA

(COMPRES-related facilities: National Synchrotron Light Source Beamline X17C)

Orthopyroxene, $(Mg,Fe)_2Si_2O_6$, crystallizes in an orthorhombic structure (space group Pbca) at ambient conditions and occurs in both igneous and metamorphic rocks and in meteorites, representing one of the most prevailing constituents of the Earth's lithosphere and upper mantle as well as the lunar mantle. In this study, compressional behavior of a natural hypersthene has been investigated at pressures up to 10.1 GPa at room temperature using in situ synchrotron X-ray diffraction in a diamond anvil cell. No phase transition was observed within the experimental pressure range. The pressure- volume data have been fitted with a third order Birch–Murnaghan equation of state, resulting in K_0 = 113.6 (6.2) GPa and K'_0 = 7.7(2.0) for the bulk modulus and its pressure derivative with a fixed unit-cell volume V_0= 854.0(6) Å^3. The unit cell parameters, a, b, and c, decrease nonlinearly with elevated pressure and show an anisotropic axial compressibility with a ratio β_a: β_b: β_c: =1:2.05:1.3. The comparison with previous results of orthopyroxene reveals that Al substitution causes a decrease in unit-cell volume and an increase in the bulk modulus, whereas the incorporation of Fe has opposite effects. The relation between unit cell volume and En/Ts contents has been obtained, V_0(Å^3) = 873.7(1.1)−40.8(1.44)×En-90.6(14.7)×Ts, which permits the prediction of unit-cell volume for Fe- and Al-bearing orthopyroxene system.

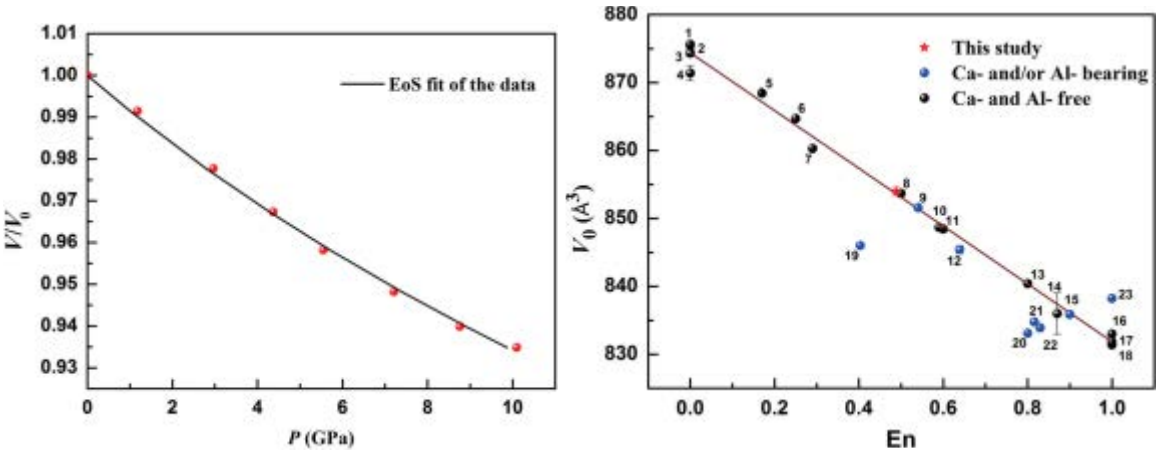

Reference
Zhishuang Xu, Maining Ma, Baosheng Li, Xinguo Hong, Lin Han & Xiaoya Zhou (2016): The elasticity of natural hypersthene and the effect of Fe and Al substitution, High Pressure Research, http://dx.doi.org/10.1080/08957959.2015.1136623

Compressibility of mimetite and pyromorphite at high pressures

Shuyi Wei[1], Maining Ma[2], Dawei Fan[1], Jing Yang[3], Wenge, Zhou[1], Baosheng Li[4], Zhiqiang Chen[4] & Hongsen Xie[1]
[1]Laboratory for High Temperature and High Pressure Study of the Earth's Interior, CAS, Guiyang, China
[2]Key Laboratory of Computational Geodynamics, CAS, Beijing, China
[3]Department of Geological Sciences, The University of Texas at Austin, Austin, USA
[4]Mineral Physics Institute, Stony Brook University, USA

(COMPRES-related facilities: National Synchrotron Light Source Beamline X17C)

High pressure X-ray diffraction experiments on mimetite [Pb5(AsO4)3Cl] and pyromorphite [$Pb_5(PO_4)_3Cl$] were performed up to 14.1 and 14.9 GPa, respectively, at 300 K, using *in situ* angle dispersive X-ray diffraction and a diamond anvil cell. No phase transition of mimetite and pyromorphite was observed within the experimental pressure range. Fitting the *P–V* data under hydrostatic stress conditions with a third-order Birch–Murnaghan Equations of State (BM-EoS) we obtained: K_0 = 46*(7)* GPa, V_0 = 680*(2)*Å^3, and K_0 = 15*(4)* for mimetite; K_0 = 44*(5)* GPa, V_0 = 636*(1)*Å^3, and $K0$ = 15*(3)* for pyromorphite. The axial compressibility was also calculated with a third-order 'linearized' BM-EoS. We obtained $K_{0a} : K_{0c}$ = 1 : 1.00 for mimetite, and $K_{0a} : K_{0c}$ = 1 : 1.28 for pyromorphite, indicating that mimetite and pyromorphite are elastically isotropic and slightly anisotropic, respectively. Comparing the previous equation of state data of vanadinite [$Pb_5(VO_4)_3Cl$] with the current results of mimetite [$Pb_5(AsO_4)_3Cl$] and pyromorphite [Pb5(PO4)3Cl], we found that the substitution ofV^{5+} by As^{5+} and P^{5+} has an insignificant effect on the bulk modulus, but has a greater effect on the axial parameters, compression ratio, and elastic anisotropy.

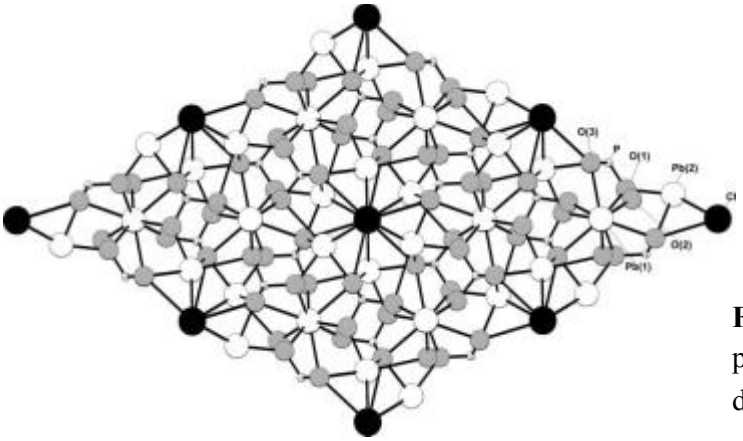

Fig. 1. Crystal structure of pyromorphite, Pb5(PO4)3Cl, viewed down the c-axis.flourapatites.

Reference

Wei, S., M. Ma , D. Fang, W. Zhou, B. Li , Z. Chen , H. Xie (2013), In situ high pressure X-ray diffraction study of mimetite and pyromorphite, Compressibility of mimetite and pyromorphite at high pressure, High Pressure Research, DOI:10.1080/08957959, 2013, 765003.

Expansivity and compressibility of strontium and barium fluorapatites: significance of the M-cations

Qiang He1, Xi Liu[1], Baosheng Li[2], Liwei Deng[1], Zhiqiang Chen[2], Xiaoyang Liu[3], Hejing Wang1
[1] Colleage of Earth and Space Sceinces, Peking University, China
[2]Mineral Physics Institute, Stony Brook University, USA
[3]Jilin University, China

(COMPRES-related facilities: National Synchrotron Light Source Beamline X17C)

Strontium fluorapatite (SrF-Ap) and barium fluorapatite (BaF-Ap) were synthesized by using a piston cylinder apparatus at 1.0 GPa and 800 ————————————C. Their thermal expansivity and compressibility were subsequently investigated by using in situ high-T powder X-ray diffraction method (up to 1,000 degree C at ambient P) and by using a diamond-anvil cell coupled with synchrotron X-ray radiation (up to about 5 GPa at room T), respectively. The derived thermal expansion coefficients and bulk moduli were combined with the literature data for calcium fluorapatite
(CaF-Ap) and lead fluorapatite (PbF-Ap) to constrain the influence of the M-site cations on the elasticity of the fluorapatites (MF-Ap). The results show that both the size of the M cations and their polarizability affect the thermal expansion coefficients of the MF-Ap. For the axial and volumetric bulk moduli, the size of the M cations plays.

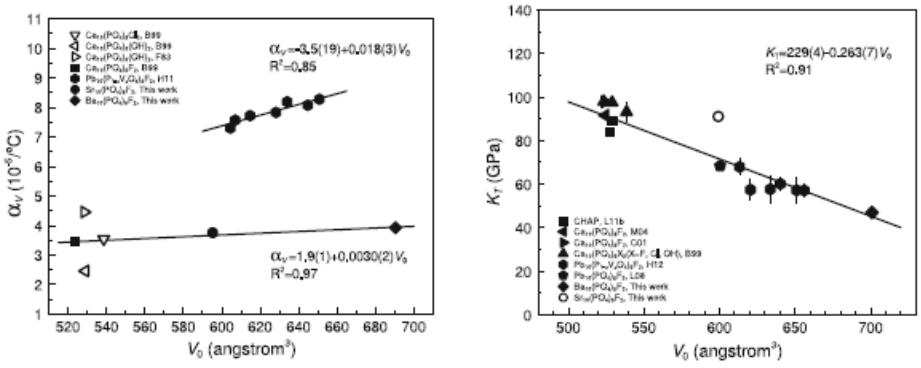

Fig. 1. (Left) Thermal expansion and (right) bulk modulus curve of strontium and barium flourapatites.

Reference

Ma, M., W. Liu, Z. Chen, Z. Liu, B. Li (2013). Compression and Structure of brucite to 31 GPa from synchrotron X-ray diffraction and Infrared spectroscopy studies, *Am Min*, 98 33-40.

Anomalous elastic properties of coesite at high pressure and implications for the upper mantle X-discontinuity

Ting Chen, Gabriel Gwanmesia, Xuebing Wang, Yongtao Zou, Robert Liebermann, Chloe Michaut, and Baosheng Li, Stony Brook University

[COMPRES Cell Assembly Project at ASU]

Compressional and shear wave velocities of coesite have been measured using ultrasonic interferometry in a multi-anvil apparatus up to 12.6 GPa at room temperature for the first time. While the *P*-wave velocity increases continuously with pressure, the *S*-wave exhibits an anomalous softening and the velocity decreases continuously with pressure. Finite strain analysis of the data yielded K_{S0}=103.6(4) GPa, G_0=61.6(2) GPa and K_0'=2.9(1), G_0'=0.3(1) for the bulk and shear moduli and their pressure derivatives, respectively. The anomalous elastic behavior of coesite results in large velocity and impedance contrasts across the coesite–stishovite transition, reaching <39% and <48% for *P* and *S*-wave velocity contrasts, and <70% and 78% for *P* and *S*-wave impedance contrasts, respectively, at pressure <8GPa, with *P* and *S*-wave velocity perturbations showing no apparent dependence on depths (i.e., $d\ln V(P \text{or} S)/dh<0$) within 8–12 GPa. These unusually large contrasts and depth independent characteristics render the transition between the two silica polymorphs one of the most plausible candidates for the cause of the seismically observed X-discontinuity. The current *P* and *S*-wave velocity perturbation dependences on the SiO_2content, $d(\ln V_P)/d(SiO_2)$ <0.43(wt%)−1and $d(\ln V_S)/d(SiO_2)$ <0.60(wt%)−1, can serve as a geophysical probe to track ancient subducted eclogite materials to gain insights on the geodynamics of the mantle.

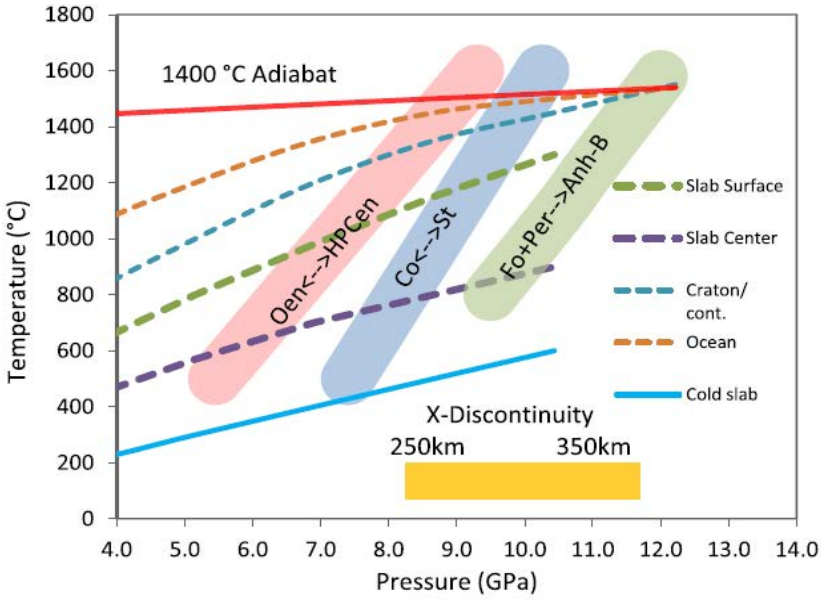

Fig. 6. (a) Phase diagram for MORB (from Ricard et al., 2005). (b) Phase boundaries for coesite–stishovite and OEn–HPC, superimposed with possible geotherms of continents, ocean, slab surface, and the interior of the slab (see Kirby et al., 1996; Peacock, 2003). Phase boundaries for coesite–stishovite include those from Akaogi et al. (2011) and Zhang et al. (1996), and Liu et al. (1996); OEn–HPCen boundaries are representative of the works by Akashi et al. (2009); Woodland and Angel (1997), Ulmer and Stalder (2001) and Pacalo and Gasparik (1990). Fo + Per → Anh-B boundary is representative of the work by Ottonello et al. (2010).

Reference: Chen, T., G. D. Gwanmesia, X. Wang, Y. Zou, R. C. Liebermann, C. Michaut and B. Li, Anomalous elastic properties of coesite at high pressure and implications for the upper mantle X-discontinuity, Earth Planet. Sci. Letters, 412, 42-51, 2015.

Spin crossover equation of state and sound velocities of $(Mg_{0.65}Fe_{0.35})O$ ferropericlase to 140 GPa

Bin Chen[1], Jennifer M. Jackson[1], Wolfgang Sturhahn[1], Dongzhou Zhang[1], Jiyong Zhao[2], June K. Wicks[1], and Caitlin A. Murphy[1]

1. Seismological Laboratory, California Institute of Technology
2. Advanced Photon Source, Argonne National Laboratory

(COMPRES-related facilities: ALS beamline 12.2.2, APS Beamline Sector 3ID-B, COMPRES gas-loading system at GSECARS)

Sound velocities and density measurements of lower mantle component minerals are essential to interpret the seismic complexities observed in Earth's lower mantle. We determined the elastic and vibrational properties of $(Mg_{0.65}Fe_{0.35})O$-ferropericlase (FP35) up to 1.4 Mbar using nuclear resonant inelastic X-ray scattering (NRIXS) and in-situ X-ray diffraction (XRD) techniques in diamond anvil cells. $(Mg_{0.65}Fe_{0.35})O$ contains the amount of iron within the estimated range expected for an aluminum-poor lower mantle assemblage. From the low-energy region of the partial phonon density of states (PDoS), in situ XRD measurements, and our equation-of-state study with smaller pressure increments (Fig. 1), we derived its shear and compressional velocities at lowermost mantle pressures (Fig. 2). From integration of the PDoS, we also determined Fe-weighted vibrational parameters as a function of pressure for this ferropericlase. Our data provide new knowledge about the effects of the spin crossover and iron content on the density and sound velocities of ferropericlase in a previous uncharted pressure-composition sector. In light of our results and seismic observations, a better understanding of the compositional variations in Earth's lowermost mantle can be achieved.

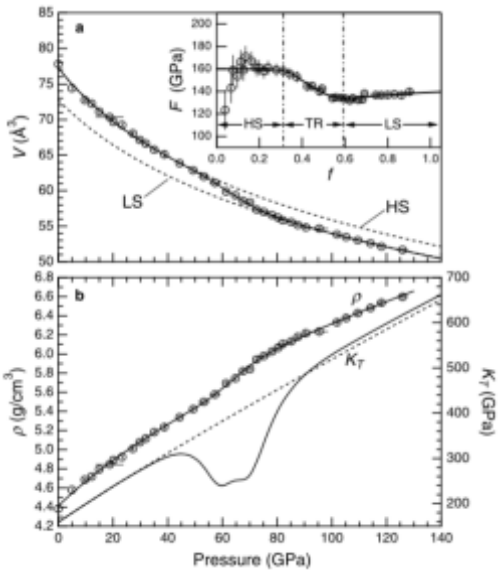

Fig. 2. Compression data of FP35 across the high-spin to low-spin transition at 300 K fitted by the spin crossover equation of state described in this paper.

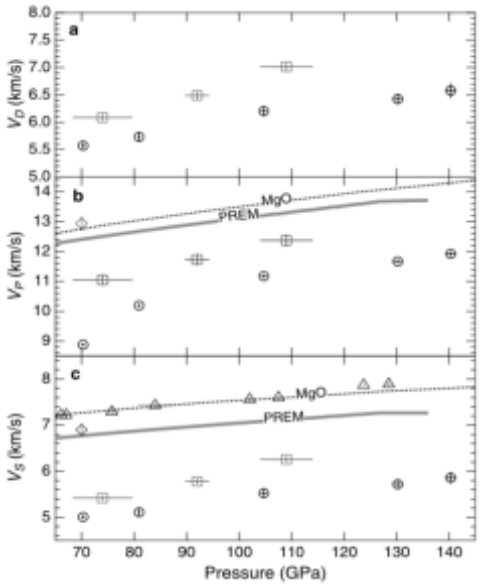

Fig. 1. Sound velocities (a) V_D, (b) V_P, and (c) V_S of MgO, $(Mg_{0.83}Fe_{0.17})O$, $(Mg_{0.75}Fe_{0.25})O$, and FP35 from 70 to 140 GPa.

Reference: Chen, B., Jackson, J.M., Sturhahn, W., Zhang, D., Zhao, J., Wicks, J.K., Murphy, C.A., 2012. Spin crossover equation of state and sound velocities of $(Mg_{0.65}Fe_{0.35})O$ ferropericlase to 140 GPa. J. Geophys. Res. Solid Earth **117**, B08208. doi:10.1029/2012JB009162

Elasticity and sound velocities of polycrystalline grossular ($Ca_3Al_2Si_3O_{12}$) at simultaneous high pressures and high temperatures

Gabriel Gwanmesia, Liping Wang, Adaire Heady and Robert Liebermann, Delaware State University and Stony Brook University

[COMPRES Multi-Anvil facilities at X17B2 at NSLS and Cell Assembly Project at ASU]

The elastic wave velocities of a dense polycrystalline specimen (99.7% of theoretical density) of synthetic grossular garnet ($Ca_3Al_2Si_3O_{12}$) were measured to pressures of 10 GPa and temperatures of 1000 K by transfer-function ultrasonic interferometry in conjunction with energy-dispersive synchrotron X-radiation in a deformation DIA-type cubic-anvil apparatus. The calculated elastic bulk (Ks) and shear (G) moduli data were fitted to functions of Eulerian strain to 3rd order, yielding the zero-pressure values [Ks = 171.2 (8) GPa; G = 107.4 (2) GPa] and their pressure derivatives [$(\partial Ks/\partial P)_T$ = 4.47 (2); $(\partial G/\partial P)_T$ = 1.29 (5)]. The temperature dependences of the elastic moduli obtained from linear regression of the entire P–T–Ks and P–T–G data are: $(\partial Ks/\partial T)_P$ = 1.38 (3) x10^{-2} GPa/K and $(\partial G/\partial T)_P$ = 1.28 (2) x10^{-2} GPa/K. These results together with those from previous studies for garnets with varying compositions suggest that most of the thermo-elastic properties of garnet are insensitive to grossular content, with the exception of the shear modulus, which significantly depends on the calcium content.

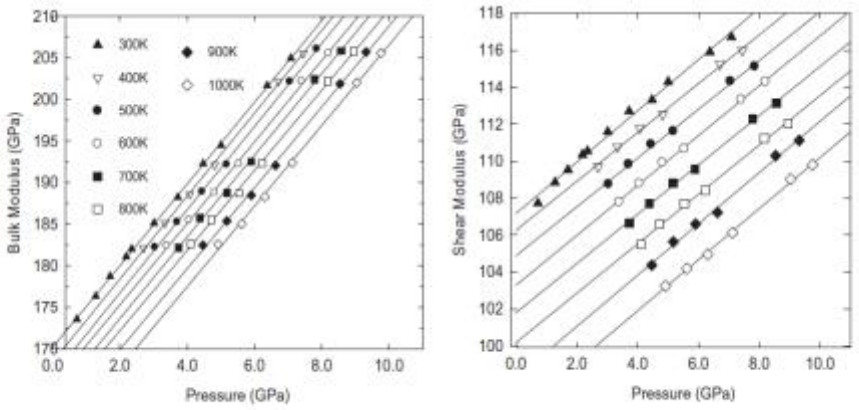

Fig. 4. The bulk (K_s) and shear (G) moduli as a function of pressure along the experimental isotherms. Lines are linear regressions through data to illustrate data trend.

Reference: Gwanmesia, G. D., L. Wang, A. Heady, and R. C. Liebermann, Elasticity and sound velocities of polycrystalline grossular ($Ca_3Al_2Si_3O_{12}$) at simultaneous high pressures and high temperatures, Phys. Earth Planet. Interiors, 228, 80-97, 2014.

Study of the Earth's interior using measurements of sound velocities in minerals by ultrasonic interferometry

Baosheng Li and Robert Liebermann, Stony Brook University

[COMPRES Multi-Anvil facilities at X17B2 at NSLS and Cell Assembly Project at ASU

This paper reviews the progress of the technology of ultrasonic interferometry from the early 1950s to the present day. During this period of more than 60 years, sound wave velocity measurements have been increased from at pressures less than 1 GPa and temperatures less than 800 K to conditions above 25 GPa and temperatures of 1800 K. This is complimentary to other direct methods to measure sound velocities (such as Brillouin and impulsive stimulated scattering) as well as indirect methods (e.g., resonance ultrasound spectroscopy, static or shock compression, inelastic X-ray scattering). Newly-developed pressure calibration methods and data analysis procedures using a finite strain approach are described and applied to data for the major mantle minerals. The implications for the composition of the Earth's mantle are discussed. The state-of-the-art ultrasonic experiments performed in conjunction with synchrotron X-radiation can provide simultaneous measurements of the elastic bulk and shear moduli and their pressure and temperature derivatives with direct determination of pressure. The current status and outlook/ challenges for future experiments are summarized.

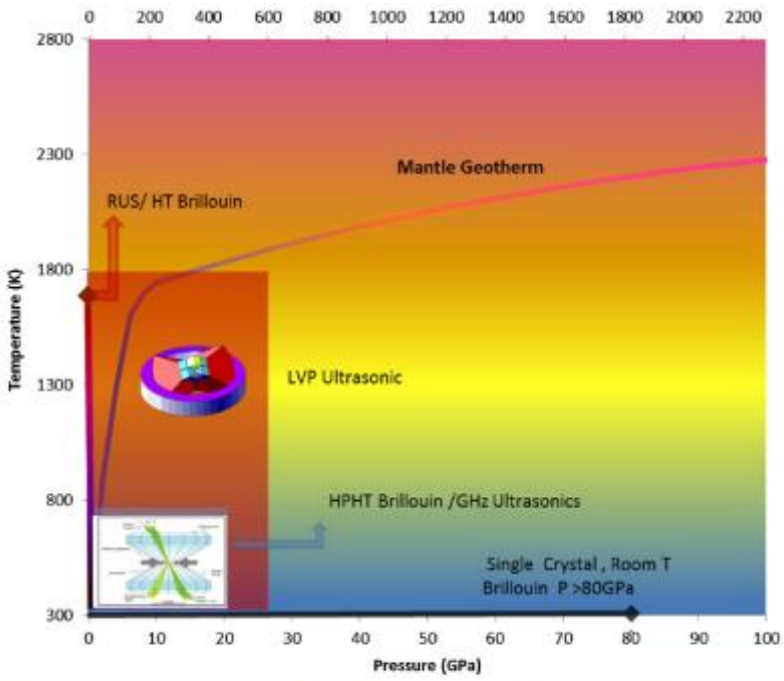

Fig. 10. Current status of sound velocity measurements in multi-anvil apparatus at high pressure and temperature in comparison to single crystal Brillouin scattering, GHz ultrasonic, and resonance ultrasonic spectroscopy investigations. For Brillouin scattering measurements on polycrystalline samples, see Speziale et al. (2014).

Reference: Li, B., and R. C., Liebermann, Study of the Earth's interior using measurements of sound velocities in minerals by ultrasonic interferometry, Phys. Earth Planet. Interiors, 233, 135-153. 2014.

Phase transition and elasticity of enstatite under pressure from experiments and first-principles calculations

Baosheng Li, Jennifer Kung, Wei Liu and Robert Liebermann, Stony Brook University

[COMPRES Multi-Anvil Facilities at X17B2 at NSLS and Cell Assembly Project at ASU

We have investigated the thermodynamic stability, crystal structure, elastic constants, and sound velocities of $MgSiO_3$-enstatite using data from X-ray diffraction and ultrasonic measurements up to 16.8 GPa and first-principles calculations up to 30 GPa. The calculated enthalpies provide theoretical support for the phase transition from Pbca to P21/c between 9 and 14 GPa previously observed in natural orthoensatite and MgSiO3 enstatite. A density increase of 1.4–1.5% for the Pbca>P21/c transition is obtained from both first-principles and experimental studies. Elastic constants of Pbca, P21/c, C2/c, P21ca and Pbca-II are all calculated, and a softening in the shear constant C_{55} is predicted for Pbca and Pbca-II phases. C_{55} of Pbca is found to be closely correlated with the A-site SiO_4 tetrahedra chain angle while C_{44} and C_{66} are correlated with the B-site chain angle. Pbca, P21/c and C2/c all exhibit similar volumetric compressibilities at all pressures. The calculated velocities of the P21/c phase at 12 GPa are equal to those of Pbca for P and 1.3% higher for S waves. The experimentally observed P and S wave velocity anomalies can be qualitatively described by the transformation from Pbca to P21/c; however, the magnitudes of the velocity decreases between 10 and 14 GPa remain to be verified by future single crystal data or polycrystalline measurements at high pressures. The predicted velocity jumps of 2.8% and 4.5% for P and S waves, respectively, between Pbca and C2/c in the pressure range of 5–12 GPa are in excellent agreement with the values of 3(1)% and 5(1)% obtained from the directly measured data, thereby making it a plausible candidate for the seismic X-discontinuity at depths of 250–300 km in the Earth's upper mantle.

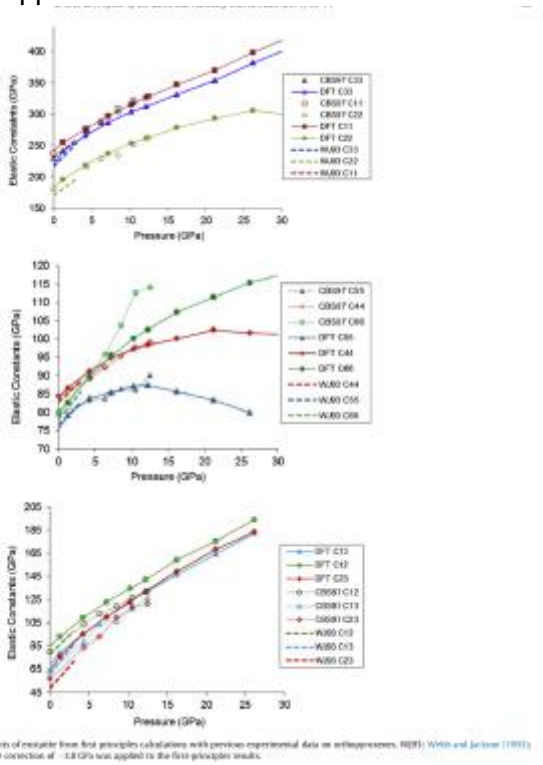

Reference:Li, B., J. Kung, W. Liu and R. C. Liebermann, Phase transition and elasticity of enstatite under pressure from experiments and first-principles calculations, Phys. Earth Planet. Interiors, 228, 63-74, 2014.

Spectroscopic and X-ray diffraction investigation of the behavior of hanksite and tychite at high pressures, and a model for the compressibility of sulfate minerals

Sarah E.M. Palaich, Craig E. Manning, Edwin Schauble, and Abby Kavner, UCLA

(COMPRES-related facilities: Advanced Light Source Beamline 12.2.2)

The rare evaporite minerals hanksite, $Na_{22}K(SO_4)_9(CO_3)_2Cl$, and tychite, $Na_6Mg_2(CO_3)_4(SO_4)$, are excellent case studies for the high-pressure behavior of ionic groups since their structures combine ionic complexity and high symmetry (hexagonal and cubic respectively). We investigated the structure and compressibility of hanksite and tychite in the diamond-anvil cell using Raman spectroscopy and X-ray diffraction and desnsity functional theory. At ambient pressure, the Raman spectrum of hanksite has a single sulfate ν_1 frequency at 992 cm^{-1} with a lower-frequency shoulder. As pressure is increased, this mode splits into two distinct peaks, which arise from two distinct local environments for the sulfate tetrahedra within the hanksite structure. X-ray diffraction data of hanksite indicate a 5% volume drop between 8–10 GPa with no apparent change of symmetry. A second-order Birch-Murnaghan fit to the data below 8 GPa yields an isothermal bulk modulus of 66(1) GPa for hanksite and 85(1) GPa for tychite, Compressibility data for a variety of sulfate minerals shows that bulk modulus decreases as the sulfate-sulfate polyhedral distance increases.

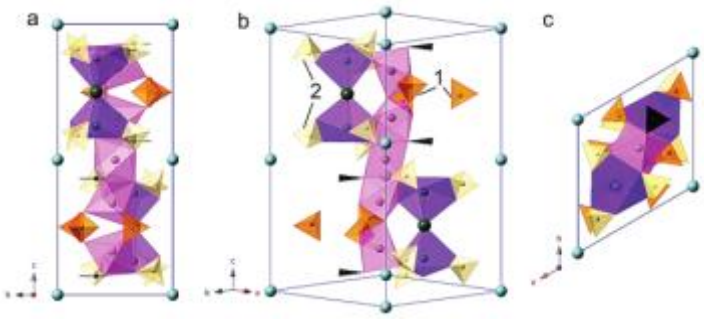

Figure 1. Three perspectives of the hanksite unit cell. Sodium octahedra are shown in light (regular) and dark (coordinated with Cl). Carbonate triangles sit parallel to the *a*-axis in line with the chlorine atoms. The two distinct sulfate tetrahedral groups are labeled 1 and 2.

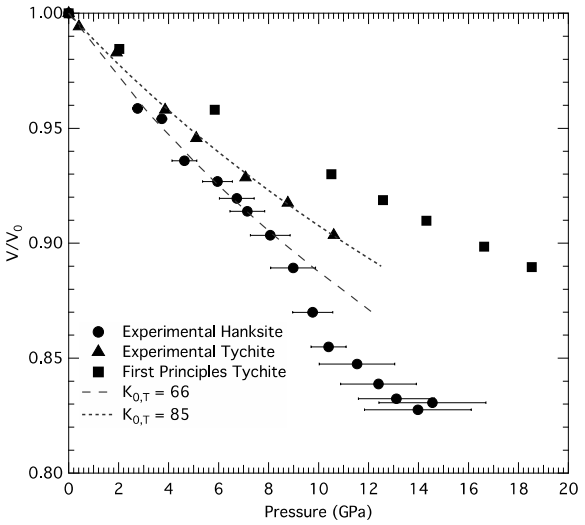

Figure 2. Plot of normalized volume as a function of pressure for hanksite (experimental: filled circle) and tychite (experimental: filled triangle, model: filled box) from X-ray diffraction data and first- principles model. Error bars on hanksite pressure represent the standard deviation of pressures measured in the DAC.

Birch-Murnaghan fits to the experimental data are shown as dotted lines [hanksite $K_{0,T} = 66(1)$ GPa; tychite $K_{0,T} = 85(1)$ GPa].

References: S. E. M. Palaich*, C. E. Manning, E. Schauble and A. Kavner, (2013), Spectroscopic and X-ray diffraction investigation of the behavior of hanksite and tychite at high pressures, *Am. Mineral.,* **98**, pp. 1543-1549.

The effect of sintering pressure on anelastictiy of pyrope garnet. (David Dobson, Simon Hunt and Oliver Lord)

Grain-boundary properties affect a diverse range of physical and chemical properties of ceramics, including optical transmission, elastic and viscous properties, partitioning of incompatible elements and electrical conductivity. Despite this, they are a largely neglected aspect of rock- and mineral-physics even though that every rock is a polyscystalline composite (natural ceramic). Here we investigate the effect of sintering pressure on anelasticity of pyrope garnet.

Garnets were synthesized from $Mg_3Al_2Si_3O_{12}$ glass at 1273 K for 24 h at pressures of between 4 and 15 GPa. The mean grain size was ~2 μm for all samples but those recovered from 15 GPa ware white while those recovered from lower pressures were grey-black. Cored cylinders of pyrope were compressed to 2.5 GPa and subjected to sinusoidally time-varying microstrains in the D-Dial press installed at X17B2 beamline of the NSLS: stress was determined using the length variation of a corundum proxy placed in series with the pyrope sample. The figures below show apparent Young's moduli based on Maxwell viscoelastic fits to the stress-strain data: (A) is for samples annealed at different pressures, all at a driving period of 160s and (B)is for the sample annealed at 4 GPa across a range of driving periods (10-360 s). All samples start off in agreement with the single-crystal average at low temperature and show viscoelastic softening ta the annealing temperature (1273 K) as is common for ceramics. At higher temperatures only the samples sintered at 10 and 15 GPa show significant recovery; the sample sintered 4GPa shows strong dispersion.

The present results show that anelastic behavior is strongly sensitive to sintering pressure, even if the anelasticity measurements are performed under identical conditions. The most likely explanation is that elastically-accommodated grain-boundary sliding is inhibited by strong intergranular bonding at high sintering pressures. This implies that studies which seek to interpret seismic Q values of the lower mantle and inner core (at pressures of 20-360 GPa) on the basis of low-pressure anelasticity measurements are likely to be erroneous.

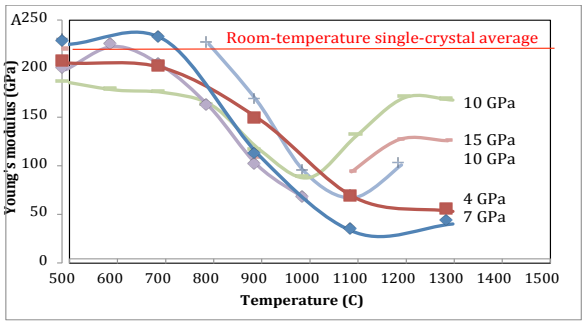

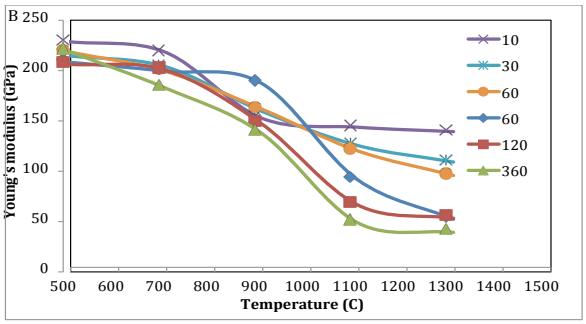

Equation of state of a synthetic ulvöspinel, $(Fe_{1.94}Ti_{0.03})TiO_4$, at ambient temperature

Using a diamond-anvil cell and synchrotron X-ray diffraction, the compressional behavior of a synthetic ulvöspinel $(Fe_{1.94}Ti_{0.03})TiO_4$ has been investigated up to about 7.05 GPa at 300 K. The pressure–volume data fitted to the second-order Birch–Murnaghan equation of state yield an isothermal bulk modulus (K_T) of 147(4) GPa (K'_T fixed as 4). This value is slightly larger than that previously determined by an ultrasonic pulse echo method (121(2) GPa; Syono et al., *J Phys Soc Jpn* **31**:471–476, 1971), but substantially smaller than that recently determined by a synchrotron X-ray diffraction technique (251(3) GPa; Yamanaka et al., *Phys Rev B* **80**:134120, 2009; *Am Mineral* **98**:736–744, 2013). Combined with the K_T of magnetite (Fe_3O_4; ~182(3) GPa), our finding suggests that the bulk modulus of the solid solutions $Fe_{3-x}Ti_xO_4$ ($0 \le x \le 1$) along the join magnetite–ulvöspinel decreases by ~20 %.

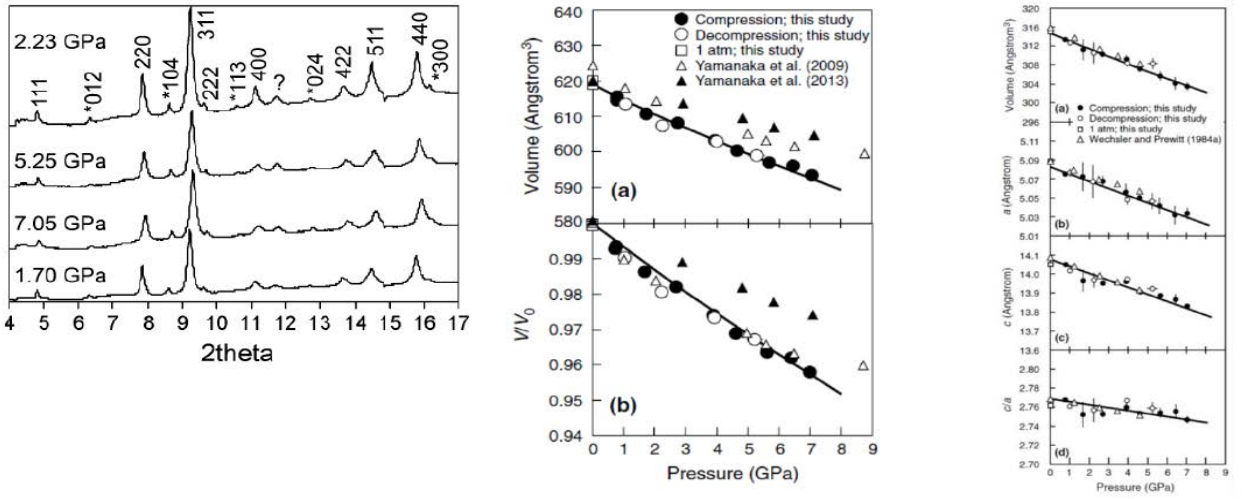

Figure 1. Left panel: Examples of X-ray diffraction patterns of ulvöspinel at 1.70, 7.05, 5.25 and 2.23 GPa. Middle panel: Effect of pressure on the unit-cell parameters of ulvöspinel at 300 K, compared to those from Yamanaka et al. (2009, 2013): **a** the volume; **b** the $V/V0$ ratio. Right panel: Effect of pressure on the unit-cell parameters of ilmenite at 300 K, compared to those from Wechsler and Prewitt (1984). *Thick curve* represents the second-order Birch–Murnaghan equation of state, established using all P–V data collected in this study.

Reference: Xiong Z, Liu X, Shieh S R, Wang F, Wu X, Hong X and Shi Y (2014) Equation of state of a synthetic ulvöspinel, $(Fe_{1.94}Ti_{0.03})TiO_4$, at ambient temperature *Phys Chem Minerals* **41**, 1–7

Equation of state of pyrope–almandine solid solution measured using a diamond anvil cell and in situ synchrotron x-ray diffraction

The pressure–volume relations of three synthetic garnet samples, $Py_{83}Alm_{17}$, $Py_{54}Alm_{46}$ and $Py_{30}Alm_{70}$,along pyrope–almandine (Py–Alm) join were measured at ambient temperature and high pressures up to 7, 21 and 19 GPa, respectively. The obtained *P–V* data were fitted to the third-order Birch–Murnaghan equation of state (EOS). The ambient cell volumes V_0 of the three samples were measured to be 1511(1), 1515(2), and 1526(1) $Å^3$ respectively. With fixed pressure derivative of the isothermal bulk modulus, K', at 4.3, isothermal bulk moduli, $K_{0,}$ of the three samples were determined to be 172(4), 174(2), and 183(2) GPa respectively. These results confirm that almandine content (iron substitution) increases the bulk modulus of the garnet join following a nearly ideal mixing model. The relation between bulk modulus and almandine mole fraction (n) in this garnet join is derived to be $K_0 = 170 + 15\ n$. These data can be used to contribute to construction of compositional models of Earth's mantle.

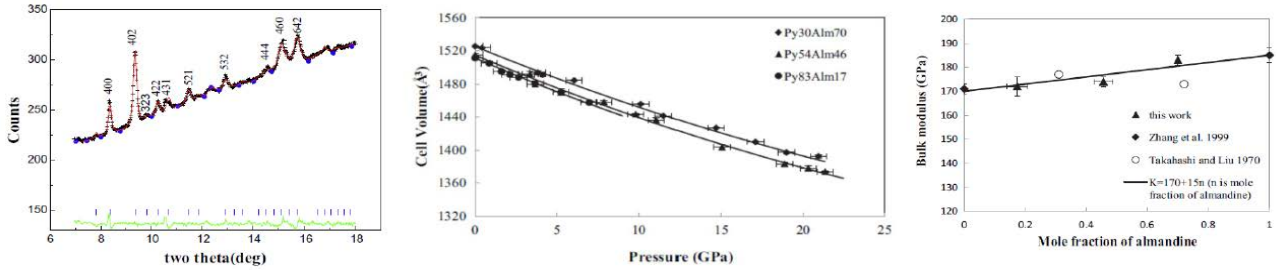

Figure 3. Left panel: Le Bail fitting of $Py_{30}Alm_{70}$ at 19 GPa and room temperature. Middle panel: Volume of Py–Alm garnets as a function of pressure measured using in situ X-ray diffraction at room temperature. Uncertainties of volume data are smaller than symbols. Solid lines represent the third order Birch–Murnagahan EOS fitting. Right panel: Bulk modulus data of almandine–pyrope binary system.

Reference: Huang S and Chen J (2014) Equation of state of pyrope-almandine solid solution measured using a diamond anvil cell and in situ synchrotron X-ray diffraction *Physics of the Earth and Planetary Interiors*, **228**: 88-91.

Elastic wave velocities of peridotite KLB-1 at mantle pressures and implications for mantle velocity modeling

Xuebing Wang, Ting Chen, Yongtao Zou, Robert Liebermann and Baosheng Li,
Stony Brook University

Compressional (V_P) and shear (V_S) wave velocities of a synthetic KLB-1 peridotite were measured for the first time up to 10 GPa using ultrasonic interferometry. Analysis of the P and S wave velocities yielded K_0 = 123(1) GPa, K_0' = 5.1(2), G_0 = 75(1) GPa, and G_0'= 1.3(1) for the bulk and shear moduli and their pressure derivatives. Comparison with Voigt-Reuss-Hill (VRH) calculations based on literature elasticity data for its constituent minerals indicates that the experimentally measured P and S wave velocities, densities, bulk sound velocities, and V_P/V_S ratios fall close to the lower limit of VRH averages associated with the uncertainties of the mineral elasticity data. A comparison with previous modeling of mantle compositions implies that the velocities for an aggregate with the pyrolitic composition of KLB-1 are in close agreement with seismic data at the depths of the Earth's upper mantle.

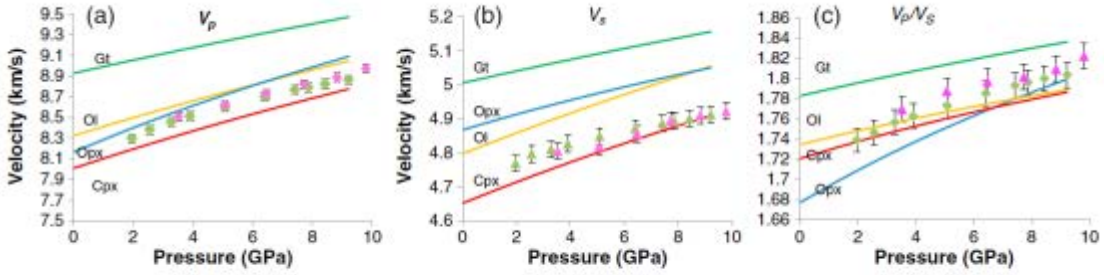

Figure 1. (a) V_P and (b) V_S for synthetic KLB-1 specimens and their comparisons with individual minerals using elastic properties from Table 2. Errors are ~0.5%. (c) Pressure dependence of V_P/V_S ratio of KLB-1 specimens and individual minerals. Errors are ~0.7%. Green diamonds: K973, pink triangles: K657.

Reference: Wang, X., T. Chen, Y. Zou, R. C. Liebermann and B. Li, Elastic wave velocities of peridotite KLB-1 at mantle pressures and implications for mantle velocity modeling, Geophys. Res. Lett., 41, doi:10.1002/2015GL063436, 2015.

Elasticity and lattice dynamics of enstatite at high pressure

D. Zhang[1,2], J. M. Jackson[1], B. Chen[1], W. Sturhahn[1], J. Zhao[2], J. Yan[3], and R. Caracas[4]
1. California Institute of Technology, 1200 E California Blvd, Pasadena, CA 91125
2. Advanced Photon Source, Argonne National Laboratory, 9700 S. Cass Ave, Argonne, IL 60439
3. Advanced Light Source, Lawrence Berkeley National Laboratory, Berkeley, CA 94720
4. Ecole Normale Supérieure de Lyon, 69364 Lyon Cedex 07, France
(COMPRES-related facilities: APS XSD 3-ID-B, ALS 12.2.2 and GSECARS gas loading system)

The elastic properties of mantle minerals are important to understand the geophysical behaviors within Earth's mantle, like the seismic velocity profiles. The behavior of synthetic powdered ^{57}Fe enriched enstatite has been explored by X-ray diffraction (XRD) and nuclear resonance inelastic X-ray scattering (NRIXS). The XRD experiments were carried out at ALS beamline 12.2.2, and the NRIXS data were collected at APS beamline 3-ID-B. The *Pbca*-structured enstatite sample was compressed in fine pressure increments for our independent XRD measurements. One structural transition between 10.1 and 12.2 GPa was identified from the XRD data. The XRD reflections observed for the high-pressure phase are best matched with space group $P2_1/c$. Density-functional theory was combined with Mössbauer spectroscopy and NRIXS to understand the local site symmetry of the Fe atoms in our sample. 3rd-order Birch-Murnaghan equations of state (BM3) give elastic parameters for the *Pbca* phase and the $P2_1/c$ phase. NRIXS measurements were performed with in-situ XRD up to 17 GPa. The partial phonon density of states (DOS) was derived from the raw NRIXS data, and from the low-energy region of the DOS, the Debye sound velocity was determined. The equation of state determined from XRD and Debye sound velocity were used to compute the isotropic compressional (V_P) and shear (V_S) wave velocities of enstatite at different pressures. The results help constrain the high-pressure properties of *Pbca*-structured enstatite in Earth's upper mantle. It is found that candidate upper mantle phase assemblages containing *Pbca*-structured enstatite are associated with shear velocity gradients that are higher than the average Earth model PREM, but lower than regional studies down to about 250 km depth.

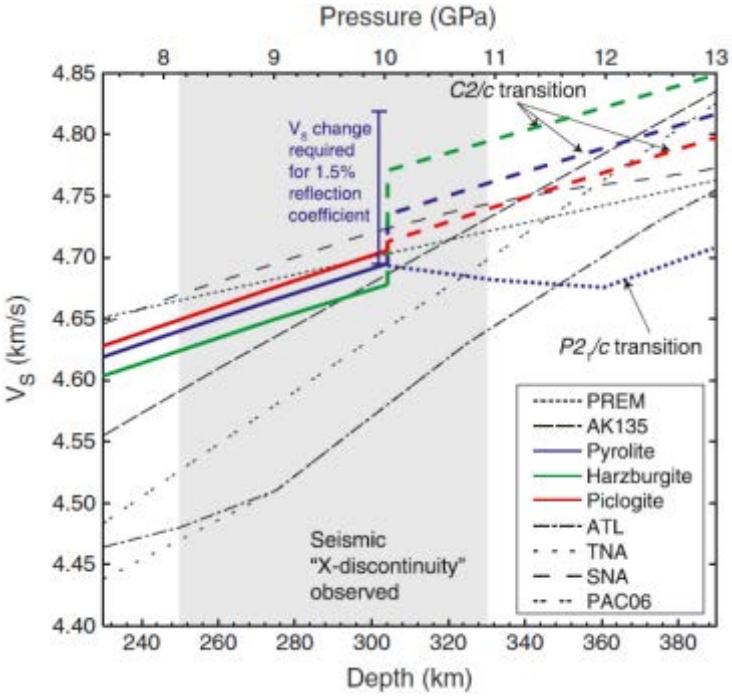

Reference: Zhang, D., J. M. Jackson, B. Chen,W. Sturhahn, J. Zhao, J. Yan, and R. Caracas (2013), Elasticity and lattice dynamics of enstatite at high pressure, *J. Geophys. Res. Solid Earth,* 118, 4071–4082.

Fig 1: Comparison of calculated shear wave velocities from candidate upper mantle petrological models with seismic profiles. At P > 10 GPa: assuming *C2/c* transition (dashed curve); speculating that the $P2_1/c$ transition occurs (dotted curve) (this study). Seismic X discontinuity observed (shaded region). Shear velocity jump required for a seismic reflection with 1.5% reflection coefficient in a pyrolytic mantle (blue

High-pressure single-crystal elasticity study of CO_2 across phase I-III transition

Jin S. Zhang[1,*], Sean R. Shieh[2], Jay D. Bass[1], Przemyslaw Dera[3] and Vitali Prakapenka[4]

[1]Department of Geology, University of Illinois, Urbana-Champaign, IL, 61801, U.S.A.
[2] Departments of Earth Sciences and Physics and Astronomy, University of Western Ontario, London, ON N6A 5B7, Canada
[3] Hawaii Institute of Geophysics and Planetology, University of Hawaii, Honolulu, HI, 96822
[4] Center for Advanced Radiation Sources, University of Chicago, Chicago, IL 60637, U.S.A.

(COMPRES-related facilities: COMPRES gas-loading system at GSECARS)

Sound velocities and elastic moduli of solid single-crystal CO_2 were measured at pressures up to 11.7(3) GPa by Brillouin spectroscopy. The aggregate adiabatic bulk modulus (K_S), shear modulus (G) and their pressure derivatives for phase I of CO_2 are K_{S0} = 3.4(6) GPa, G_0 = 1.8 (2) GPa, $(dK_S/dP)_0$ = 7.8(3), $(dG/dP)_0$ = 2.5(1), $(d^2K_S/dP^2)_0$ = -0.23(3) GPa^{-1} and $(d^2G/dP^2)_0$ = -0.10(1) GPa^{-1}. A small increase of elastic properties was observed between 9.8(1) and 10.5(3) GPa, in agreement with the CO_2 I-III transition pressure determined from previous X-ray diffraction experiments. Above the transition pressure P_T, we observed a mixture dominated by CO_2-I, with minor CO_2-III. The CO_2-I + III mixture shows slightly increased sound velocities compared to pure CO_2-I. Elastic anisotropy calculated from the single-crystal elasticity tensor exhibits a decrease with pressure beginning at 7.9(1) GPa, which is lower than P_T. Our results coincide with recent X-ray Raman observations, suggesting that a pressure-induced electronic transition is related to local structural and optical changes.

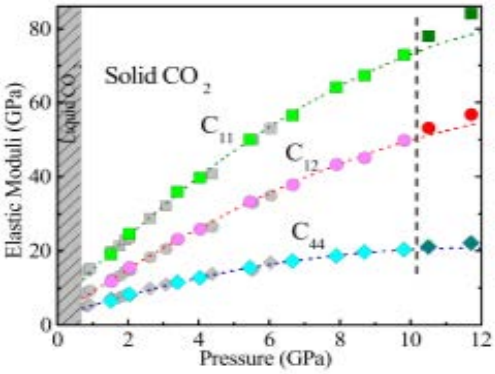

Figure. 1. Single-crystal elastic moduli C_{11}, C_{12}, C_{44}, versus pressure. Green squares, pink circles, cyan diamonds, denote C_{11}, C_{12} and C_{44}, respectively, for CO_2-I; whereas olive squares, red circles, dark cyan diamonds are for CO_2-III. Vertical black dashed straight lines indicate transition pressure boundary. Most experimental uncertainties are within symbols. Dashed curves with olive, red and navy color are the corresponding 2nd order polynomial fits. Previous results for C_{11}, C_{12}, C_{44}, of CO_2-I at high pressures, denoted by grey squares, circles, diamonds respectively.

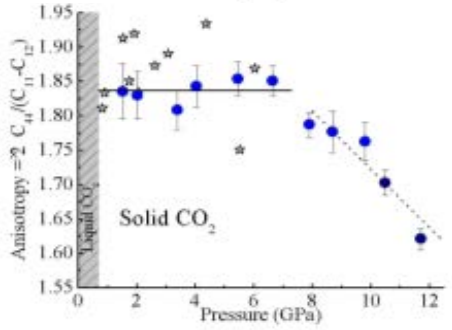

Figure. 2. Plot of elastic anisotropy (A) as a function of pressure. Navy circles and grey stars denote anisotropy measured by this study and Shimizu *et al*. Dash-dot line is the polynomial fit of the Cij's. The horizontal solid line denotes the averaged anisotropy at pressures to ~7 GPa. The decrease of elastic anisotropy starts from ~7.5 GPa and a much more significant decrease occur at above 10 GPa.

Reference: Zhang, J. S., Shieh, S., Bass, J.D., Dera, P. and V. B. Prakapenka (2014), High-pressure single-crystal elasticity study of CO_2 across phase I-III transition, *Appl. Phys. Lett.* **104**, 141901. doi:10.1063/1.4870526

Compressional behavior of omphacite to 47 GPa

D. Zhang[1], Y. Hu[1,2], P. K. Dera[1,2]
1. Hawai'i Institute of Geophysics and Planetology, University of Hawaii at Manoa, 1680 East West Road, Honolulu, HI 96822
2. Department of Geology and Geophysics, University of Hawaii at Manoa, 1680 East West Road, Honolulu, HI 96822
(COMPRES-related facilities: Partnership for Extreme Crystallography)

Omphacite is an important mineral component of eclogite. Single crystal synchrotron X-ray diffraction data on natural $(Ca,Na)(Mg,Fe,Al)Si_2O_6$ omphacite have been collected at the Advanced Photon Source beamlines 13-BM-C and 13-ID-D up to 47 GPa at ambient temperature. Unit cell parameter and crystal structure refinements were carried out to constrain the isothermal equation of state and compression mechanism. The 3rd order Birch-Murnaghan equation of state (BM3) fit of all data gives V_0=423.9(3) Å^3, K_{T0}=116(2) GPa and K_{T0}'=4.3(2). These elastic parameters are consistent with the general trend of the diopside-jadeite join. The eight-coordinated polyhedra (M2 and M21) are the most compressible, and contribute to majority of the unit cell compression, while the SiO_4 tetrahedra (Si1 and Si2) behave as rigid structural units and are the most incompressible. Axial compressibilities are determined by fitting linearized BM3 equation of state to pressure dependences of unit cell parameters. Throughout the investigated pressure range, the **b**-axis is more compressible than the **c**-axis. The axial compressibility of the **a**-axis is the largest among the three axes at 0 GPa, yet it quickly drops to the smallest at pressures above 5 GPa, which is explained by the rotation of the stiffest major compression axis toward the **a**-axis with the increase of pressure.

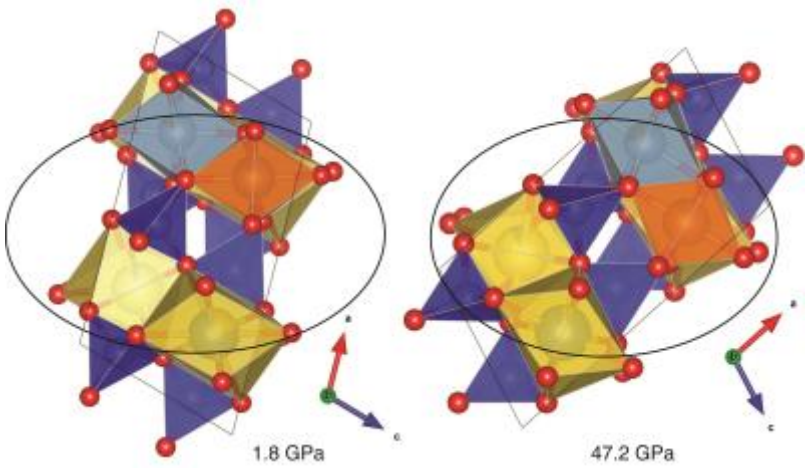

Figure 1. The orientations of the representation quadric in the **a-c** plane for the isothermal compressibility tensor of omphacite at 1.8 GPa and 47.2 GPa, viewed down **b**-axis.

Reference: Zhang D., Hu Y., and Dera P. (2016) "Compressional behavior of omphacite to 47 GPa" Phys. Chem. Minerals. DOI: 10.1007/s00269-016-0827-4

Iron isotope fractionation in the Earth's interior investigated by Nuclear Resonant IXS

Jin Liu[1], Nicolas Dauphas[2], Mathieu Roskosz[3], Michael Y. Hu[4], Hong Yang[5], Wenli Bi[4,6], Jiyong Zhao[4], Jung-Fu Lin[1]
[1]Department of Geological Sciences, Jackson School of Geosciences, University of Texas at Austin, Austin, Texas 78712, USA
[2]Origins Laboratory, Department of the Geophysical Sciences and Enrico Fermi Institute, The University of Chicago, Chicago, IL 60637, USA
[3]IMPMC – UMR CNRS 7590, Sorbonne Universités, UPMC, IRD, MNHN, Muséum National d'Histoire Naturelle, 61 rue Buffon, 75005 Paris, France
[4]Advanced Photon Source, Argonne National Laboratory, Argonne, Illinois 60439, USA
[5]Center for High Pressure Science and Advanced Technology Research (HPSTAR), Pudong, Shanghai 201203, China
[6]Department of Geology, University of Illinois at Urbana-Champaign, Urbana, Illinois 61801, USA

(COMPRES-related facilities: Advanced Photon Source, beamline 3-ID)

Using the Nuclear Resonant Inelastic X-ray Scattering (NRIXS) facility at XOR3 of the Advanced Photon Source, we have investigated iron force constants in iron alloys and silicate materials at high pressures in order to understand the iron isotope fractionation in the deep Earth. Iron isotope ratios have been extensively studied to decipher the origin and evolution of planetary bodies. The enrichment of terrestrial basalts in heavy iron isotopes relative to chondrites was proposed to be a fingerprint of core-mantle segregation. However, the extent of iron isotopic fractionation between molten iron-rich alloys and silicate melts under conditions relevant to core formation is poorly known. Here, we report the experimental determination by NRIXS coupled with a high-pressure diamond anvil cell of the mean force constant $\langle F \rangle$ of iron bonds and reduced isotopic partition function ratios (β-factors) of a basaltic glass, pure iron, and iron-rich Fe-Ni-Si alloy at high pressures. We find that all $\langle F \rangle$ values increase with pressure, and that the $\langle F \rangle$ values of silicate glass are comparable to those of metal. The calculated equilibrium iron isotope fractionation between silicate and iron at conditions relevant to high-pressure core formation in Earth is negligible relative to the measured iron isotope enrichment in terrestrial basalts of ~+0.1 ‰.

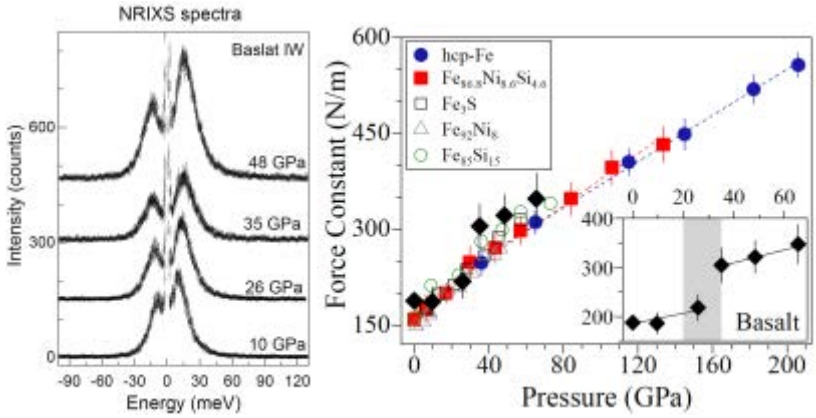

Figure 1. (Left) NRIXS spectra of basaltic glass at high pressures. (Right) Force constants $\langle F \rangle$ of iron bonds in the basaltic glass and Fe-rich alloys at high pressures.

References: J. Liu, Dauphas, N., M. Roskosz, M. Hu, H. Yang, W. Bi, J. Zhao., J., **J. F. Lin**, Iron isotopic fractionation between silicate mantle and metallic core under high-pressure conditions, submitted to Nature Comm., 2016.

Electronic transitions of iron in almandine-composition glass to 91 GPa

S. M. Dorfman, Department of Geological Sciences, Michigan State University, East Lansing, Michigan 48824, U.S.A.
S. E. Dutton, Department of Physics, University of Cambridge, Cambridge CB3 0HE, U.K.
V. Potapkin, Bayerisches Geoinstitut, University of Bayreuth, 95440 Bayreuth, Germany
A. I. Chumakov, European Synchrotron Radiation Facility, BP 220, F-38043 Grenoble, France
J.-P.l Rueff, Synchrotron SOLEIL, L'Orme des Merisiers, BP 48 Saint-Aubin, F-91192 Gif-sur-Yvette, France; Sorbonne Universités, UPMC Université Paris 06, Laboratoire de Chimie Physique-Matière et Rayonnement, F-75005, Paris, France
P. Chow and Y. Xiao, HPCAT, Geophysical Laboratory, Carnegie Institution of Washington, Argonne, Illinois 60439, U.S.A.
R. J. Cava, Department of Chemistry, Princeton University, Princeton, New Jersey 08544, U.S.A.
T. S. Duffy, Department of Geosciences, Princeton University, Princeton, NJ 08544, USA Department of Geosciences, Princeton University, Princeton, New Jersey 08544, U.S.A.
Philippe Gillet, Earth and Planetary Science Laboratory, Ecole polytechnique fédérale de Lausanne, Station 3, CH-1015 Lausanne, Switzerland

The behavior of silicate glasses at high pressures is a key analogue for silicate liquids in the deep Earth, from regions of partial melt to the magma ocean early in Earth's history. While liquids are challenging to study due to high temperatures and limitations of analytical methods, glasses are relatively stable and can be characterized by additional techniques including Mössbauer spectroscopy. We performed a multi-technique high-pressure study of glass isochemical with almandine garnet, a major component of Earth's mantle. Glass starting materials were characterized using the APS sector 3 ^{57}Co-source Mossbauer spectrometer. Nuclear forward scattering, synchrotron Mössbauer source and X-ray emission spectroscopy were used to constrain changes in the electronic environment of iron in almandine glass to 91 GPa. These complimentary techniques demonstrate a high-to-low spin transition in Fe^{3+} in the glass below ~30 GPa and suggest a gradual increase in bonding coordination of Fe^{2+}.

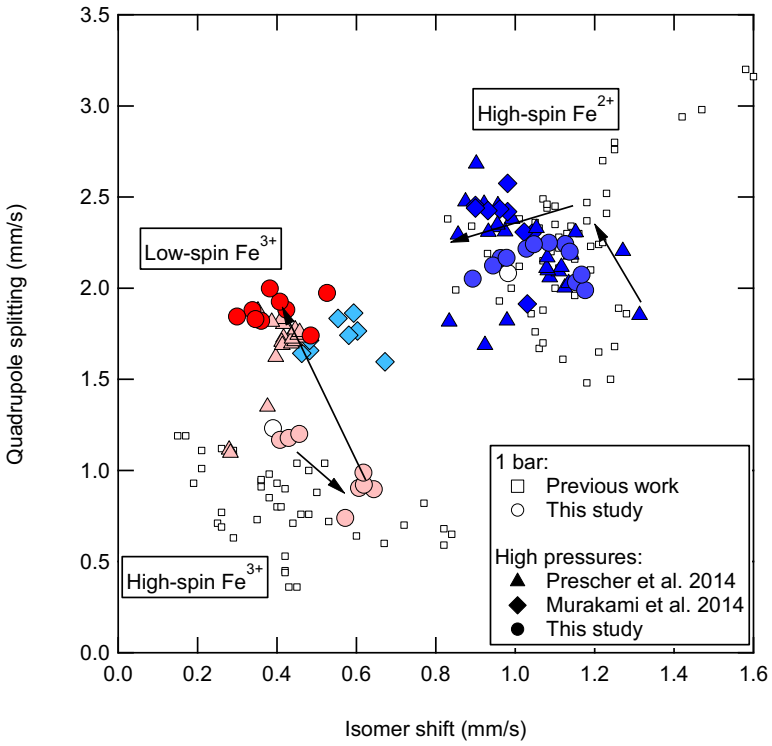

Dorfman, S. M. et al. (2016), Electronic transitions of iron in almandine-composition glass to 91 GPa, *American Mineralogist*, in press, doi:10.2138/am-2016-5606.

Pressure-induced Phase Transition in $MnCO_3$ and its Implications on the Deep Carbon Cycle

E Boulard, A Goncharov, M Blanchard, WL Mao, Stanford University, Carnegie Institution of Washington, CNRS France

(COMPRES-related facilities: National Synchrotron Light Source beamline U2A, Advanced Light Source Beamline 12.2.2)

The high-pressure behavior of Mn-rich carbonate, rhodochrosite, has been characterized up to 62GPa using synchrotron-based midinfrared spectroscopy and X-ray diffraction through diamond anvil cell at U2A, NSLS and ALS 12.2.2. Modifications in both the infrared spectra and the X-ray diffraction patterns were observed above ~35GPa, indicating the presence of a high-pressure phase transition at these pressures. We found that rhodochrosite adopts a structure close to $CaCO_3$-VI with a triclinic unit cell (Fig.1). Using first-principles calculations based on density functional theory, we confirmed these observations and assigned modes in the new infrared signature of the high-pressure phase. These results suggest that high-pressure metastable phase of calcite may play an important role in carbon storage and transport in the deep Earth.

Figure 1. Structure of the high-pressure phase related to the $CaCO_3$-VI phase of calcite [Merlini et al., 2012a]. CO_3 groups appear in black, and Mn^{2+} atoms are shown as violet spheres.

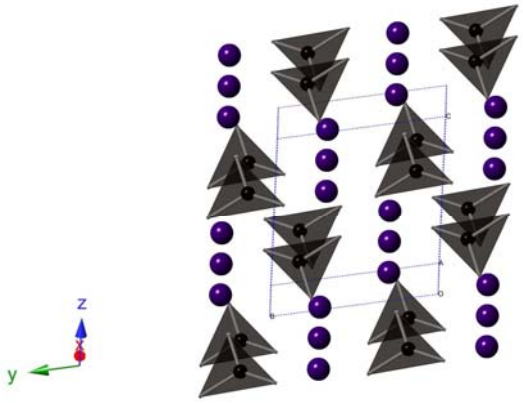

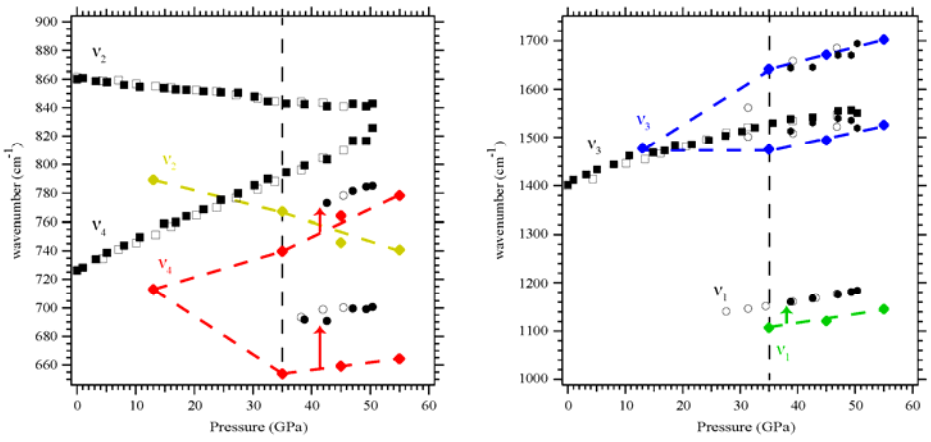

Figure 2. Theoretical (colored symbols) and experimental (black symbols) band positions as a function of pressure. The lines between the calculated band positions are guides for the eye. The arrows indicate assignments of the experimental modes. The vertical lines indicate the pressure of the phase transition (~35 GPa

References: E Boulard, A Goncharov, M Blanchard, W Mao, Pressure-induced Phase Transition in $MnCO_3$ and its Implications on the Deep Carbon Cycle, *J. Geophys. Res.*, **120**(6), 4069-4079 (2015).

Tetrahedrally Coordinated Carbonates in Earth's Lower Mantle

E Boulard, D Pan, G Galli, Z Liu, W Mao, Stanford University, University of Chicago and Carnegie Institution of Washington

(COMPRES-related facilities: National Synchrotron Light Source beamline U2A)

Carbonates are fundamentally distinct from silicates in the Earth's crust in that carbon binds to 3 oxygen atoms, while silicon is bonded to 4 oxygens. Carbonates are the main species that bring carbon deep into our planet through subduction. In order to get insights on the C-O bondings at Earth's mantle conditions, we performed *in situ* Infrared Spectroscopy up to pressure of 103 GPa at NSLS U2A beamline. An unequivocal spectroscopic signature of the high-pressure phase of $(Mg,Fe)CO_3$ was observed above 80 GPa (Fig. 1). Using ab-initio calculations, we assign this new IR signature to C–O bands associated with tetrahedrally coordinated carbon (Fig.2). Tetrahedrally coordinated carbonates are expected to exhibit substantially different reactivity than low-pressure threefold coordinated carbonates, as well as different chemical properties in the liquid state which may have significant implications for carbon reservoirs and fluxes, and the global geodynamic carbon cycle.

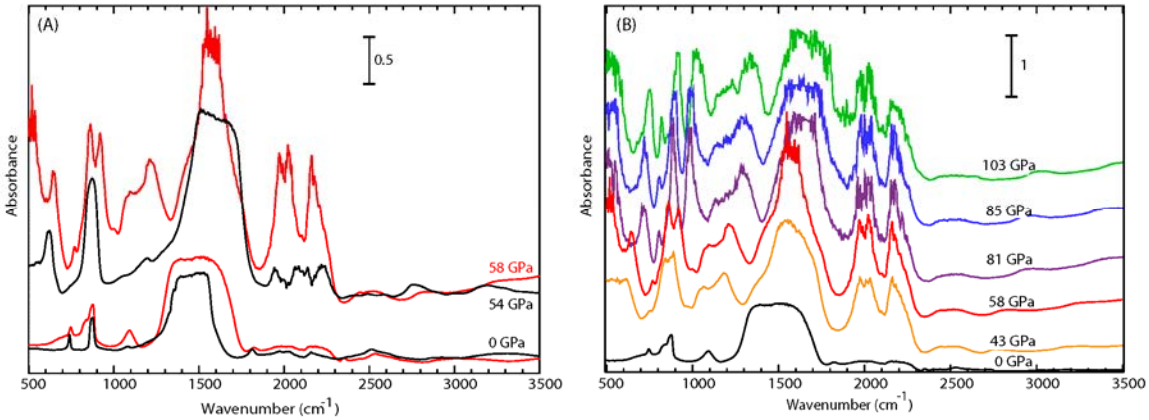

Figure 1. (A) IR spectra collected on compression of the ferromagnesite (black lines) at 0 and 54 GPa, and on decompression of the high-pressure phase (red lines) at 58 and 0GPa. (B) IR spectra collected on the decompression of the post-magnesite phase from 103 to 0GPa. The scale bars give the absorbance scale for each panel.

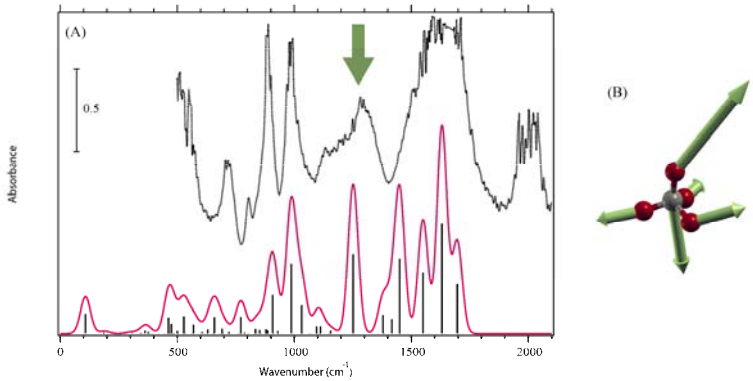

Figure 2. (A) Calculated IR intensities (black lines) and spectrum (solid red line) of the high-pressure phase at 82 GPa. The experimental spectrum collected at 81 GPa is shown as a dotted line. (B) The vibrational mode at 1,252 cm^{-1} (marked by the arrow on A) is identified as a unique signature of the high-pressure phase.

References: E Boulard, D Pan, G Galli, Z Liu, W Mao, Tetrahedrally Coordinated Carbonates in Earth's Lower Mantle, *Nat. Commun.*, **6**, 6311 (2015).

Complex effects of alumina/silica on ferric/ferrous iron in the lower mantle

S. M. Dorfman, Department of Geological Sciences, Michigan State University, East Lansing, Michigan 48824, U.S.A.

The incorporation of iron in bridgmanite, the lower mantle's dominant mineral, is critical to the chemistry and physical properties of the deep Earth. Iron is the most complex major element in the Earth, with multiple possible valence and spin states. Aluminum has been shown to modify the behavior of iron in the mantle by promoting formation of ferric iron over ferrous iron. However, enrichment in silicon is also important to the crystal chemistry of bridgmanite. Iron-rich bridgmanite was synthesized in the laser-heated diamond anvil cell from synthetic ^{57}Fe-enriched enstatite and almandine-composition glass, both compositions rich in ferrous iron and silicon. The valence and spin state of iron in these bridgmanite samples was analyzed by nuclear forward scattering at sector 3 of the Advanced Photon Source and synchrotron Mössbauer spectroscopy at ID18 of the European Synchrotron Radiation Facility. Both Al-free enstatite and Al-bearing almandine samples exhibit at least 75% ferrous iron: in both of these compositions the high Si-content of the bridgmanite B-site promotes ferrous iron over ferric iron. Spectra also show an increase in quadrupole splitting of the ferrous iron with pressure, consistent with previous studies and density functional theory predictions of electronic changes in the A-site of bridgmanite.

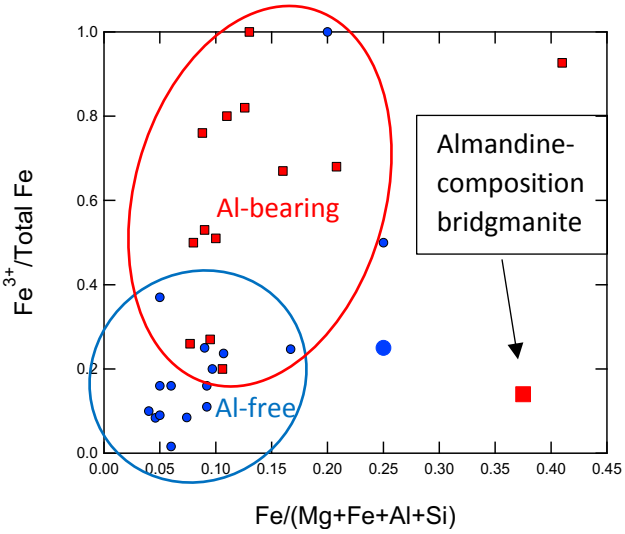

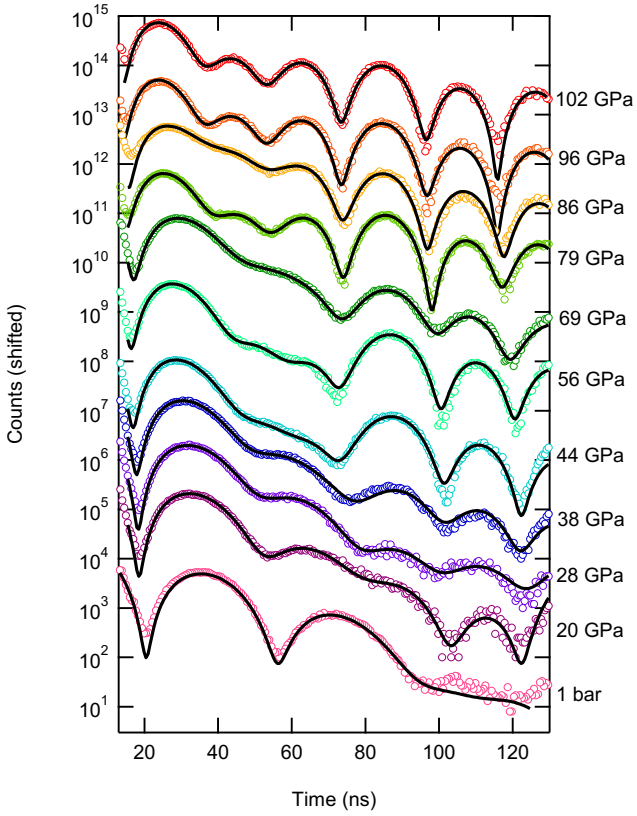

Dorfman, S. M., V. Potapkin, I. Kupenko, A. I. Chumakov, F. Nabiei, A. Magrez, L. Dubrovinsky, C. A. McCammon, and P. Gillet (2014), Complex Effects of Alumina/Silica on Ferric/Ferrous Iron in Earth's Lower Mantle, *American Geophysical Union Fall Meeting 2014*, San Francisco.

Dorfman, S. M., S. E. Dutton, L. Gao, R. J. Cava, Y. Meng, J. Zhao, E. E. Alp, and T. S. Duffy, Synchrotron Mossbauer spectroscopy of perovskite and post-perovskite synthesized from almandine end-member, in prep.

Effect of iron on the physical properties of ferropericlase

Natalia V Solomatova, Wolfgang Sturhahn, Jennifer M Jackson
Seismological Laboratory, Caltech, Pasadena, CA, United States

(COMPRES facilities used: Sector 3 at the Advanced Photon Source, Chicago area, IL and Beamline 12.2.2 at the Advanced Light Source, Berkeley, CA)

Iron plays an essential role in controlling the behavior of materials on the surface and interior of Earth. The lower mantle, which occupies more than half of Earth's volume, is composed primarily of bridgmanite, Ca-perovskite and ferropericlase. Knowledge of the elastic and structural properties of lower mantle minerals is essential for interpreting complexity in the deep Earth, which in turn can drive dynamics of material transport. We have examined the high-pressure behavior of polycrystalline (Mg,Fe)O containing 48 mol% FeO, loaded hydrostatically with neon as a pressure medium. Using x-ray diffraction and synchrotron Mössbauer spectroscopy at Sector 3 of the Advanced Photon Source (Argonne National Laboratory, IL), we measured the equation of state to about 83 GPa and hyperfine parameters to 107 GPa at 300 K. A gradual volume drop corresponding to a high-spin (HS) to low-spin (LS) crossover was observed between ~45 and 83 GPa with a volume drop of 1.85% at 68.8(2.7) GPa, the calculated spin transition pressure (*Solomatova et al.* 2016). A systematic analysis of all reported data using similar techniques is presented and clear compositional trends in spin transition pressure and width are observed.

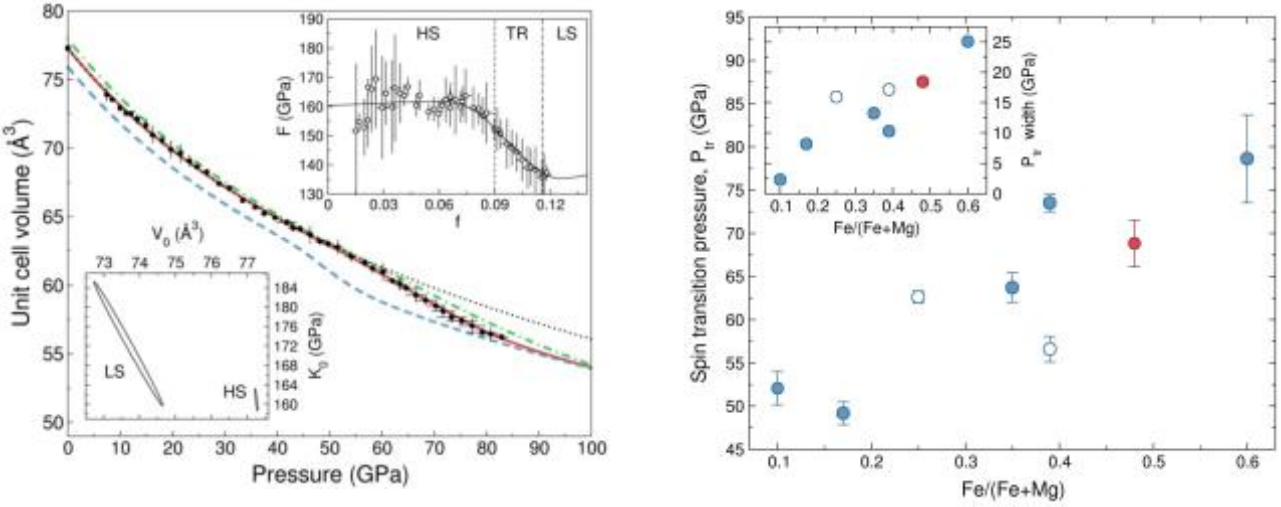

Figure 1. (left) Pressure-volume relationship of Fp48 at 300 K (data points, solid red curve), using a spin crossover equation of state to fit and analyze the data (Sturhahn, www.nrixs.com 2016). Normalized pressure (F) versus Eulerian strain (f) is, as well as the covariance ellipses for the HS and LS states for the parameters, K_{0T} and V_0, where $K'_{0T,LS}$ was fixed to 4, for Fp48. The dashed blue curve and dashed dotted green curve are the spin crossover EOS's fitted with MINUTI to (Mg,Fe)O data with 17 mol% and 60 mol% FeO, respectively. **(right)** Spin transition pressure and width of $(Mg_{(1-x)}Fe_x)O$ as a function of iron concentration, the latter defined as the 20-80% volume drop. $(Mg_{(1-x)}Fe_x)O$ with x=0.10 (Marquardt et al., 2009), x=0.17 (Lin et al., 2005), x=0.25 (Mao et al., 2011), x=0.35 (Chen et al., 2012), x=0.39 (Zhuravlev et al., 2010; Fei et al., 2007), x=0.48 (Solomatova et al. 2016), and x=0.60 (Lin et al., 2005).

Solomatova, N.V., Jackson, J.M., Sturhahn, W., Wicks, J.K., Zhao, J., Toellner, T.S., Kalkan, B., Steinhardt, W.M. (2016): Equation of state and spin crossover of (Mg,Fe)O at high pressures, American Mineralogist, 101, 1084-1093.

Thermal equation of state and stability of $(Mg_{0.06}Fe_{0.94})O$

J. Wicks,[1,2] J. M. Jackson,[2] W. Sturhahn,[1] K. K. Zhuravlev,[3] S. N. Tkachev,[3] V. B. Prakapenka,[3]
[1]*Division of Geological and Planetary Sciences, California Institute of Technology, Pasadena, CA*
[2]*Department of Geosciences, Princeton University, Princeton, NJ*
[3]*Center for Advanced Radiation Sources, University of Chicago, Chicago, IL*

(COMPRES-related facilities: Advanced Photon Source, the gas-loading system at GSECARS and conventional Mössbauer spectroscopy laboratory at Sector 3)

We measured the pressure–volume–temperature (P–V–T) equation of state of polycrystalline $(Mg_{0.06}Fe_{0.94})O$ (Mw94) determined from laser-heated X-ray diffraction experiments up to 122 GPa and 2100 K, conditions approaching those of the deep mantle. In the sampled P–T range of the high temperature part of this study, only the B1 structure of Mw94 was observed, indicating that the addition of Mg to FeO stabilizes the B1 phase with respect to the B8 phase at these conditions. Fitting to a Birch–Murnaghan and Mie–Grüneisen–Debye thermal equation of state was carried out using a new open-source fitting routine (seos) within the MINeral physics Utility software package (MINUTI, www.nrixs.com). We've also compared the thermal equation of state of Mw94 to that of wüstite and conclude that Mw94 has measurably distinct thermoelastic properties compared with those of wüstite.

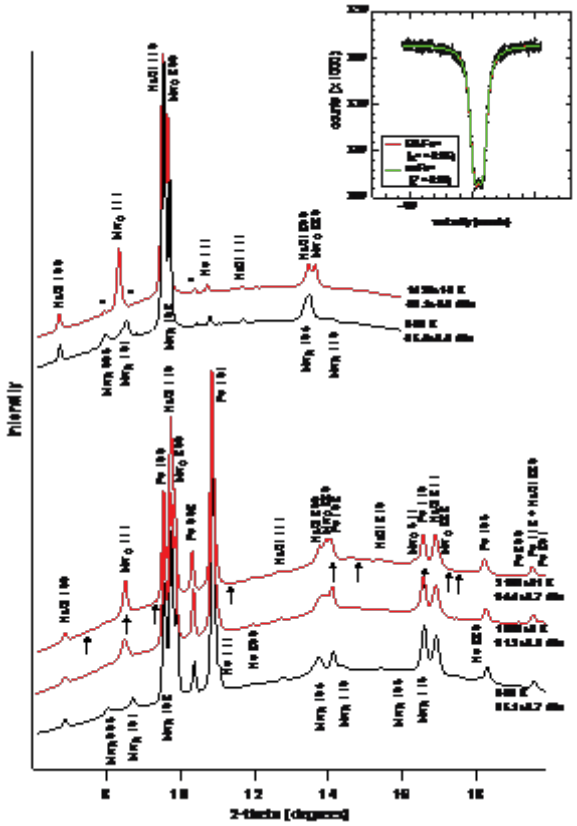

Figure 1. Example integrated XRD patterns showing peak identifications for *B2*-NaCl, *hcp*-Fe, and Ne. Pressures were determined using the equation of state of *B2*-NaCl (Fei et al., 2007) for the unbuffered dataset (top two patterns), and hcp-Fe (Dewaele et al., 2006; Murphy et al., 2011) for the buffered dataset (bottom three patterns). $(Mg_{0.06}Fe_{0.94})O$ is rhombohedral at room temperature (Mw_R, *R-3m*) and cubic at high temperature (Mw_C, *Fm-3m*). Unidentified peaks are labeled with *. Arrows indicate location of expected B8 peaks at these conditions (Ozawa et al., 2011). Inset: A conventional Mössbauer spectrum of Mw94 before heating at 1 bar (Wicks, 2013), with two example fits (no Fe^{3+}, green, and 5% Fe^{3+}, red.)

References: J. Wicks, J. M. Jackson, W. Sturhahn, K. K. Zhuravlev, S. N. Tkachev, and V. B. Prakapenka, Phys. Earth Planet. Int. **249**, 28—42 (2015).

Report from Yale Karato's lab

Deformation experiments under the deep mantle conditions

Using NSLS I, we have conducted deformation experiments at high pressure and temperature under the controlled strain-rate. The experiments were conducted using the RDA (rotational Drickamer apparatus) designed in the Karato's lab using the white x-ray beam facility at NSLS I (X-17B2). The main thrust has been to extend the pressure range. At the time of writing, the maximum pressure we conducted deformation experiments is 28 GPa (at T=2100 K) and we made the first deformation experiments on the bridgmanite + ferropericlase mixtures to large strain (**Fig. 1a, b**). The results showed a large contrast in creep strength between these two minerals suggesting that deformation in the lower mantle might be localized (Girard et al., 2016).

Similarly we conducted deformation experiments on wadsleyite, ringwoodite and MgO under the deep mantle conditions.

(1) (2)

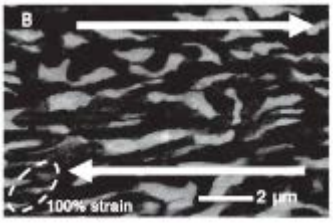

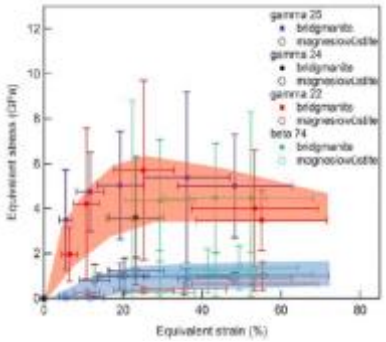

Fig. (1): SEM photograph of deformed bridgmanite + ferropericlase aggregate (brighter one is ferropericlase).

Fig. (2): Strength of bridgmanite and ferropericlase as a function of strain (at P=27 GPa and T-2100 K and strain rate of ~10^{-5} s^{-1}.

Synchrotron Mössbauer studies

We also use the synchrotron Mössbauer facility at APS to study the formation of metallic Fe in the lower mantle. We have clear evidence of co-existence of metallic Fe with ferric Fe in bridgmanite (closed system behavior) but also evidence of formation of metallic Fe in (Mg,Fe)O by reduction (open system behavior). The results of this study has an important implication for melting in the lower mantle.

Reference

Girard, J., Amulele, G., Farla, R. and Karato, S., 2016. Shear deformation experiment of bridgmanite + magnesiowüstite aggregates under the lower mantle conditions, *Science,* 351: 144-147.

Enhancement of Thermoelectric Performance with Pressure in $Ce_{0.8}Fe_3CoSb_{12.1}$

Matthew K. Jacobsen , Wei Liu and Baosheng Li (all at Stony Brook University)

(COMPRES-related facilities: Multi-anvil Cell Assemblies Facility)

Transport properties (resistivity, thermal conductivity, and Seebeck coefficient) and sound velocities have been determined for the skutterudite $Ce_{0.8}Fe_3CoSb_{12.1}$ with pressure up to 14 GPa. From these measurements, high pressure anomalous features were found in all transport properties. By correlating these with results from previous x-ray work, it has been determined that there is likely an electronic topological transition in this material induced by pressure. This is possibly due to the known pressure variation of valence in the void-filling Ce atom and has been found to induce an improved figure of merit at higher pressures, which shows a nearly two-fold increase with applied pressure. At higher pressures, it was determined that this anomalous behavior is suppressed and is possibly induced by insertion of Sb from the cage into the remaining central voids of the structure, similar to that seen in the $CoSb_3$ parent compound.

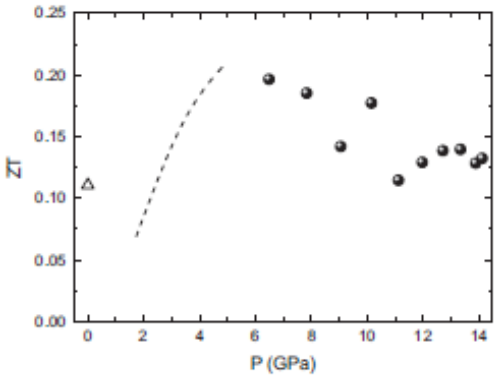

Fig. 1. ZT value as a function of pressure determined in this study for $Ce_{0.8}Fe_3CoSb_{12.1}$.

Reference

Jacobsen, M., W. Liu, B. Li (2014), Enhancement of Thermoelectric Performance with Pressure in $Ce_{0.8}Fe_3CoSb12.1$, Journal of Physics and Chemistry of Solids, 75, 1017–1023, 2014.

Hexagonal-structured ε-NbN:ultra-incompressibility, high shear rigidity, and a possible hard superconducting material

Yongtao Zou[1,2], Xuebing Wang[3], Ting Chen[3], Xuefei Li[1], Xintong Qi[3], David Welch[4,5], Pinwen Zhu[2], Bingbing Liu[2], Tian Cui[2] & Baosheng Li[1]
[1]Mineral Physics Institute, State University of New York, USA
[2]College of Physics, Jilin University, China.
[3]Department of Geosciences, State University of New York, USA.
[4]Department of Materials Science and Engineering, State University of New York, USA.
[5]Condensed Matter Physics and Materials Science Department, BNL, USA.

(COMPRES-related facilities: Multi-anvil Cell Assembly Facility)

Exploring the structural stability and elasticity of hexagonal ε-NbN helps discover correlations among its physical properties for scientific and technological applications. Here, for the first time, we measured the ultra-incompressibility and high shear rigidity of polycrystalline hexagonal ε-NbN using ultrasonic interferometry and in situ X-ray diffraction, complemented with first-principles density-functional theory calculations up to 30 GPa in pressure. Using a finite strain equation of state approach, the elastic bulk and shear moduli, as well as their pressure dependences are derived from the measured velocities and densities, yielding B_{S0} = 373.3(15) GPa, G_0 = 200.5(8) GPa, $\partial B_S/\partial P$ = 3.81(3) and $\partial G/\partial P$ = 1.67(1). The hexagonal ε-NbN possesses a very high bulk modulus, rivaling that of superhard material cBN (B_0 = 381.1 GPa). The high shear rigidity is comparable to that for superhard γ-B (G_0 = 227.2 GPa). We found that the crystal structure of transition-metal nitrides and the outmost electrons of the corresponding metals may dominate their pressure dependences in bulk and shear moduli. In addition, the elastic moduli, Vickers hardness, Debye temperature, melting temperature and a possible superconductivity of hexagonal ε-NbN all increase with pressures, suggesting its exceptional suitability for applications under extreme conditions.

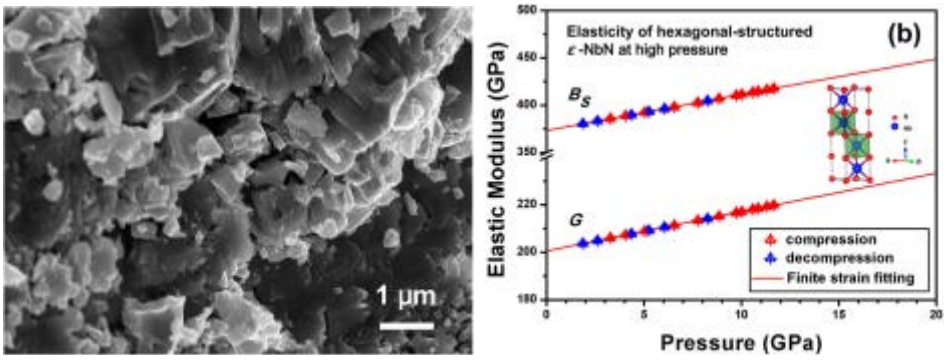

Fig. 1. SEM image (left) and the elastic moduli as a function of pressure (right).

Reference

Zou Y., X. Li, X. Wang, T. Chen, X. Qi, D. Welch, P. Zhu, B. Liu, T. Cui, and B. Li (2015). Hexagonal-structured ε-NbN: ultra-incompressibility, high shear rigidity, and a possible hard superconducting material, Scientific Reports 5, doi:10.1038/srep10811.

High-pressure behavior and thermoelastic properties of niobium studied by in situ x-ray diffraction

Yongtao Zou, Xintong Qi, Xuebing Wang, Ting Chen, Xuefei Li, David Welch, and Baosheng Li (all at Mineral Physics Institute, Stony Brook University, U.S.A)

(COMPRES-related facilities: National Synchrotron Light Source beamline X17B2, X17C)

In situ synchrotron energy dispersive x-ray diffraction (XRD) experiments on Nb have been conducted at pressures up to 6.4 GPa and temperatures up to 1073 K. From the pressure volume-temperature measurements, thermoelastic parameters were derived for the first time for Nb based on the thermal pressure (DPth) equation of state (EOS), modified high-T Birch-Murnaghan EOS, and Mie-Gruneisen-Debye EOS. With the pressure derivative of the bulk modulus K0 T fixed at 4.0, we obtained the ambient isothermal bulk modulus K_{T0} = 174(5) GPa, the temperature derivative of bulk modulus at constant pressure $[dK_T/dT]_P$ = -0.060(8) GPa K^{-1} and at constant volume $[dK_T/dT]_V$ = 0.046(8) GPa K^{-1}, the volumetric thermal expansivity $\alpha_T(T)$ = 2.3(3) x10^{-5} + 0.3(2) x 10-8T (K^{-1}), as well as the pressure dependence of thermal expansion $[d\alpha = dP]_T$ = -2.060(4) x 10^{-6} K^{-1} GPa^{-1}. Fitting the present data to the Mie-Gruneisen-Debye EOS with Debye temperature 276.6K gives γ_0 =1.27(8) and K_{T0} =171(3) GPa at a fixed value of q = 3.0. The ambient isothermal bulk modulus and Gruneisen parameter derived from this work are comparable to previously reported values from both experimental and theoretical studies. An in situ high-resolution, angle dispersive XRD study on Nb did not indicate any anomalous behavior related to pressure-induced electronic topological transitions at ~5 GPa as has been reported previously.

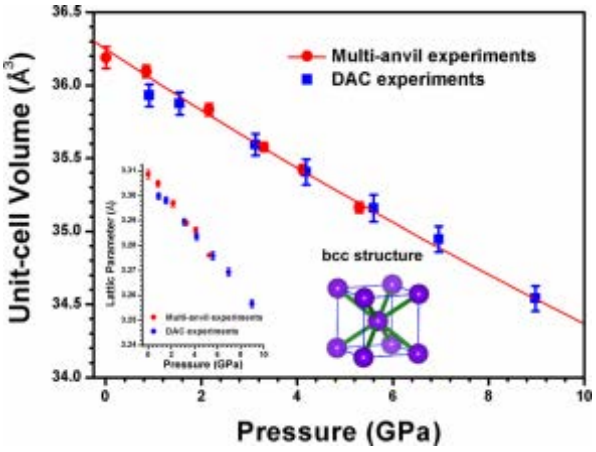

Fig. 1. P-V relations for Nb at room temperature obtained from the current multi-anvil experiment (solid red circles), in comparison with those fromour DAC experiments (blue squares). The red curve shows the fitting results of this study using the third-order Birch-Murnaghan equation of state.

Reference

Zou, Y., X. Qi, X. Wang, T. Chen, X. Li, D. Welch, and B. Li (2014), High-pressure behavior and thermoelastic properties of niobium studied by in situ x-ray diffraction, J. Appl. Phys. 116, 013516, 2014..

Discovery of Superconductivity in Hard Hexagonal ε-NbN

Yongtao Zou[1,2], Xintong Qi[2], Cheng Zhang[3], Shuailing Ma[1], Wei Zhang[4], Ying Li[2], Ting Chen2, Xuebing Wang[2], Zhiqiang Chen[2], David Welch[2,3], Pinwen Zhu[1], Bingbing Liu[1], Qiang Li[3], Tian Cui[1] and Baosheng Li[2]

[1]Jilin University [2]State University of New York [3]Brookhaven National Laboratory

[4]Southwest University of Science and Technology;

(COMPRES-related facilities: National Synchrotron Light Source Beamline X17C)

Since the discovery of superconductivity in boron-doped diamond with a critical temperature (T_C) near 4 K, great interest has been attracted in hard superconductors such as transition-metal nitrides and carbides. Here we report the new discovery of superconductivity in polycrystalline hexagonal ε-NbN synthesized at high pressure and high temperature. Direct magnetization and electrical resistivity measurements demonstrate that the superconductivity in bulk polycrystalline hexagonal ε-NbN is below ~11.6 K, which is significantly higher than that for boron-doped diamond. The nature of superconductivity in hexagonal ε-NbN and the physical mechanism for the relatively lower T_C have been addressed by the weaker bonding in the Nb-N network, the co-planarity of Nb-N layer as well as its relatively weaker electron-phonon coupling, as compared with the cubic δ-NbN counterpart. Moreover, the newly discovered ε-NbN superconductor remains stable at pressures up to ~20 GPa and is significantly harder than cubic δ-NbN; it is as hard as sapphire, ultra-incompressible and has a high shear rigidity of 201 GPa to rival hard/superhard material γ-B (~227 GPa). This exploration opens a new class of highly desirable materials combining the outstanding mechanical/elastic properties with superconductivity, which may be particularly attractive for its technological and engineering applications in extreme environments.

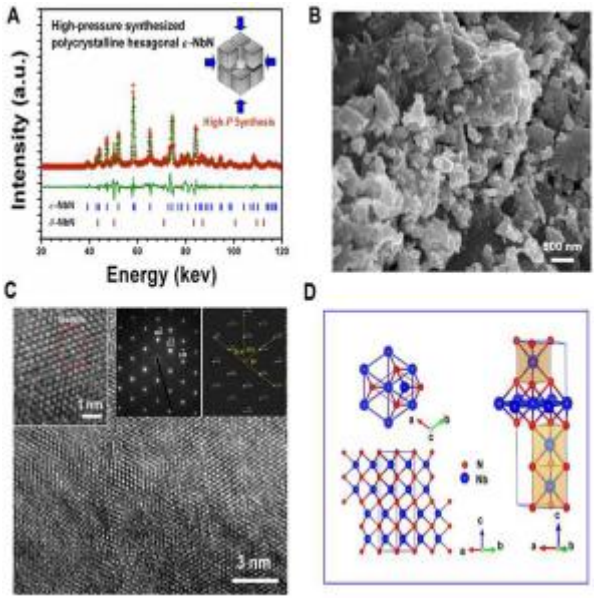

Figure 1. (A). Observed (red crosses) and fitted (olivine lines) X-ray diffraction pattern of the polycrystalline niobium nitride specimen. The peak positions of the hexagonal ε-NbN and cubic δ- structures are denoted by tick marks.
(B). SEM image showing the microstructure of the synthesized polycrystalline hexagonal-structured ε-NbN for the current measurements.
(C). High resolution TEM (HRTEM) of the synthesized specimen; the corresponding observed and simulated SAED patterns and the enlarged portion of the HRTEM image are displayed as insets.
(D) Crystal structure of the hexagonal ε-NbN ($P6_3/mmc$). The blue large and red small spheres represent Nb and N atoms, respectively.

Reference

Zou, Y., X. Qi, C. Zhang, S. Ma, W. Zhang, Y. Li, T. Chen, X. Wang, Z. Chen, D. Welch, P. Zhu, B. Liu, Q. Li, T. Cui, B. Li (2016). Discovery of Superconductivity in Hard Hexagonal ε-NbN, *Scientific Reports*, 6, 22330, doi:10.1038/srep22330.

Experimental and first-principles studies on the elastic properties of α-hafnium metal under pressure

Xintong Qi, Xuebing Wang, Ting Chen, and Baosheng Li (Mineral Physics Institute, Stony Brook University, U.S.A)

(COMPRES-related facilities: Multi-anvil Cell Assembly Facility)

Compressional and shear wave velocities of the a phase of hafnium have been measured up to 10.4 GPa at room temperature using ultrasonic interferometry in a multi-anvil apparatus. A finite strain equation of state analysis yielded K_{S0} = 110.4(5) GPa; G_0 = 54.7(5) GPa; K_0' = 3.7; and G_0' = 0.6 for the elastic bulk and shear moduli and their pressure derivatives at ambient conditions. Complementary to the experimental data, the single crystal elastic constants, the elastic anisotropy, and the unit cell axial ratio c/a of a-hafnium at high pressures were investigated by Density Functional Theory (DFT) based first principles calculations. A c/a value of 1.605 is predicted for α-Hf at 40GPa, which is in excellent agreement with previous experimental results. The low-pressure derivative of the shear modulus observed in our experimental data up to 10 GPa was found to originate from the elastic constant C44, which exhibits negligible pressure dependence within the current experimental pressure range. At higher pressures (>10GPa), C44 was predicted to soften and the shear wave velocity trended to decrease with pressure, which can be interpreted as a precursor to the a-x transition similar to that observed in other group IV elements (titanium and zirconium). The acoustic velocities, the bulk and shear moduli, and the acoustic Debye temperature (240.1 K) determined from the current experiments were all compared well with those predicted by our theoretical DFT calculations.

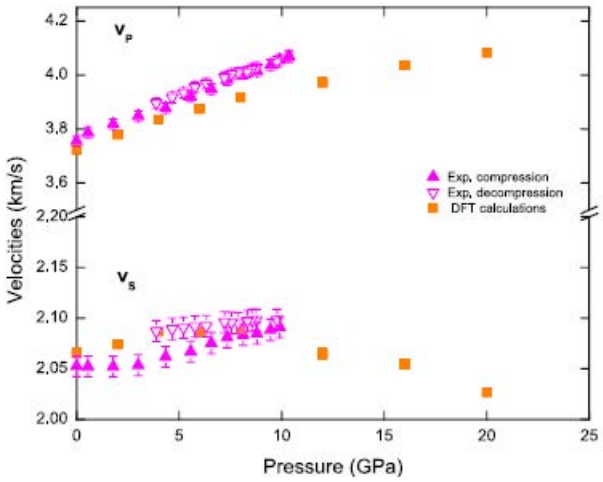

Fig. 1 Compressional (V_P) and shear (V_S) wave velocities of a-hafnium as a function of pressure. The triangles are data from high pressure experiment, and the squares are data from DFT calculations.

Reference

Qi, X., X Wang, T Chen, B Li(2016), Experimental and first-principles studies on the elastic properties of α-hafnium metal under pressure, J App Phys,119, 125109.

Pressure-induced Stiffness of Nano Au to 71 GPa under Quasi-hydrostatic Loading

Xinguo Hong[1], Thomas S. Duffy[2], Lars Ehm[1,3] and Donald J. Weidner[1]

[1]*Mineral Physics Institute, Stony Brook University, Stony Brook, NY 11794, USA*
[2]*Department of Geosciences, Princeton University, Princeton, NJ 08544, USA*
[3]*Photon Sciences Directorate, Brookhaven National Laboratory, Upton, NY 11973, USA*

The mechanical properties of nanoparticles defined by both elastic and plastic properties are fundamental quantities in physics, engineering and geoscience, and can be determined by X-ray diffraction at high pressure. The compressibility of nanocrystalline gold (n-Au, 20 nm) has been studied by X-ray total scattering using high-energy monochromatic X-rays in the diamond anvil cell (DAC) under quasi-hydrostatic conditions up to 71 GPa. The bulk modulus, K_0, of the n-Au obtained from fitting to a Vinet equation of state is ~196(3) GPa, which is about 17% higher than for the corresponding bulk materials (K_0: 167 GPa). At low pressures (<7 GPa), the compression behavior of n-Au shows little difference from that of bulk Au. With increasing pressure, the compressive behavior of n-Au gradually deviates from the equation of state (EOS) of bulk gold. Analysis of the pair distribution function (PDF), peak broadening and Rietveld refinement reveals that the microstructure of n-Au is nearly a single-grain/domain at ambient conditions, but undergoes substantial pressure-induced reduction in grain size until 10 GPa. Full-pattern analysis confirms that significant changes in grain size, stacking faults, grain orientation and texture occur in n-Au at high pressure. We have observed direct experimental evidence of a transition in compression mechanism for n-Au at ~20 GPa, i.e., from deformation dominated by nucleation and motion of lattice dislocations (dislocation-mediated) to a prominent grain boundary mediated response to external pressure. The internal microstructure inside the nanoparticle (nanocrystallinity) plays a critical role for the macro-mechanical properties of nano-Au.

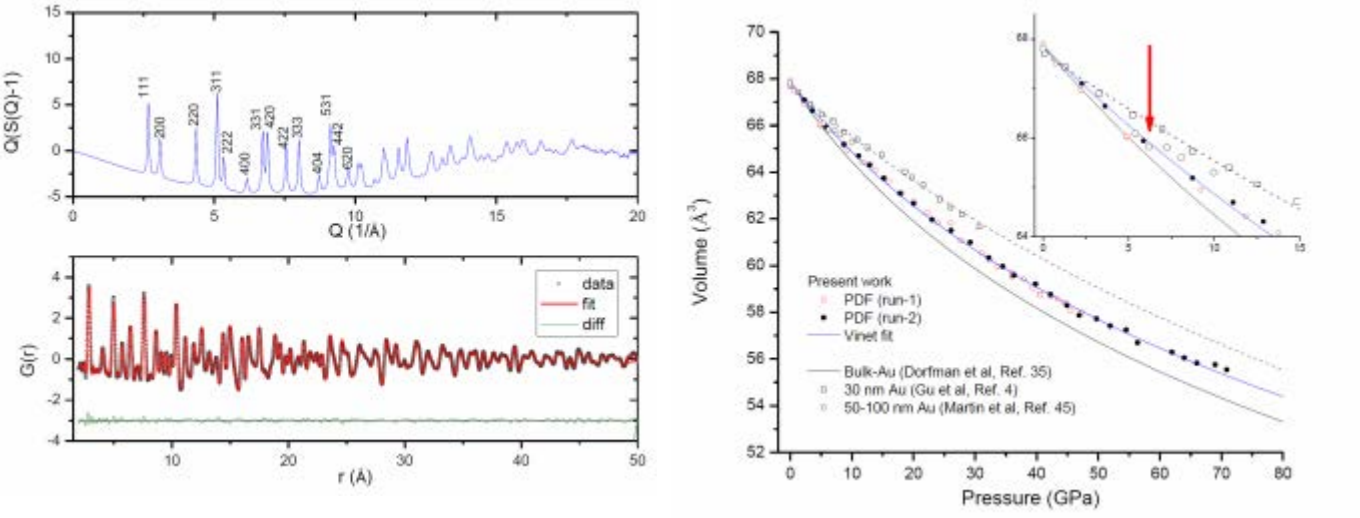

Left: (Upper panel) Total scattering function *F(Q)* of nano Au powder at ambient pressure using high-energy X-ray microbeam (81.400±0.024 keV). (Lower panel) Points are the measured PDF function *G(r)* while lines are the simulated PDFs for 22 nm n-Au with a fit residual, R_w, of 0.094. **Right:** Pressure dependence of the unit cell volume of n-Au compared to previously reported data for 30 nm Au (dashed line) and the bulk material (solid line). Vinet EOS fit is shown for the PDF data of run-1 and run-2.

Reference: Hong, X., T. S. Duffy, L. Ehm and D. J. Weidner, Pressure-induced stiffness of Au nanoparticles to 71 GPa under quasi-hydrostatic loading, *Journal of Physics: Condensed Matter* **27**: 485303, 2015.

Polyhedral Units and Network Connectivity in GeO_2 Glass at High Pressure: an X-Ray Total Scattering Investigation

Xinguo Hong[1], Lars Ehm[1,2] and Thomas S. Duffy[3]

1Mineral Physics Institute, Stony Brook University, Stony Brook, NY 11794
2Photon Sciences Directorate, Brookhaven National Laboratory, Upton, NY 11973
3Department of Geosciences, Princeton University, Princeton, New Jersey 08544

Pressure-induced structural changes of the 'strong' network-forming SiO_2 and GeO_2 glasses have been extensively studied due to their importance in glass, materials and geological sciences. Accurate determination of the pressure-dependent structure is necessary for understanding the mechanisms of network compression and corresponding property changes in SiO_2 and GeO_2 glasses. Germanium dioxide (GeO_2) is regarded as a chemical and structural analogue of silica (SiO_2) with similar pressure response at lower pressures due to the larger ionic radius of Ge^{4+}. The authors report a pressure-induced dense tetrahedral intermediate state via Ge–O–Ge rotation formed at 3–5 GPa and the polyhedral relations in GeO_2 glass up to 17.5 GPa using in situ X-ray total scattering and X-ray absorption (XAFS) techniques. It was found that the nearest-neighbor Ge–Ge correlations show a decrease reaching a minimum between 4 and 6 GPa, and exhibit negative compression behavior at 7–17.5 GPa. The Ge–Ge distance determined by XAFS shows a substantial reduction, i.e., normal compression behavior, at 7–17.5 GPa. The comparison with the theoretical g(r) function for rutile-type GeO_2 (16.1GPa) indicates that the negative compression of intermediate range order reflects the direct formation of GeO_6 octahedral units. Results of coordination number analysis show that GeO_2 glass undergoes a transition from tetrahedral GeO_4, to GeO_5 units (possibly triangular bipyramidal), and finally to octahedral GeO_6 units. The present investigation provides the structural details of the polyhedral units and their relationships in GeO_2 glass at high pressure.

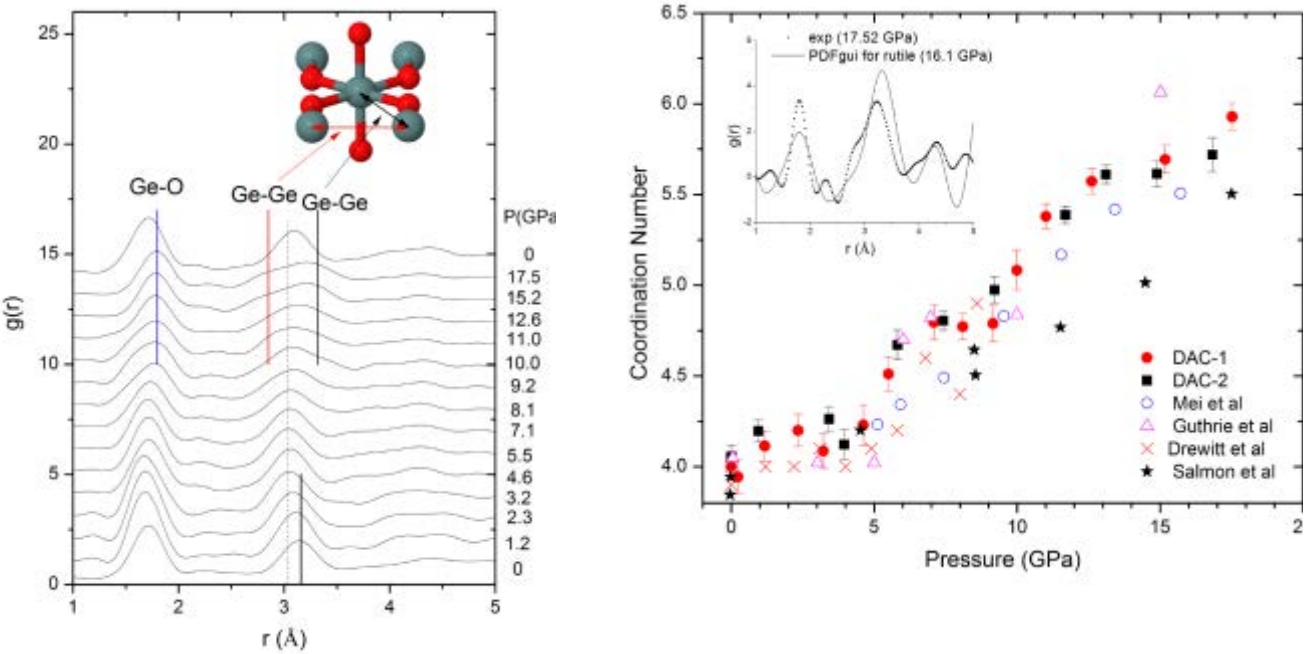

Left: Pair distribution function *g(r)* for GeO_2 glass; **Right**: The pressure evolution of the mean coordination number N_{Ge}^{O} for GeO_2 glass

Reference: Hong, X., L. Ehm and T. S. Duffy, Polyhedral units and network connectivity in GeO_2 glass at high pressure: An X-ray total scattering investigation, *Applied Physics Letters*, **105**: 081904, 2014.

High-Pressure X-Ray Absorption Spectroscopy (HP-XAFS) of GeO_2 Glass to 64 GPa

Xinguo Hong[1], Matt Newville[2], Thomas S. Duffy[3], Stephen R. Sutton[2,4], and Mark L. Rivers[2,4]

[1]Mineral Physics Institute, Stony Brook University, Stony Brook, NY 11794
[2]Consortium for Advanced Radiation Sources and [4]Department of Geophysical Sciences, University of Chicago, Chicago, Illinois 60637
[3]Department of Geosciences, Princeton University, Princeton, New Jersey 08544

XAFS can be a powerful tool to determine the local (SRO) and higher-order (IRO) structure around absorber atoms at high pressures. However, due to the Bragg reflections from the diamond anvils, it has long been regarded unsuitable for the DAC environment. In this study, the authors have reported a further development of HP-XAFS and applications to the structure of GeO_2 glass up to 64 GPa. It is found that the difference between the nearest Ge–O distances of glassy and rutile-type GeO_2 disappears at the Ge–O distance maximum at 20 GPa. The mean-square displacement σ^2 of the Ge–O distance in the first Ge–O shell increases progressively to a maximum at 10 GPa, followed by a substantial reduction at higher pressures. The differences in Ge–O distance and density between the glass and the crystals are gradually eliminated over the 20–40 GPa pressure range. Above 40 GPa, GeO_2 forms a dense octahedral glass with a compressibility similar to that of the corresponding crystalline phase (α-PbO_2 type). The Ge–O bond distance shows little change between 45–64 GPa, and this may reflect a balance between bond shortening and a gradual coordination number increase with compression. The density data provide evidence for a possible discontinuity and change in compressibility at 40–45 GPa, but there are no major changes in the corresponding EXAFS spectra. A pyrite-type local structural model for the glass can provide a reasonable fitting to the XAFS spectra at 64 GPa.

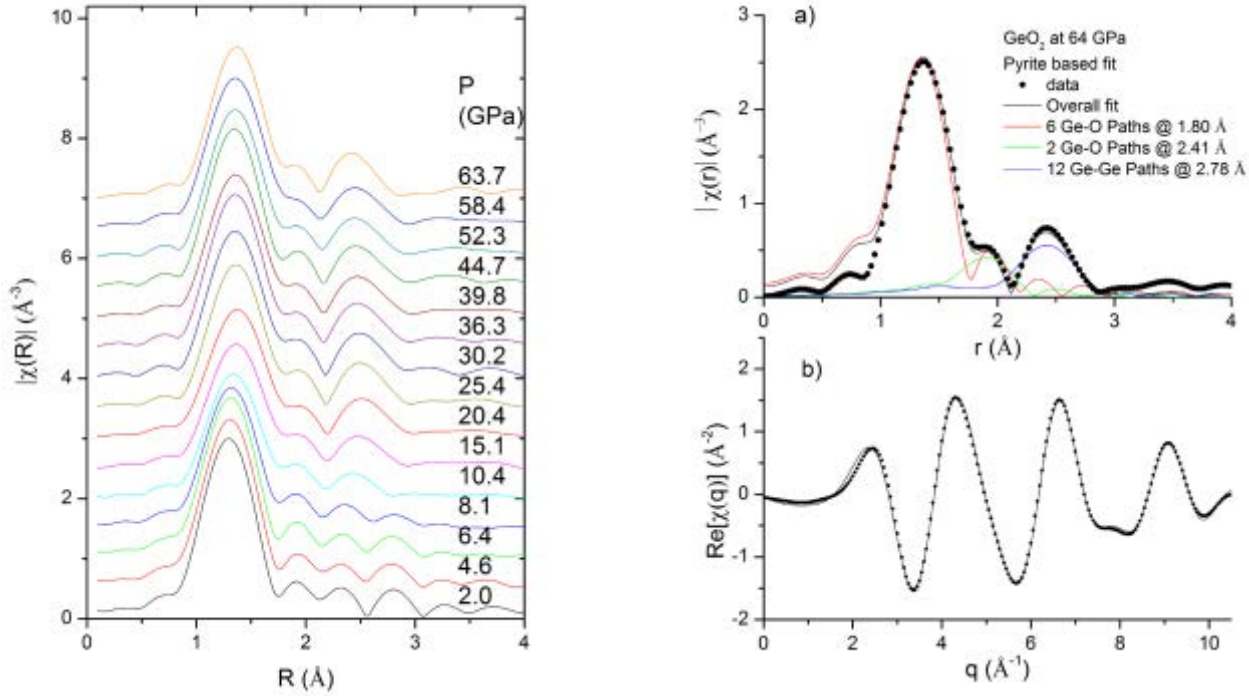

Left: XAFS Fourier transform, $|\chi(R)|$, for GeO_2 glass at high pressures. Note the merging of two peaks (2.2—3Å) at 10.4 GPa. **Right**: The pyrite-based structural modelling for GeO_2 glass at 63.7 GPa.

Reference: Hong, X., M. Newville, T. S. Duffy, S. R. Sutton and M. L. Rivers, X-ray absorption spectroscopy of GeO_2 glass to 64 GPa, *Journal of Physics: Condensed Matter*, **26**: 035104, 2014.

Pressure-driven variations of hydrogen bonding energy in ammonium azide (NH4N3): IR absorption and Raman scattering studies

Xiaoxin Wu, Fengxian Ma, Chunli Ma, Hang Cui, Zhenxian Liu (GL-CIW), Hongyang Zhu, Xiaoli Wang, and Qiliang Cui, Jilin University

(COMPRES-related facilities: NSLS, U2A Beamline at Brookhaven National Laboratory)

In this study, high pressure infrared (IR) absorption and Raman scattering studies for ammonium azide (NH_4N_3) were carried out at room temperature up to 20 GPa and 22 GPa, respectively. The recorded vibrational data consistently indicated a pressure-induced phase transition at 2.9 GPa. All observed vibrational modes maintained their identities at the high pressure phase, indicating that NH_4N_3 was still presented in the form of ammonium cations and azide anions linked by the hydrogen bond (N–H…N). The hydrogen bonding energy exhibited a weakening (0 - 2.9 GPa), strengthening (2.9 - 12 GPa), and then again weakening (12 - 22 GPa) phenomena with the increasing of compression. The hydrogen bonding energy variation with the increase of pressure can be ascribed to a phase transition at 2.9 GPa and a rotational or bending behavior of azide ions at 12 GPa.

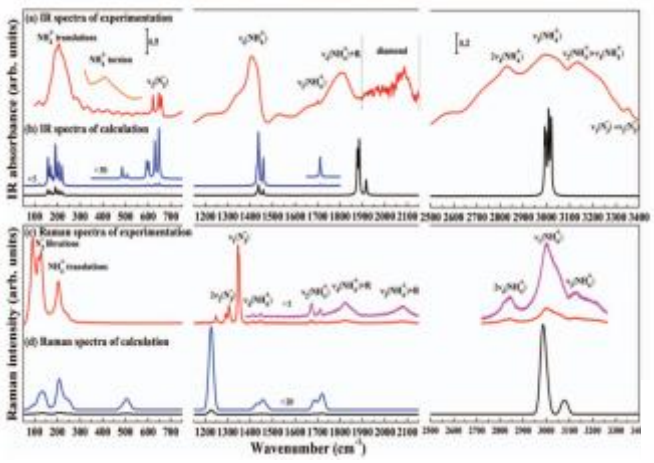

Figure 1. Experimental and calculated IR and Raman spectra of NH_4N_3 at ambient conditions. The red lines in (a) and (c) are experimental spectra and the black lines in (b) and (d) are calculated spectra. The orange line in (a) is the spectrum of the NH_4^+ torsion mode which was obtained only from the far-IR experiment with the thick sample.

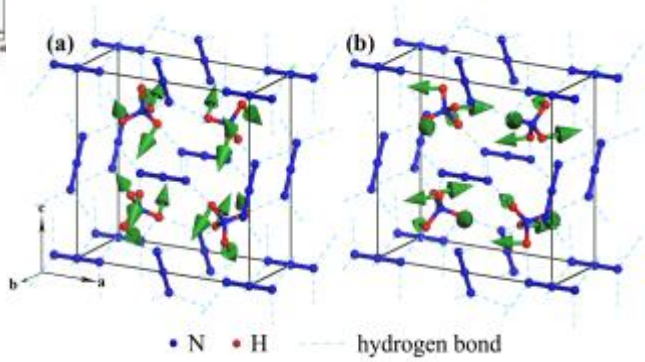

Figure 2. The simulated eigenvectors of the torsional modesat (a) 485 cm^{-1} and (b) 505 cm^{-1}.
(The blue and red colored spheres denote N and H atoms, respectively. The dashed lines denote the hydrogen bonds.)

Reference: .Xiaoxin Wu, Fengxian Ma, Chunli Ma, Hang Cui, Zhengxian Liu, Hongyang Zhu*, Xiaoli Wang, Qiliang Cui, (2014), Pressure-driven variations of hydrogen bonding energy in ammonium azide (NH_4N_3): IR absorption and Raman scattering studies, *J. Chem. Phys.* **141,** pp. 024703

Claperyon slope reversal in $AuGa_2$ at 5.5 GPa

Z. M. Geballe[1], S.V. Raju[2], B.K. Godwal[1] and R. Jeanloz[1]

[1]University of California, Berkeley; [2]Advanced Light Source (LBL), Berkeley

(COMPRES-related facilities: ALS 12.2.2)

We use X-ray diffraction in a resistively heated diamond anvil cell to extend the melting curve of $AuGa_2$ beyond its minimum at 720K, and to constrain the high-temperature phase boundaries between cubic (fluorite structure), orthorhombic (cottunite structure) and monoclinic phases (Fig. 1). We document a large change in Claperyon slope that coincides with the structural phase transitions from cubic to lower symmetry phases, showing that a structural transition is the direct cause of the change in slope (Fig.2). Studies of negative Claperyon slopes have motivated variety of theoretical explanations. For example the change in slope of melting curve from positive to negative in simple metals, lithium and sodium are possibly due to coupled structural and electronic phase transitions. In addition, moderate (~30 K) to large (90 K) hysteresis is detected between melting and freezing, from which we infer that at high pressures, $AuGa_2$ crystals can remain in a metastable state at more than 5% above the thermodynamic melting temperature.

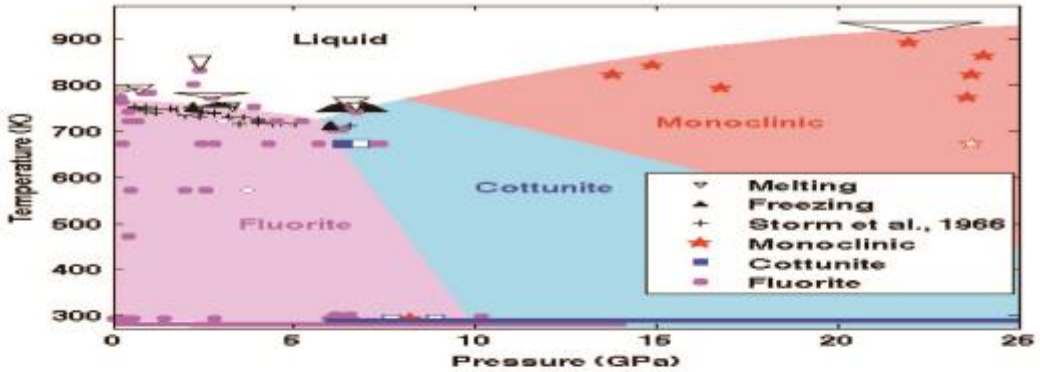

Fig. 1 Phase diagram of AuGa2 based on evidence of melting (open triangles), freezing (solid triangles) and three crystalline phases up to 15 GPa: triangle bases show pressure uncertainty for melting and freezing, determined from scatter in pressures measured at several 10s of degrees below melting; triangle heights show the interval over which we heated or cooled between X-ray diffraction patterns. The data of Storm et al.3 (1966) are shown as plus symbols. Crystalline phases identified in the present study are shown as polygons indicating the pressure–temperature conditions at which each phase was observed. In the special case that a crystalline phase was the product of a phase transition, an open symbol is used to mark the first observation of the new phase. Thick pink and blue lines show regions of stability for the fluorite and cottunite phases at room temperature. Shaded regions indicate phase fields

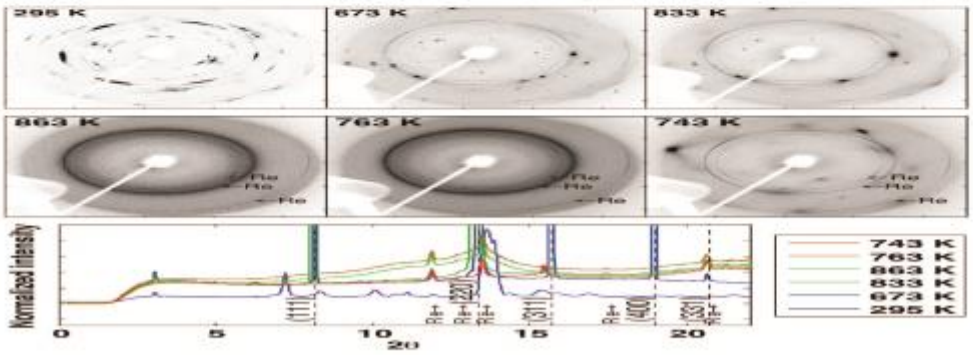

Fig. 2 Evolution of diffraction patterns upon increase and decrease of temperature at ~ 3 GPa. Top rows show raw data. Bottom row shows integrated patterns that are normalized to collection time and x-ray intensity. The room-temperature image shows that the dominant phase is the Fm3m starting material (upper left) at 10 GPa. The sample becomes purely cubic upon heating as pressure drops to 4 GPa at 673 K and 2.3 GPa at 833 K. From 673 to 833 K, single crystals grow (top row). At 863 K, AuGa2 melts completely, creating a diffuse ring; the remaining lines are from the rhenium gasket (second row, left). When temperature is decreased to 743 K, broad peaks of the Fm3m phase appear (second row, right). Integrated patterns show a sudden increase in diffuse scattering upon heating from 833 to 863 K, and a decrease upon cooling from 763 to 743 K. AuGa2 peaks are marked by vertical lines and labeled by their Miller indices.

References: Z.M. Geballe, S.V. Raju, B.K. Godwal and R. Jeanloz J. Phys.:Condens. Matter 25, 415401 (2013); A. R. Storm, J. H. Wernick and A. Jayaraman, J. Phys. Chem. Solids, **27**, 1227 (1966); B. K. Godwal, S. Stackhouse, J. Yan, S. Speziale, B. Militzer and R. Jeanloz, Phys. Rev. B, **87**, 100101(R) (2013)

Co-Determination of Crystal Structures at High Pressure: Combined Application of Theory and Experiment to the Intermetallic Compound $AuGa_2$

B.K. Godwal[1], S. Stackhouse[2], J. Yan[3], S. Speziale[4], Burkhard Militzer[1] and R. Jeanloz[1]

[1]University of California Berkeley; [2]University of Leeds, UK; [3]Advanced Light Source, LBL; [4]Deutsches GeoForschungsZentrum, Potsdam, Germany

(COMPRES-related facilities: ALS 12.2.2)

A combination of X-ray diffraction at high pressures and first-principles calculations reveals the sequence of crystal-structural phase transitions in $AuGa_2$ from cubic ($Fm\bar{3}m$) to orthorhombic (*Pnma*) at 10 (± 4) GPa and then to monoclinic ($P2_1/n$) at 33 (± 6) GPa. Neither theory nor experiment would have been adequate, on their own, in documenting this sequence of phases, but together they confirm a sequence differing from the $Fm\bar{3}m \rightarrow Pnma \rightarrow P6_3/mmc$ transitions predicted for CaF_2 and $Pnma \rightarrow P112_1/a$ transition reported for $PbCl_2$ and $SnCl_2$. The combined results from theory and ADXRD experiments at ALS, also allow us to constrain the equations of state of the three phases of $AuGa_2$. This has important implications for the determination of structure of unknown high pressure phases in materials of interest to Geosciences and Material Science as the deterioration in the quality of diffraction data from powdered samples make the structure determination difficult. Calculations on the analog $PbCl_2$ predict a transition to the $P2_1/n$ phase seen in $AuGa_2$ that could, therefore, be a common high-pressure phase for $PbCl_2$-structured compounds which are analog to CaF_2.

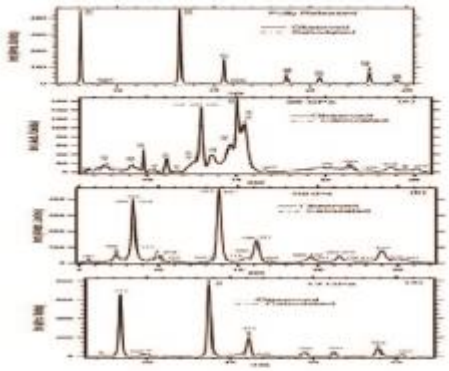

Fig. 1. Comparison of observed and calculated diffraction patterns for the (a) cubic ( ) at 13 GPa, (b) orthorhombic (Pnma) at 16 GPa and (c) monoclinic (P21/n) phases at 36 GPa. Fully relaxed pattern (top panel) reveals that AuGa2 transforms back to its ambient phase. The Rietveld refinement of experimental data was performed using atomic coordinates from the theoretical calculations. The weak peaks indicated by * in Fig. (a) are due to orthorhombic phase.

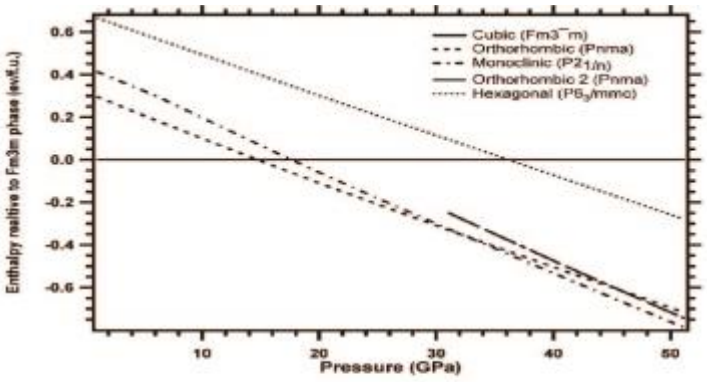

Fig. 2. Calculated enthalpies of all phases studied, relative to that of the cubic structure. The computed enthalpies suggest a transition from the cubic (Fm3m) to orthorhombic (Pnma) phase at about 14 GPa and from the latter to the monoclinic (P21/n) phase at about 32 GPa.

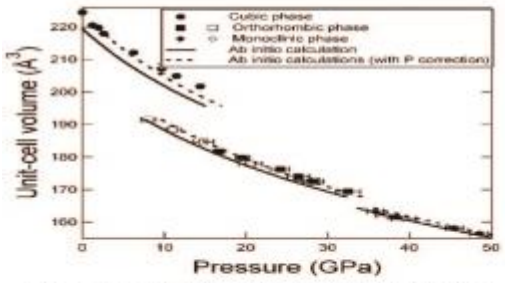

Fig. 3. Experimental unit-cell volumes determined for AuGa2 under static compression. The data shows three separate regions: a low pressure region (≤ 13 GPa) corresponding to the cubic ( ) phase; an intermediate-pressure region (8 GPa ≤ P ≤ 35 GPa) corresponding to the orthorhombic (Pnma) phase; and a high-pressure region (> 35 GPa) corresponding to the monoclinic (P21/n) phase. The filled and open symbols represent compression and decompression respectively. The dashed and solid lines are the P-V compression curves from theory with and without pressure correction respectively.

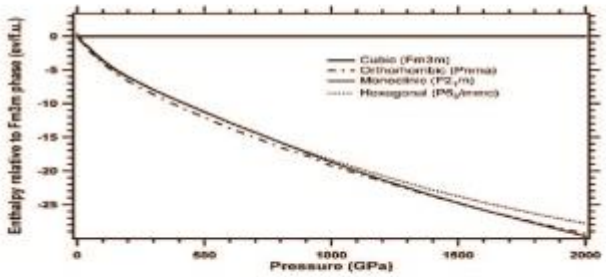

Fig.4 Calculated enthalpies of all phases of PbCl2 studied, relative to that of the cubic ( ) structure. The calculations suggest a displacive transition from the ambient orthorhombic structure (Pnma) to the Co2Si-type structure (Pnma) at low pressure and then to the monoclinic (P21/n) phase at about 1600 GPa. Metallization begins at about 100 GPa.

References: B.K. Godwal , S. Stackhouse, J. Yan, S. Speziale, B. Militzer and R. Jeanloz, Phys. Rev. B 87, 100101(R) (2013), Co-Determination of Crystal Structures at High Pressure: Combined Application of Theory and Experiment to the Intermetallic Compound $AuGa_2$

High Pressure and Temperature structure of Liquid and Solid Cd: Implications for the melting curve of Cd

S. V. Raju[1,2], Z. M. Geballe[3], B. Kalkan [2], B. K. Godwal[3], Q. A Williams[1] and R. Jeanloz[3]

[1] University of California, Santa Cruz ; [2]Advanced Light Source, LBL, Berkeley; [3]University of California, Berkeley

(COMPRES-related facilities: ALS 12.2.2)

The structure of cadmium was characterized in both the solid and liquid forms at pressures to 8 GPa using in-situ x-ray diffraction measurements in a resistively heated diamond anvil cell (Fig. 1 shows melting and freezing at 8 GPa ; Fig. 2 provides liquid structure factor S(Q) and radial distribution function g(r) at 2 and 6.8 GPa). The distortion of the hexagonal structure of solid cadmium markedly increases at high temperatures, with anomalously large c/a ratio of Cd becoming larger as the melting curve is approached (Fig. 3). The measured structure factor S(Q) for the melt reveals that the cadmium atoms are spaced about 0.6 Angstroms apart (Fig. 2). The melt structure remains notably constant with increasing pressure, with the first peak in the structure factor remaining mildly asymmetric, in accord with the persistence of an anisotropic bonding environment within the liquid. Evolution of powder diffraction patterns up to the temperature of melting revealed the stability of the ambient-pressure hcp structure up to a pressure of 10 GPa. The melting curve has a positive Clausius-Clapeyron slope, and its slope is in good agreement with data from other techniques (Fig. 4). We find deviations in the melting curve from Lindermann Law type behavior for pressures above 1 GPa.

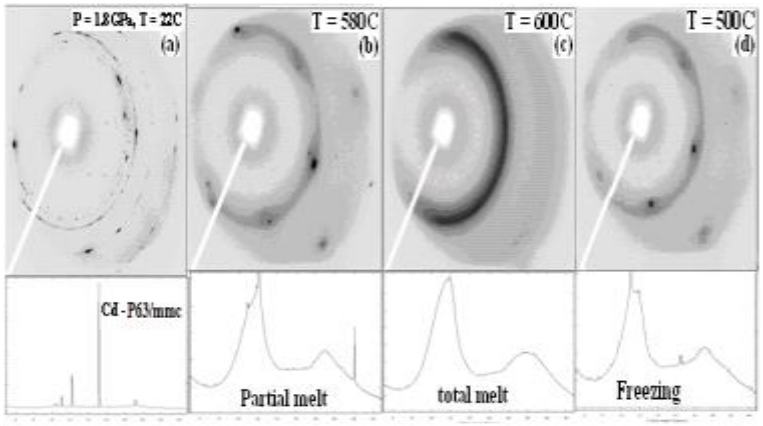

Fig. 1: Melting and freezing of Cadmium under high pressure at ~6.8 GPa.

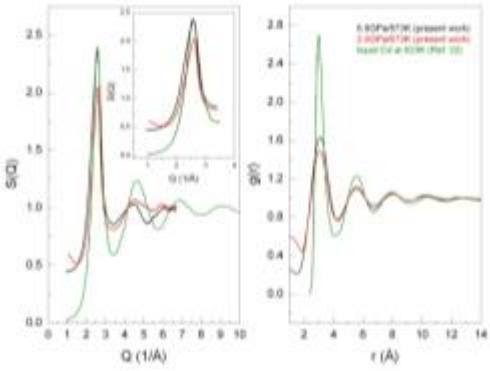

Fig. 2. Structure factor S(Q) and Radial distribution function g(r) obtained from melt data.

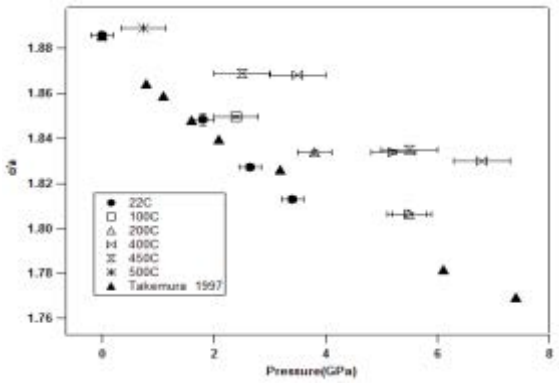

Fig.3. The variation of the c/a ratio with pressure at high temperatures up to temperatures up to 500°C. Solid symbols represent the c/a ratio obtained at respective temperature indicated in the figure. Solid triangles represent room temperature data from Takemura(1997).

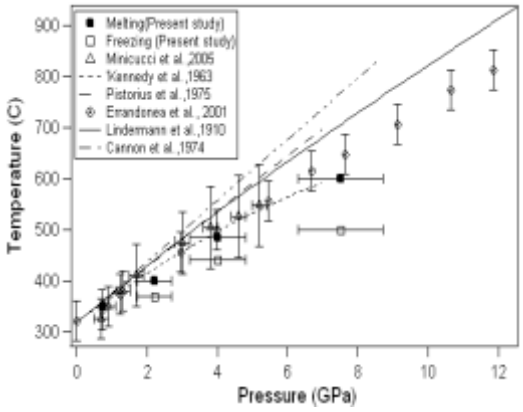

Fig. 4 . Comparison of different cadmium melting data.

S. V. Raju, Z. M. Geballe, B. Kalkan , B. K. Godwal, Q. A Williams and R. Jeanloz , High Pressure and Temperature structure of Liquid and Solid Cd: Implications for the melting curve of Cd; Material Research Express 1, 046502 (2014) (For all the references in the figures refer to this); B.K. Godwal, S.V. Raju, Z. Geballe and R. Jeanloz J. Phys.: Conf. Series 377, 012033 (2012), Electronic phase transitions in Cd.

A new lithium-rich anti-spinel in Li–O–Br system

The spinel structure is a common structure in a wide variety of crystalline materials. The general composition for the spinel structure is AB_2X_4, derived from mineral spinel $MgAl_2O_4$, which crystallizes in the space group of Fd-3m (227). In a normal AB_2X_4 spinel, the A ions are in the tetrahedral sites and the B ions are in the octahedral sites. When A ions occupy one half of the octahedral sites and B ions occupy the other half of the octahedral and all tetrahedral sites, the structure is called inverse spinel, generally expressed as $B[AB]X_4$ (e.g., magnetite). There is yet a third family of materials crystallized in the defect spinel structure (e.g., gama-Fe_2O_3), indicating that the spinel structure can accommodate a substantially large amount of vacancies in the crystal lattice. In all known materials that exhibit the spinel structure, both A and B ions are cations and X is an electronegative divalent anion such as O^{2-} and S^{2-}. However, despite its flexibility to a wide range of compositions and vacancies, the spinel structure with inverted cation and anion positions, the so-called anti-spinel, has yet been reported in any material system. We report here the first discovery of an 'electronically inverted' anti-spinel. The new anti-spinel was synthesized in the system Li–O–Br under pressures (P) less than 2 GPa and temperatures (T) below 330 °C at COMPRES-supported MAC facility (X17B2-NSLS/6BMB-APS). The synthesis processes were monitored by in situ and real-time synchrotron X-ray diffraction, and the new phase is formed during the following breakdown reaction: $Li_5Br(OH)_4 = Li_3OBr + 2LiOH + H_2O$.

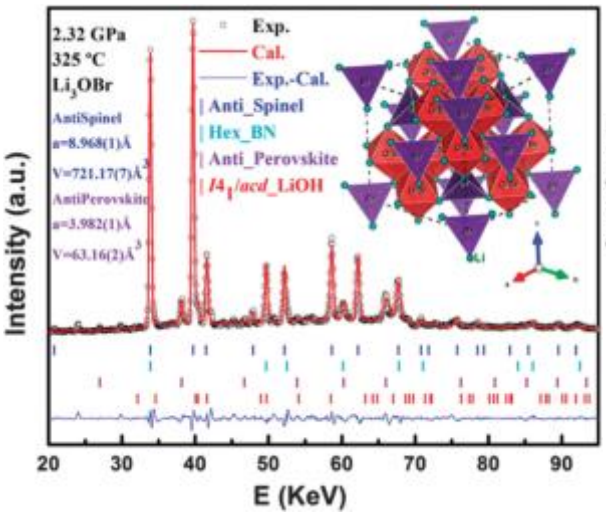

Figure 1 Le Bail fit of the observed pattern at 2.32 GPa and 325 °C. The inset shows the crystal structure of anti-spinel with space group Fd-3m.

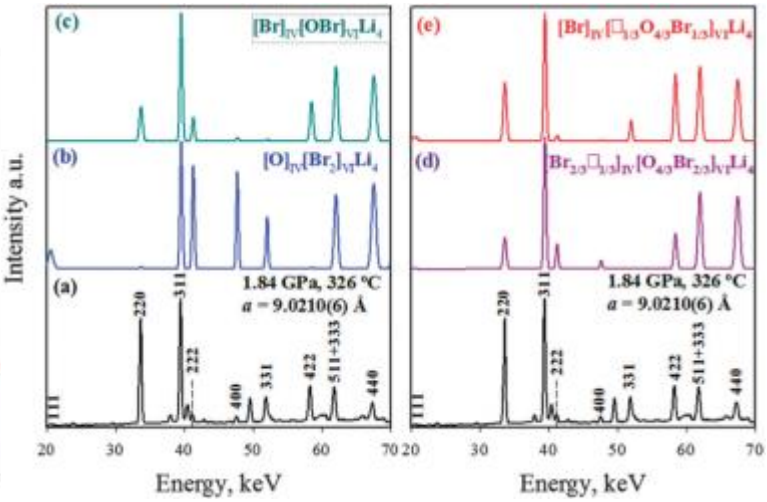

Figure 2 Observed (a) and simulated X-ray patterns (b–e) for anti-spinel structure of various anion and vacancy distributions. All simulated patterns were generated by using a GSAS + ExpGUI software package with space group Fd-3m and a lattice parameter of 9.02 Å. An isotropic thermal vibration parameter of 0.025 was used for all atoms. Patterns (d) and (e) best match the observed diffraction pattern for anti-spinel.

Zhang, JZ; Zhu, JL; Wang, LP; Zhao, YS (2015) A new lithium-rich anti-spinel in Li–O–Br system. ***Chemical Communications***, 51, 9666-9669, DOI: 10.1039/c5cc01109d.

Magnetism of europium under extreme pressures

W. Bi,[1, 2] J. Lim,[3] G. Fabbris,[1,3,4] J. Zhao,[1] D. Haskel,[1] E. E. Alp,[1] M. Y. Hu,[1] P. Chow,[5]
Y. Xiao,[5] W. Xu,[6] and J. S. Schilling[3]
[1]*Advanced Photon Source, Argonne National Laboratory, Argonne, IL*
[2]*Department of Geology, University of Illinois at Urbana-Champaign, Urbana, IL*
[3]*Department of Physics, Washington University, St. Louis, MO*
[4]*Department of Condensed Matter Physics and Materials Science, Brookhaven National Laboratory, Upton, NY*
[5]*High Pressure Collaborative Access Team, Geophysical Laboratory, Carnegie Institution of Washington, Argonne,*
[6]*Beijing Synchrotron Radiation Facility, Institute of High Energy Physics, Chinese Academy of Sciences*
(COMPRES-related facilities: Advanced Photon Source, beamline 3-ID)

Using synchrotron-based Mössbauer and x-ray emission spectroscopies, we explore the evolution of magnetism in elemental (divalent) europium as it gives way to superconductivity at extreme pressures. Magnetic order in Eu is observed to collapse just above 80 GPa as superconductivity emerges, even though Eu cations retain their strong local $4f^7$ magnetic moments up to 119 GPa with no evidence for an increase in valence. We speculate that superconductivity in Eu may be unconventional and have its origin in magnetic fluctuations, as has been suggested for high-T_c cuprates, heavy fermions and iron-pnictides.

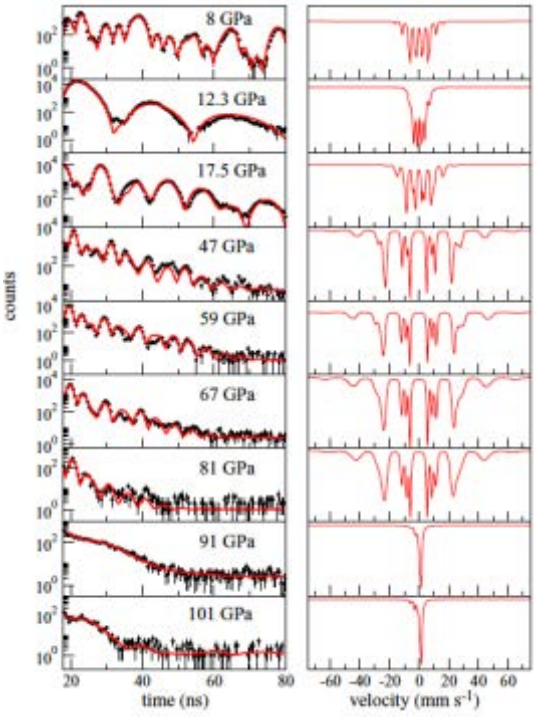

Figure 1 (left column) Representative SMS spectra of Eu at high pressure and 11 K. Black dots are data and red lines are fits from CONUSS. (right column) Simulated spectra in energy domain from fits of the time-domain data (red lines in left column).

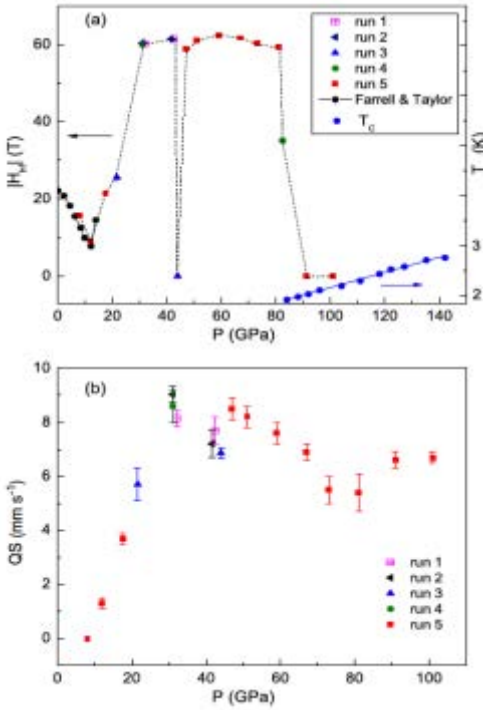

Figure 2 Extracted hyperfine parameters from SMS spectra at 11 K. (a) Absolute value of magnetic hyperfine field $|H_{hf}|$ versus pressure compared to previous at 44 K. Dashed lines through data are guides to the eye. Lower right: superconducting transition temperature T_c versus pressure. (b) Quadrupole splitting (QS) versus pressure. Error bars come from CONUSS fits to $|H_{hf}|$ and quadrupole splitting.

References: W. Bi, J. Lim, G. Fabbris, J. Zhao, D. Haskel, E.E. Alp, M.Y. Hu, P. Chow, Y. Xiao, W. Xu, and J.S. Schilling, Phys. Rev. B **93**, 184424 (2016).

Pressure-induced collapse of magnetism in Greigite (Fe_3S_4)

Wenli Bi (UIUC and APS, ANL), J. Zhao, E. E. Alp (APS, Argonne National Laboratory)
J. S. Tse (Department of Physics and Engineering Physics, University of Saskatchewan, Canada)

COMPRES-related facilities:
Advanced Photon Source, beamline 3-ID and offline Mössbauer Lab

Greigite (Fe_3S_4) is a ferrimagnetic mineral with vital bio-geochemical cycle. At ambient pressure greigite has an inverse spinel structure, in analogy to magnetite (Fe_3O_4) [1, 2, 3]. However, how the magnetic behave under high pressure is still unknown. We have performed conventional Mössbauer experiment at ambient conditions as well as synchrotron Mössbauer experiment under high pressure using an ultrahigh purity synthetic sample. We have found that hyperfine magnetic fields from both tetragonal and octahedral Fe sites decrease slowly with pressure. The magnetic field starts to collapse above 2.3 GPa and greigite becomes completely nonmagnetic at 3.6 GPa. These results warrant further investigation of the electronic and crystal structure of greigite under high pressure.

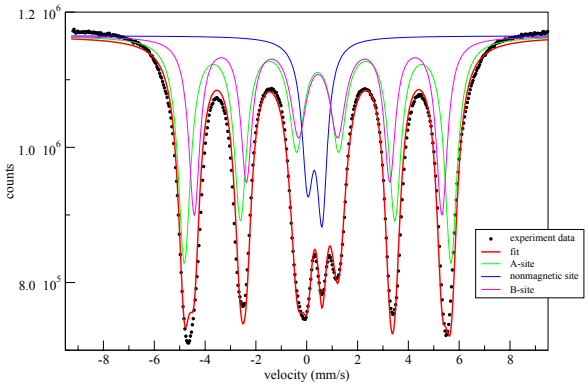

Figure 1 Conventional Mössbauer spectrum of Fe_3S_4 at ambient conditions. The fit to the data includes Fe A- and B-sites and a nonmagnetic component.

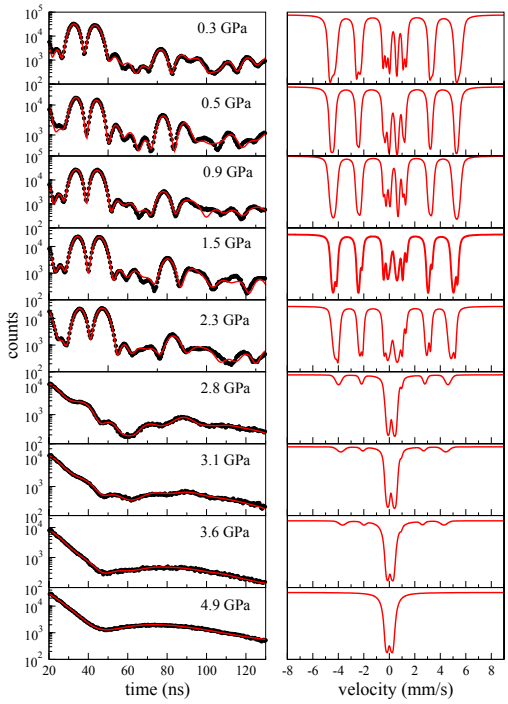

Figure 2 (Left column) SMS spectra of Fe_3S_4 at various pressures at room temperature. Black dots are experiment data and red lines are fits from CONUSS. (right column) Simulated spectra in energy domain corresponding to fit of the time domain data.

References:

[1] M. Wu, J.S. Tse, and Y. Pan, Sci. Rep. **6**, 21637 (2016).
[2] G. Li, B. Zhang, F. Yu, A.A. Novakova, M.S. Krivenkov, T.Y. Kiseleva, L. Chang, J. Rao, A.O. Polyakov, G.R. Blake, R.A. De Groot, and T.T.M. Palstra, Chem. Mater. **26**, 5821 (2014).
[3] L. Chang, A.P. Roberts, Y. Tang, B.D. Rainford, A.R. Muxworthy, and Q. Chen, J. Geophys. Res. Solid Earth **113**, 1 (2008).

Porous Ice Phases with VI and Distorted VII Structures Constrained in Nanoporous Silica

Jinlong Zhu, Zewei Quan, Yu-Shen Lin, Ying-Bing Jiang, Zhongwu Wang, Jianzhong Zhang, Changqing Jin, Yusheng Zhao, Zhenxian Liu, C. Jeffrey Brinker, and Hongwu Xu, UNLV

(COMPRES-related facilities: National Synchrotron Light Source I U2A)

High-pressure compression of water contained in nanoporous silica allowed fabrication of novel porous ice phases as a function of pressure. The starting liquid nanoporous H_2O transformed to ice VI and VII at 1.7 and 2.5 GPa, respectively, which are 0.6 and 0.4 GPa higher than commonly accepted pressures for bulk H_2O. The continuous increase of pressure drives the formation of a tetragonally distorted VII structure with the space group I4mm, rather than a cubic Pn3m phase in bulk ice. The enhanced incompressibility of the tetragonal ice is related to the unique nanoporous configuration, and the distortion ratio c/a gradually increases with increasing pressure. The structural changes and enhanced thermodynamic stability may be interpreted by the two-dimensional distribution of silanol groups on the porous silica surfaces and the associated anisotropic interactions with H_2O at the interfaces.

Figure 1. The infrared absorption spectroscopy of water interactions with different pore sized silica. The broad peaks at ~ 3400-3500 cm^{-1} are from the water interacted with the surface hydrophilic OH groups (~ 3750 cm^{-1}). The small shoulders at ~ 3700 cm^{-1} are from the water inside the nanoporous wall. The blue shift effect (opposite to increasing pressure) could come from the capillary and constrained effect. All the nano amorphous silica samples have the hydrophilic -OH groups attached on the surface, as evidenced by the sharp IR peaks at ~3750 cm^{-1}.

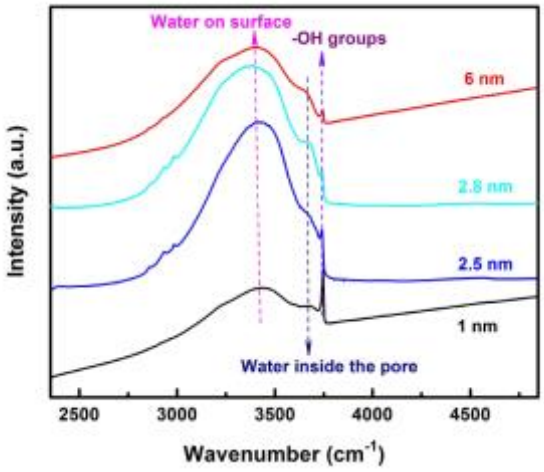

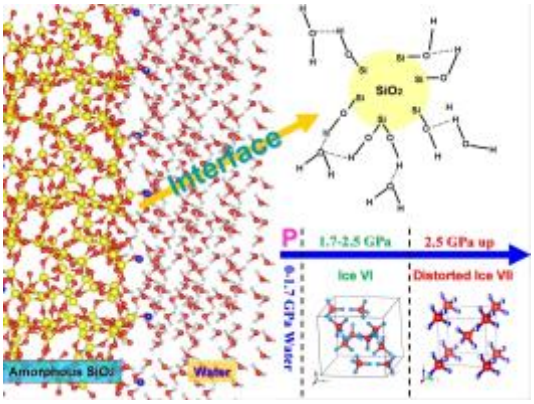

Figure 2. Schematic show of bonding interaction at the interface of porous silica and H_2O; the red balls represent oxygen, yellow represent silicon, light gray represent hydrogen of water, and the blue balls represent the hydrogen of the Si–OH group on silica surface. Left lower panel gives the shifted transition pressure from water to ice VI and distorted ice VII.

References: J. Zhu, Z. Quan, Y. Lin, Y. Jiang, Z. Wang, J. Zhang, C. Jin, Y. Zhao, Z. Liu, C. J. Brinker, and H. Xu, (2014) Porous Ice Phases with VI and Distorted VII Structures Constrained in Nanoporous Silica, *Nano Letters* **14**, pp. 6554-6558.

Pressure-induced Insulator- metal transition in single molecular radicals and metallicity of doped Mg_2Si thermoelectric compounds

John. S. Tse, University of Saskatchewan, Canada

(COMPRESS related facilities: U2A- NSLS-I)

We have employed themed and far-IR facilities atU2A to study band gap closure in the transmission spectra and the estimation of frequency dependent optical conductivity in the reflective mode. A major project is the investigation of the electronic properties of a series of organic single radical solids consisted of the fundamental building block **I** with different alkyl groups and halides substitutions under pressure and, occasionally at low temperature. The basic idea is to use manipulate the spin-coupling between the single spin radical units in the crystal by adjusting the spearations using pressure. Since crystals are very compressible, very lowpressure of a few GPa is often required. We successfully demonstrated the magnetic property of the systems can be altered from paramagnetic, to ferro-and/or antiferromagntic and, for the first time, we succeeded to metalize in avariety of neutral molecular radical systems without decomposition or polymerization. Some examples are illustrated below.

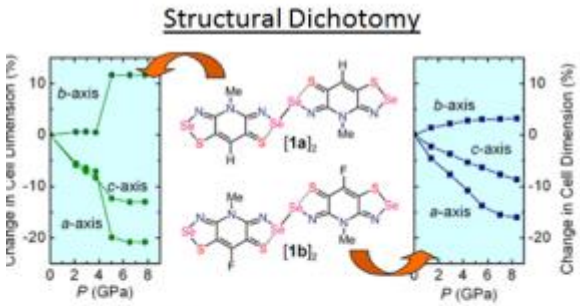

Cryst Growth & Design, 12, 4076 (2012)

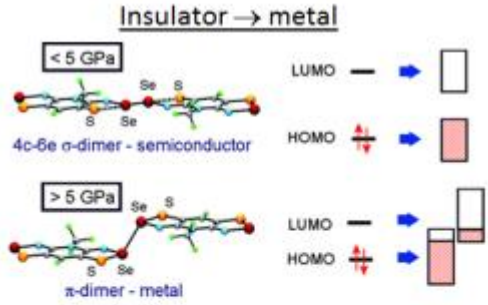

JACS, 132, 4876 (2010)

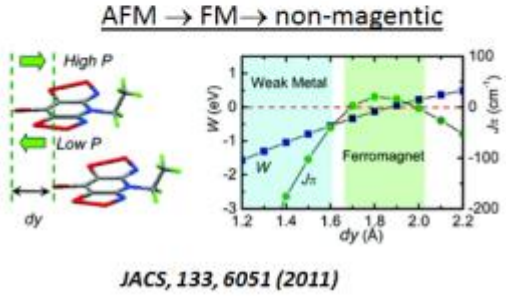

JACS, 133, 6051 (2011)

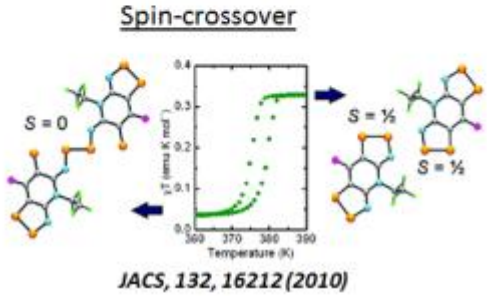

JACS, 132, 16212 (2010)

We have used IR spectroscopy to characterize the metallicity of doped-Mg_2Si, a potential efficient thermoelectric material. The goao is to extract the dielectric functions from the far and mid-IR spectra. A recent example is the elucidation of the mechanism on pressure-enhanced thermopower of an Al-doped sample.

References:J. Zhao, *et.al., J. Appl. Phys*., **118**, 145902 (2015); D. Tian, *et.al., J. Amer. Chem. Soc*., **13**7, 14136, 2015; J.W. Wong, et.al., *J. Amer. Chem. Soc*., **136**, 1070, 2014.